Mathematical Models of Mitochondria in the Kidney and Liver

by

T. William Bell

A thesis
presented to the University of Waterloo
in fulfillment of the
thesis requirement for the degree of
Masters of Mathematics
in
Applied Mathematics

Waterloo, Ontario, Canada, 2021

Author's Declaration

I hereby declare that I am the sole author of this thesis. This is a true copy of the thesis, including any required final revisions, as accepted by my examiners.

I understand that my thesis may be made electronically available to the public.

Abstract

Mitochondria are key players in several kinds of tissue injury, and are even the site of mechanism of certain diseases. In this work we introduce new models of mitochondrial ATP generation in multiple tissues, including liver hepatocytes and the medullary thick ascending limb in the kidney. Using this model, we predict these tissues' responses to hypoxia, uncoupling, ischemia-reperfusion, and oxidative phosphorylation dysfunction. Our results suggest mechanisms explaining differences in robustness of mitochondrial function across tissues.

The medullary thick ascending limb and proximal tubule in the kidney both experience a high metabolic demand, while having lower baseline activity of oxidative phosphorylation relative to the liver. These factors make these tissues susceptible to dysfunction in Complex III. A lower baseline oxygen tension observed in the thick ascending limb makes it susceptible to Complex IV. On the other hand, since the liver lacks these risk factors, and has higher baseline rates of glycolysis, it is less susceptible to all kinds of oxidative phosphorylation dysfunction.

Ischemia-reperfusion is an intriguing example of a non-equilibrium behaviour driven by a change in tissue oxygen tension. Ischemia involves prolonged hypoxia, followed by the sudden return of oxygen during reperfusion. During reperfusion, we predict that the build up of succinate causes the electron transport chain in the liver to temporarily be in a highly reduced state. This can lead to the production of reactive oxygen species. We accurately predict the timescale on which the electron transport chain is left in a reduced state, and we observe levels of reduction likely to lead to reactive oxygen species production.

Aside from the above, we predict thresholds for ATP depletion from hypoxia, and we predict the consequences for oxygen consumption of uncoupling. We find that once again, the kidney tissues considered are more at risk from hypoxia. We predict that hypoxia represents a danger of ATP depletion in the proximal tubule below 10 mmHg of oxygen partial pressure, and in the thick ascending limb below 3 mmHg.

We examine at length the effects of diabetes on the liver and kidney, and we find that it may leave the kidney especially at greater risk for ATP depletion and reactive oxygen species formation. This is particularly true during hypoxia (and uncoupling in the case of ATP depletion).

Our modelling efforts indicate the viability of modelling mitochondrial pathologies with mechanistic models. We demonstrate that even simple models of mitochondrial dysfunction may effectively reproduce experimental results.

Acknowledgements

I would like to thank all the people who came together to help make this thesis. Anita Layton was my most consistent collaborator in producing this work, she has gone over every page of my thesis and given me direction on the scientific and mathematical substance of it. Aurélie Edwards and Rui Hu also graciously and responsively gave me direction in posing certain key problems for this work, and in the estimation of several important quantities for this work. I would like to thank Sameera Singh for reviewing parts of my manuscript. My work builds on the work of many people, but aside from the above, I would also like to highlight the foundational work of Fred Palm, Fan Wu, and Dan Beard, without whom this model might not exist. Along the way I have had the opportunity to work alongside several colleagues whose collaboration has been valuable in less tangible ways to the completion of this work, among them (non-exhaustively), Mehrshad Sadria, Stéphanie Abo, Anderson White, Aiden Huffman, Dania Sheaib, Delaney Smith, and Melissa Stadt. My work has benefited from their influence. I also would like to thank many people who've been there for me throughout the completion of this work (aside from those mentioned above), including Casey Vaillancourt, Haroon Shaffiulla, Trupti Jayakumar, Catherine Bell, Lorie Bell, my girlfriend Salina Mathur, and my parents, Sharon Bell and Neal Thomas. Throughout the pandemic, the thoughtfulness and astuteness of the above figures was crucial for the completion of my work.

"The ancient philosophical problematic, 'how do we get from the Many to the One?' (corresponding to a phenomenological transit) becomes the mathematical problematic, 'how do we get from the local to the global?' (technical transit), which, in turn, can be subdivided into the questions (i) 'how do we differentially register the local?' and (ii) 'how do we globally integrate those registers?'"

- Zalamea, *Synthetic Philosophy of Contemporary Mathematics*

Here we begin work on the first step of this process.

Table of Contents

List of Figures

List of Tables

Chapter 1

Introduction

The body is composed of a variety of tissues, and mitochondrial respiration varies starkly among them [13]. There are several reasons to care about these differences: first, there is significant tissue specificity to many forms of mitochondria-mediated cellular injury [169] and second, tissues contribute in very different ways to whole-body metabolism [204, 206]. Those tissue-specific contributions to whole-body metabolism depend on many subcellular differences, and especially the behaviour of mitochondria [65]. For these reasons, both to understand tissue-specific responses to whole-body functioning, and whole-body responses to local dysfunction it is valuable to understand physiological diversity in mitochondrial function.

Below we map out some of these differences in epithelial cells of the proximal tubule & medullary thick ascending limb of the kidney, and hepatocytes of the liver. We also examine how these tissues' mitochondria act differently due to diabetes.

1.1 Mitochondria

The mitochondrion is a cellular organelle crucial to the performance of several functions of the animal cell, including aerobic cellular respiration and apoptosis. The importance of mitochondria to these cellular functions doesn't exhaust its uniqueness among animal cellular organelles. The mitochondria are unique for their structure, relative independence, and origins. These features are closely connected and are all due to the origins of mitochondria. Mitochondria were originally endosymbionts living inside the common ancestor of today's eukaryotes [67, 152]. That is, they were originally free-living prokaryotes that were most likely endocytosed by a proto-eukaryote [67]. They eventually developed a symbiotic relationship with the species that (most likely) endocytosed it [26], becoming the mitochondria we know today. Due to this strange natural history, mitochondria have their own DNA that we'll call mtDNA to distinguish it from the DNA found in the cell's nucleus [196]. Today the mitochondrial genome only codes for a few proteins, all localized to the mitochondrion, as

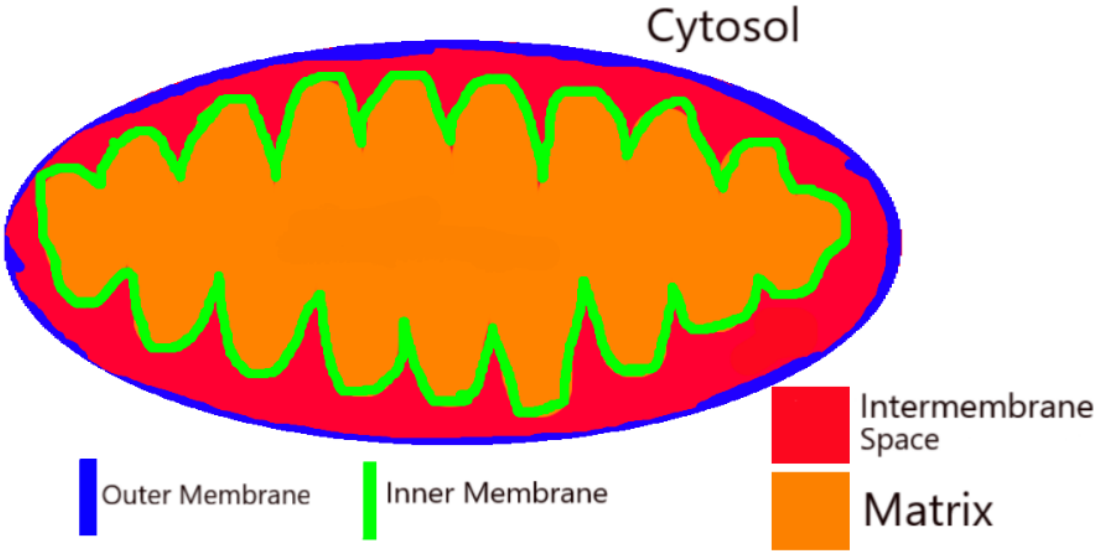

Figure 1.1: A mitochondrion with its interior spaces and surrounding cytosol labelled. The cytosol and intermembrane space are separated by the mitochondrion's outer membrane. The intermembrane space and mitochondrial matrix are separated by the mitochondrion's inner membrane. The folds in the inner membrane are known as cristae. Cristae increase the surface area available for reactions.

well as a full set of tRNAs [196]. Mitochondria are also left with another reminder of their history: they have two membranes. This is believed by some to be a biproduct of the originating endocytotic event which could have left the cell inside an extra membrane [26]. This double membrane structure creates two compartments within the mitochondrion: the mitochondrial matrix and the intermembrane space, this is depicted in Figure 1.1.

Below we wish to briefly outline the main steps of cellular respiration. For a more detailed account one may consult Cox and Nelson's *Lehninger Principles of Biochemistry* [33]. As part of aerobic cellular respiration, the mitochondria use several metabolites, including fatty acids (for instance via beta-oxidation) and pyruvate (via pyruvate oxidation). These metabolites are primarily converted into acetyl-CoA, which enters the Tricarboyxlic Acid (TCA) or Krebs cycle. The TCA cycle occurs in the mitochondrial matrix. The TCA cycle produces ATP, NADH, and $FADH_2$. The latter two products of the TCA cycle reduce components of the electron transport chain, NADH reduces Complex I and $FADH_2$ reduces Complex II. Both Complex I and II reduce coenzyme Q, which in turn reduces Complex III. Complex III reduces Cytochrome C, which reduces Complex IV. Complex IV reduces oxygen, the final electron acceptor of the electron transport chain. The complexes noted above are localized on the inner membrane of the mitochondrion. They use the energy from the above redox reactions they participate in to move hydrogen ions into the intermembrane space. The hydrogen gradient that they create provides the potential that drives the production of

ATP via ATP Synthase (also known as F_0F_1-ATPase or Complex V). ATP Synthase phosphorylates ADP to ATP while allowing hydrogen ions to travel across the inner membrane. Together the processes of the electron transport chain and ATP production by ATP Synthase are known as oxidative phosphorylation. Dysfunction of oxidative phosphorylation is tied to several diseases, including most known mitochondrial diseases and diabetic end-organ damage. Dysfunctions of this kind, caused by reduced activity of enzymes involved in oxidative phosphorylation, will appear in our modelling work as a potential cause of ATP depletion.

The cell does not ever do the above procedure with optimal efficiency, although this is not necessarily maladaptive [135, 157]. Two ways in which cellular respiration functions suboptimally are via uncoupling and free radical (mainly reactive oxygen species) production. Uncoupling is the leakage of hydrogen ions across the inner membrane of the mitochondrion [157]. This shunting of hydrogen gradient means that more hydrogen needs to be pumped by the electron transport chain into the intermembrane space for the same amount of ATP synthesized. This inefficiency is best measured by the P/O ratio (phosphate/oxygen ratio), which is defined for our model as the ratio of ATP Synthase activity to Complex IV activity [44]. As an aside, not all experimentalists define the P/O ratio this way, it depends on how they measure oxygen consumption [19]. This will be discussed in more detail in Chapter 4. The potential adaptive purpose of uncoupling is tied to free radical production, which we turn to now.

Mitochondrial free radical production primarily occurs when electrons are transferred by Complex I or III to something other than another member of the electron transport chain [73]. Free radicals have an unpaired electron that make them reactive. The most significant free radical produced by the electron transport chain is O_2^-, or superoxide, a reactive oxygen species [73]. Free radicals frequently react with important biomolecules, causing cellular injury [73]. Notably, reactive oxygen species released by mitochondria are already nearby the mtDNA, putting the mtDNA at risk. Consequently, mtDNA mutations are the most prevalent causes of mitochondrial disease [1] (mitochondrial turnover, on the timescale of weeks, ensures that inherited mitochondrial diseases are the major cause of long-term mitochondrial dysfunction [38]). The protein-coding sequences of mtDNA exclusively code for proteins involved in oxidative phosphorylation and the construction of the mitochrondial ribosome [1]. For this reason, the vast majority of mitochondrial diseases are known to cause dysfunction of oxidative phosphorylation [1]. Reactive oxygen species are produced by components of the electron transport chain when they are in a reduced state but are not able to reduce their typical cofactors or other targets. Let's consider an example: Complex I is typically reduced by NADH and oxidized by coenzyme Q [33]. If there are sufficient quantities of oxidized coenzyme Q or NAD^+, then Complex I will reduce those rather than producing reactive oxygen species. If there are not, or Complex I is prevented from reducing those cofactors (for instance by rotenone), then Complex I will produce superoxide and hydrogen peroxide instead [128]. This is the direct mechanism for reactive oxygen species production from Complex I. However it is important to note that the activity of Complex I exhibits exponential dependence on the proton motive force [175]. The production of reactive oxygen species is

highly sensitive to the proton motive force [39]. A consequence of this is that uncoupling may significantly reduce reactive oxygen species production, since it directly reduces the proton motive force [55, 73].

Ischemia-reperfusion injury is tightly linked to this process of free radical production. We say a tissue is ischemic when it is not being perfused with blood. Ischemic tissues experience hypoxia and a lack of nutrient perfusion from the blood [30]. However, ischemia (particularly with modern methods used in for instance, organ transplantation) does not usually kill the cell or cause lasting injury [82]. Instead there is a massive build up of succinate during the ischemic phase, and the rapid consumption of this succinate during reperfusion leaves the electron transport chain in a highly reduced state, causing free radical formation through the process outlined above over the course of only a few minutes [30]. As Jassem and Roake memorably put it, ischemia-reperfusion injury "consists of two distinct phases: ischaemia, which is the biological equivalent of loading and cocking a gun, and reperfusion, which is analogous to pulling the trigger" [82].

This is sufficient detail on the mitochondrion's role in cellular respiration for our discussion. However an exposition of mitochondrial function would be incomplete without discussing their role in calcium homeostasis and apoptosis. Calcium is stored in large quantities in the mitochondrial matrix [45, 64]. The cell is extremely sensitive to deviations from calcium homeostasis. If there is too much calcium in the cytosol, mitochondrial permeability transition pores open on the inner membrane [45]. These pores are non-selective, allowing for the movement of many small particles across the inner membrane. This causes the collapse of the proton motive force across the inner membrane and allows more leakage of calcium. This process ultimately triggers apoptosis [45]. Calcium homeostasis is the crux of many mitochondria-mediated diseases, among them, the most common variant of autosomal dominant polycystic kidney disease [134]. During autosomal dominant polycystic kidney disease, polycystin-1, a protein involved in the regulation of calcium transfer between the endoplasmic reticulum and mitochondria, is dysfunctional. This disrupts calcium homeostasis, and may be a key pathway underlying the progression of the disease [134]. Ultimately however this will be outside the scope of our work, as discussed below.

1.2 Tissues and their Mitochondria

In our work we consider three cell types across two organs: epithelial cells from the proximal convoluted tubule (PT) and medullary thick ascending limb of the loop of Henle (mTAL) in the kidney (these tissues occur in each nephron, the functional unit of the kidney), and hepatocytes in the liver lobules (the functional unit of the liver). The kidney is divided up into three layers, the inner medulla in its core, the outer medulla outside the inner medulla, and the cortex which surrounds the medulla. The nephron travels from the cortex (where the Bowman space and proximal convoluted tubule are) into the inner medulla (via the loop of Henle) and back out, before travelling back into the medulla via the collecting duct. The

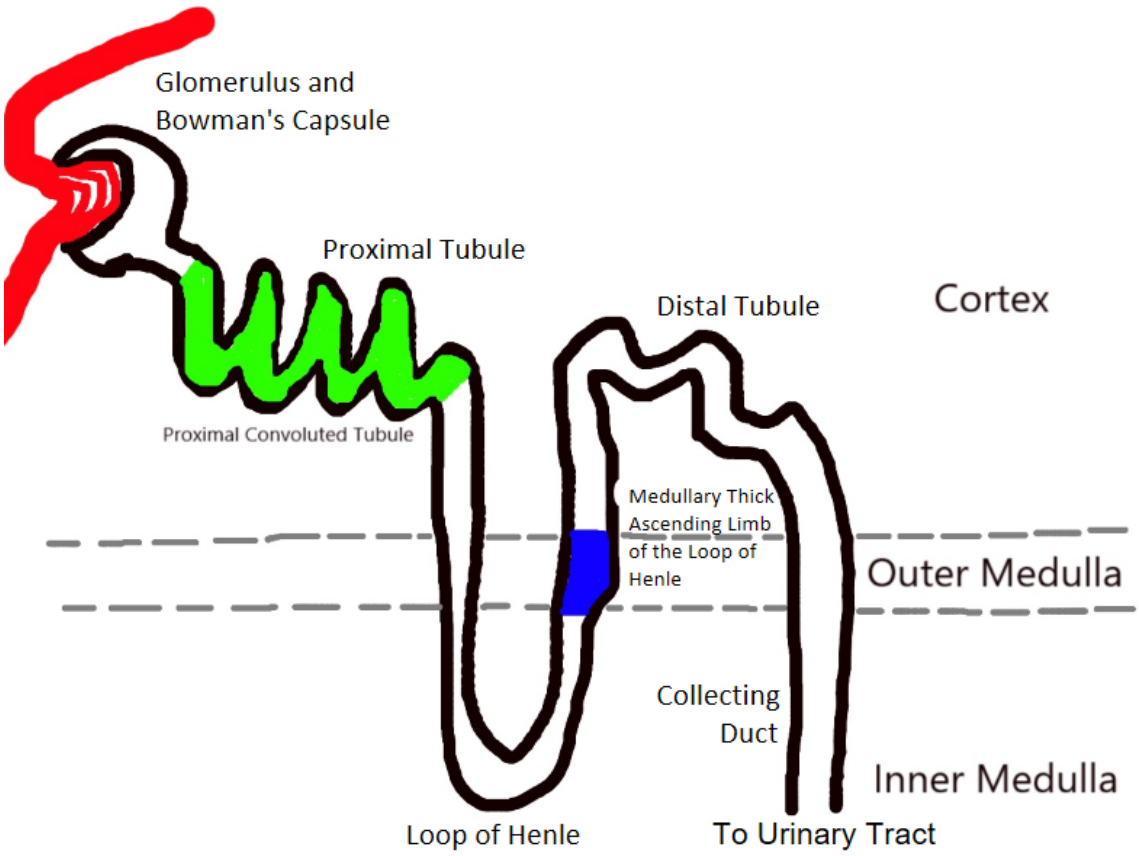

Figure 1.2: A nephron in the kidney, with some kidney and nephron sections labelled, the proximal convoluted tubule and medullary thick ascending limb of the loop of Henle are coloured green and blue respectively.

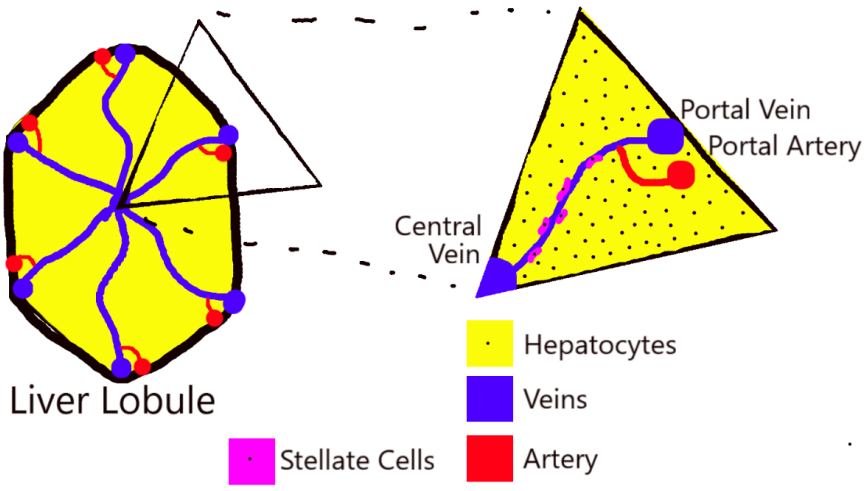

Figure 1.3: A lobule in the liver, with labelled circulatory structures and cell types.

PT (in the cortex) is the site of the majority of reabsorption of ions and nutrients from the glomerular filtrate (which will eventually become urine), and has a high metabolic demand [44]. The PT (and kidney cortex in general) is highly oxygenated [47]. The mTAL (in the outer medulla) is the site of a significant amount of active reabsorption of sodium, it in fact has a higher metabolic demand than the PT [181]. The mTAL (and kidney medulla) is less well oxygenated [47]. Due to the high metabolic demand in the kidney tissues we consider, they are at risk of ATP depletion. We show a nephron, with the PT and mTAL highlighted in Figure 1.2.

The liver is primarily composed of rice-sized units called lobules [12]. The liver hepatocytes are the majority of liver tissue by volume [11]. The liver is crucial to the body's metabolic homeostasis, particularly for glucose [12]. Many liver pathologies are mitochondria-mediated [195]. Unlike the kidney cells we consider, these pathologies typically involve the production of reactive oxygen species by the liver mitochondria [124, 195]. The liver lobules have oxygen gradients from the edge of the liver lobule to its center, but generally the oxygen tension is somewhere between that of the kidney cortex and medulla [12]. We show a liver lobule, with various structures and cell-types labelled in Figure 1.3.

1.3 Mechanistic Mathematical Modelling of Mitochondrial Respiration

Mitochondrial respiration has been a subject of biological research for an extended period of time and consequently it has been subject to intense research by mathematical biologists [e.g. 7, 44, 151, 193]. In this introduction we focus on mechanistic models of cellular metabolism that include detailed models of mitochondria. There are many such models. Among the earliest was a model by Kohn and Garfinkel in 1983 [91] for cardiac muscle cells in rats, which is also a direct source for much of the kinetics in our model. Other kinetic models have been developed independently of the model by Kohn and Garfinkel, including Bohnensack 1981 [16], Magnus and Keizer 1998 [120], Demin et al. 2001 [36], Jin and Bethke 2002 [83], Cortassa et al. 2003 [32], Gauthier et al. 2013 [60], Mulukutla et al. 2015 [126], and Leung et al. 2021 [109]. These models differ in their focus and completeness. Some, such as Magnus and Keizer's [120], do not explicitly represent the TCA cycle. Instead the Magnus and Keizer model focuses on pyruvate dehydrogenase and transporters that they understand to be limiting steps for the process. Several include models of glycolysis, calcium regulation, or other cellular processes [109, 120, 126]. Others restrict their focus to a subset of mitochondrial respiration [16], such as the electron transport chain [60, 83].

If we focus on models that have been the basis of extensive further work, a few stand out. A reconstruction of Kohn and Garfinkel's model [92] was the starting point for Wu et al's more recent model [113, 193] which includes mechanistic modelling of pyruvate oxidation, the TCA cycle, oxidative phosphorylation, and key transporters regulating mitochondrial respiration. That model is the basis for our work. Already in work like Kohn and Garfinkel's

they note a strong dependence of alphaketogluterate dehydrogenase flux on coenzyme A state, a finding comes up in our analysis of our model for renal tissues [90] (see Section 3.3.3). The Wu et al. model adapts the Kohn and Garfinkel model and fits in with the advantage of better computing power, which was not available to Kohn and Garfinkel [193]. The Wu et al. thermodynamic model with major changes was adapted for the lung in Zhang et al. [203, 202]. In that model they include vasculature and several parallel pathways such as the pentose phosphate and glycolysis pathways. The Wu et al. model was also adapted with more minor adjustments by Edwards et al. [44] for the proximal tubule. In Edwards et al. they adjust the kinetics of hydrogen and potassium leakage used in the model to more closely match observed kinetics of hydrogen leak [149]. This change makes the model consistent with other recent models of mitochondrial respiration that are also derived from Wu et al's model [9, 75]. The leak kinetics will be outlined in Section 2. Edwards et al. studies at length the proximal tubule mitochondria's response to diabetic uncoupling, and is the first paper to predict certain oxygen-efficiency measurements of the proximal tubule *in vivo* such as the P/O ratio. In Kohn and Garfinkel [92], and all the subsequent models noted above, biophysical assumptions from thermodynamics are used to describe the kinetics. To further this work, thermodynamic parameters of reactions involved in mitochondrial respiration have been compiled in a database by the Beard group [113]. Other mathematical models of the electron transport chain have used more thoroughly mechanistic models of its dynamics [60].

Magnus and Keizer's model for β cells in the pancreas [120] was the basis for work by Bertram et al. [14], and Saa & Siqueira [151]. Bertram et al. make several simplifications and adjustments inspired by Cortassa et al's more recent model [14, 32]. Among these adjustments are changes to the kinetics of pyruvate dehydrogenase [151]. Saa & Siqueira uses more complete experimental information in order to more carefully introduce steady state assumptions [151]. Saa & Siqueira develop a smaller model of cellular respiration and calcium homeostasis which they can subject to analytical techniques [151]. This family of models provide excellent tools for studying the effects of adding cytosolic calcium. Mulukutla et al's recent model [126] in mammalian cell cultures has formed the basis for novel work by Roy and Finley [150] studying mitochondrial respiration in pancreatic cancer cells. Leung et al's model of a neuron includes comparable equations for the mitochondrion as reaction terms in a larger reaction-diffusion model [109]. Leung et al also includes calcium homeostasis [109].

Due to mitochondrial respiration's importance and the intensive research work on it, it has been the subject of comparatively more modelling analysis than other subcellular processes. The above mathematical models cover a range of physiological subjects and levels of detail most comparable with our work. If we broaden our focus, then there are many other mitochondrial models. The MitoCore model describes the same chemical-kinetic scale at a lower level of detail, using flux balance analysis it aims to reproduce the correct stoichiometry but not kinetics of subcellular mitochondrial processes [170]. Instead of representing the system's kinetics, this model instead only enforces the stoichiometry of mitochondrial reactions. This restriction allows the model to be used in multiscale applications and to more quickly incorporate new reactions & metabolites. On the other hand, if we branch out from simply

considering mitochondrial respiration, there are many other significant mechanistic models, such as models of mitochondrial calcium homeostasis alone [45, 74], population genetics of mitochondria [79, 94], and reaction-diffusion models of mitochondrial metabolites & products in cardiac muscle [146]. While our modelling work is in a central area within the broader modelling of mitochondria, it is only part of a larger picture.

Chapter 2

Exposition of our Model

Our model includes 53 state variables representing concentrations in three compartments, and the electrical potential gradient across the inner membrane of the mitochondrion. We include the full table of state variables (see Table 2.12), a table of adjustable parameters for the cytosol, membrane fluxes, and buffering reactions (see Table 2.13), and a table of physical parameters (see Table 2.14 at the end of this chapter, we characterize less important kinetic parameters in the section with the relevant flux or reaction in a table (for further discussion see the supplementary material to Wu et al. [193], our exposition draws heavily on Wu et al.). Our model includes the process of pyruvate oxidation, the TCA cycle, and oxidative phosphorylation. Aside from this we also include a couple significant reactions in the matrix and cytosol, several transporter activities on the inner membrane of the mitochondrion, and several passive diffusive fluxes across the outer membrane of the mitochondrion. We begin by showing our model from a bird's eye view, with the fluxes and reactions between state variables represented but with the details of the kinetics left out. Then we will dive into the exact kinetics after that. In the work of Wu et al. [193], 35 parameters were estimated. Many more parameters are taken from direct experimental estimates as discussed in the supplementary material to Wu et al [193]. In our model, we include a new enzyme activity, glutamate dehydrogenase. For that enzyme we use experimental estimates for both its activity and Michaelis constant [84]. Since we are considering two novel tissues we identify experimental measurements for several key parameters that are specific to those tissues, and we fit or refit multiple parameters. Each chapter includes a table listing experimental sources for parameters that were changed based on direct measurements. Other parameter changes are discussed in the text itself.

The electrical potential gradient depends on the difference in charges across the inner membrane of the mitochondrion, and drives the activity of ATP synthase. The gradient is determined by the net flux across the inner membrane of the mitochondrion, in our model the net charge across the inner membrane is influenced by the members of the electron transport chain (J_{C1}, J_{C3}, and J_{C4}), hydrogen leak (J_{Hle}), ATP synthase (J_{F1}), and adenosine nucleotide

translocase (J_{ANT}). Notably, while the stoichiometry of all these fluxes are well-understood aside from ATP synthase, where the necessary hydrogen flux is controversial, thus the flux term for ATP synthase has a parameter n_A that determines the stochiometry of the flux. In our model, n_A is three. The electrical potential gradient is reported in millivolts.

$$\frac{d\Delta\Psi}{dt} = \left(+4J_{\mathrm{C1}} + 2J_{\mathrm{C3}} + 4J_{\mathrm{C4}} - n_A J_{\mathrm{F1}} - J_{\mathrm{ANT}} - J_{\mathrm{Hle}} - J_{\mathrm{Kle}} + J_{\mathrm{ASPGLU}}\right)/C_{\mathrm{IM}} \tag{2.1}$$

The proton motive force may be calculated using the electrical potential gradient and the hydrogen ion concentrations in the matrix and intermembrane space as follows:

$$\mathrm{PMF} = \Delta\Psi + \frac{RT\ln(10)}{F}(\log_{10}([\mathrm{H}_i^+]) - \log_{10}([\mathrm{H}_x^+])) \tag{2.2}$$

By far the most important compartment for our model is the mitochondrial matrix. The mitochondrial matrix includes all of the reactions involved in the TCA cycle (J_{acon}, J_{isod}, J_{akgd}, J_{scoas}, J_{sdh}, J_{fum}, J_{mdh}, J_{got}, and J_{cits}) and pyruvate oxidation (J_{pdh}). Aside from these reactions, there are several fluxes that we identify as significant, both the ones related to oxidative phosphorylation mentioned before, several transporters that control the quantities of TCA cycle intermediates within the mitochondrial matrix (J_{PYRH}, J_{MALPI}, J_{SUCPI}, J_{SUCMAL}, J_{AKGMAL}, and J_{CITMAL}), and several other transporters (J_{PIHt}, J_{ANT}, J_{KH}, J_{GLUH}, and J_{ASPGLU}). The concentrations of certain essential compounds are fixed, most notably the oxygen concentration. We consider a range of oxygen concentrations in our work. In what follows, we use the subscript 'x' for matrix concentrations, 'i' for intermembrane space concentrations, and 'c' for cytosolic concentrations.

$$\frac{d[\mathrm{ATP}]_{\mathrm{x}}}{dt} = \left(+J_{\mathrm{ndk}} + J_{\mathrm{F1}} - J_{\mathrm{ANT}}\right)/W_{\mathrm{x}} \tag{2.3}$$

$$\frac{d[\mathrm{ADP}]_{\mathrm{x}}}{dt} = \left(-J_{ndk} - J_{F1} + J_{ANT}\right)/W_{\mathrm{x}} \tag{2.4}$$

$$\frac{d[\mathrm{AMP}]_{\mathrm{x}}}{dt} = 0/W_{\mathrm{x}} \tag{2.5}$$

$$\frac{d[\mathrm{GTP}]_{\mathrm{x}}}{dt} = \left(+J_{\mathrm{scoas}} - J_{\mathrm{ndk}}\right)/W_{\mathrm{x}} \tag{2.6}$$

$$\frac{d[\mathrm{GDP}]_{\mathrm{x}}}{dt} = \left(-J_{\mathrm{scoas}} + J_{\mathrm{ndk}}\right)/W_{\mathrm{x}} \tag{2.7}$$

$$\frac{d[\mathrm{PI}]_{\mathrm{x}}}{dt} = \left(-J_{\mathrm{scoas}} - J_{\mathrm{F1}} + J_{\mathrm{PIHt}} - J_{\mathrm{SUCPI}} - J_{\mathrm{MALPI}}\right)/W_x \tag{2.8}$$

$$\frac{d[\mathrm{NADH}]_{\mathrm{x}}}{dt} = \left(+J_{\mathrm{pdh}} + J_{\mathrm{isod}} + J_{\mathrm{akgd}} + J_{\mathrm{mdh}} - J_{\mathrm{C1}}\right)/W_x \tag{2.9}$$

$$\frac{d[\mathrm{QH_2}]_\mathrm{x}}{dt} = \left(+J_\mathrm{sdh} + J_\mathrm{C1} - J_\mathrm{C3}\right)/W_\mathrm{x} \tag{2.10}$$

$$\frac{d[\mathrm{PYR}]_\mathrm{x}}{dt} = \left(-J_\mathrm{pdh} + J_\mathrm{PYRH}\right)/W_\mathrm{x} \tag{2.11}$$

$$\frac{d[\mathrm{ACCOA}]_\mathrm{x}}{dt} = \left(-J_\mathrm{cits} + J_\mathrm{pdh}\right)/W_\mathrm{x} \tag{2.12}$$

$$\frac{d[\mathrm{CIT}]_\mathrm{x}}{dt} = \left(+J_\mathrm{cits} - J_\mathrm{acon} + J_\mathrm{CITMAL}\right)/W_\mathrm{x} \tag{2.13}$$

$$\frac{d[\mathrm{ICIT}]_\mathrm{x}}{dt} = \left(+J_\mathrm{acon} - J_\mathrm{isod}\right)/W_\mathrm{x} \tag{2.14}$$

$$\frac{d[\mathrm{AKG}]_\mathrm{x}}{dt} = \left(+J_\mathrm{isod} - J_\mathrm{akgd} - J_\mathrm{got} + J_\mathrm{AKGMAL}\right)/W_\mathrm{x} \tag{2.15}$$

$$\frac{d[\mathrm{SCOA}]_\mathrm{x}}{dt} = \left(+J_\mathrm{akgd} - J_\mathrm{scoas}\right)/W_\mathrm{x} \tag{2.16}$$

$$\frac{d[\mathrm{COASH}]_\mathrm{x}}{dt} = \left(-J_\mathrm{pdh} - J_\mathrm{akgd} + J_\mathrm{scoas} + J_\mathrm{cits}\right)/W_\mathrm{x} \tag{2.17}$$

$$\frac{d[\mathrm{SUC}]_\mathrm{x}}{dt} = \left(+J_\mathrm{scoas} - J_\mathrm{sdh} + J_\mathrm{SUCMAL}\right)/W_\mathrm{x} \tag{2.18}$$

$$\frac{d[\mathrm{FUM}]_\mathrm{x}}{dt} = \left(+J_\mathrm{sdh} - J_\mathrm{fum}\right)/W_\mathrm{x} \tag{2.19}$$

$$\frac{d[MAL]_x}{dt} = \left(+J_\mathrm{fum} - J_\mathrm{mdh} + J_\mathrm{MALPI} - J_\mathrm{AKGMAL} - J_\mathrm{CITMAL} - J_\mathrm{SUCMAL}\right)/W_\mathrm{x} \tag{2.20}$$

$$\frac{d[\mathrm{OAA}]_\mathrm{x}}{dt} = \left(-J_\mathrm{cits} + J_\mathrm{mdh} + J_\mathrm{got}\right)/W_\mathrm{x} \tag{2.21}$$

$$\frac{d[\mathrm{GLU}]_\mathrm{x}}{dt} = \left(+J_\mathrm{got} + J_\mathrm{GLUH} - J_\mathrm{ASPGLU}\right)/W_\mathrm{x} \tag{2.22}$$

$$\frac{d[\mathrm{ASP}]_\mathrm{x}}{dt} = \left(-J_\mathrm{got} + J_\mathrm{ASPGLU}\right)/W_\mathrm{x} \tag{2.23}$$

$$\frac{d[\mathrm{O_2}]_\mathrm{x}}{dt} = 0/W_\mathrm{x} \tag{2.24}$$

$$\frac{d[\mathrm{CO_2tot}]_\mathrm{x}}{dt} = 0/W_\mathrm{x} \tag{2.25}$$

For the liver, our model includes the activity of glutamate dehydrogenase (J_gdh), which converts glutamate into alpha-ketogluterate. With this adjustment the model has the following structure:

$$\frac{d[\mathrm{AKG}]_\mathrm{x}}{dt} = \left(+J_\mathrm{isod} - J_\mathrm{akgd} - J_\mathrm{got} + J_\mathrm{AKGMAL} + J_\mathrm{gdh}\right)/W_\mathrm{x} \tag{2.26}$$

$$\frac{d[\mathrm{GLU}]_\mathrm{x}}{dt} = \left(+J_\mathrm{got} + J_\mathrm{GLUH} - J_\mathrm{ASPGLU} - J_\mathrm{gdh}\right)/W_\mathrm{x} \tag{2.27}$$

$$\frac{d[\mathrm{NADH}]_{\mathrm{x}}}{dt} = \left(+J_{\mathrm{pdh}} + J_{\mathrm{isod}} + J_{\mathrm{akgd}} + J_{\mathrm{mdh}} - J_{\mathrm{C1}} + J_{\mathrm{gdh}}\right)/W_x \tag{2.28}$$

The intermembrane space connects the mitochondrial matrix and the cytosol (or for isolated mitochondria, the surrounding compartment). The inner membrane is relatively impermeable, relying on several transporters to maintain the flux of solutes between the matrix and the intermembrane space (transporters and oxidative phosphorylation complexes mentioned previously). On the other hand, the outer membrane is highly permeable, and so the intermembrane space & cytosol are coupled by passive diffusion in multiple solutes (J_{ATP}, J_{ADP}, J_{AMPt}, J_{PIt}, J_{PYRt}, J_{CITt}, J_{ICITt}, J_{AKGt}, J_{SUCt}, J_{MALt}, J_{GLUt}, and J_{ASPt}). These two connections give us the following equations:

$$\frac{d[\mathrm{Cred}]_{\mathrm{i}}}{dt} = \left(+2J_{\mathrm{C3}} - 2J_{\mathrm{C4}}\right)/W_{\mathrm{i}} \tag{2.29}$$
$$\frac{d[\mathrm{ATP}]_{\mathrm{i}}}{dt} = \left(+J_{\mathrm{ATP}} + J_{\mathrm{ANT}} + J_{\mathrm{AKi}}\right)/W_{\mathrm{i}} \tag{2.30}$$
$$\frac{d[\mathrm{ADP}]_{\mathrm{i}}}{dt} = \left(+J_{\mathrm{ADP}} - J_{\mathrm{ANT}} - 2J_{\mathrm{AKi}}\right)/W_{\mathrm{i}} \tag{2.31}$$
$$\frac{d[\mathrm{AMP}]_{\mathrm{i}}}{dt} = \left(J_{\mathrm{AMPt}} + J_{\mathrm{AKi}}\right)/W_{\mathrm{i}} \tag{2.32}$$
$$\frac{d[\mathrm{PI}]_{\mathrm{i}}}{dt} = \left(-J_{\mathrm{PIHt}} + J_{\mathrm{PIt}} + J_{\mathrm{MALPI}}\right)/W_{\mathrm{i}} \tag{2.33}$$
$$\frac{d[\mathrm{PYR}]_{\mathrm{i}}}{dt} = \left(-J_{\mathrm{PYRH}} + J_{\mathrm{PYRt}}\right)/W_{\mathrm{i}} \tag{2.34}$$
$$\frac{d[\mathrm{CIT}]_{\mathrm{i}}}{dt} = \left(-J_{\mathrm{CITMAL}} + J_{\mathrm{CITt}}\right)/W_{\mathrm{i}} \tag{2.35}$$
$$\frac{d[\mathrm{ICIT}]_{\mathrm{i}}}{dt} = \left(-J_{\mathrm{ICITMAL}} + J_{\mathrm{ICITt}}\right)/W_{\mathrm{i}} \tag{2.36}$$
$$\frac{d[AKG]_{i}}{dt} = \left(-J_{\mathrm{AKGMAL}} + J_{\mathrm{AKGt}}\right)/W_{\mathrm{i}} \tag{2.37}$$
$$\frac{d[\mathrm{SUC}]_{\mathrm{i}}}{dt} = \left(+J_{\mathrm{SUCt}} - J_{\mathrm{SUCMAL}}\right)/W_{\mathrm{i}} \tag{2.38}$$
$$\frac{d[\mathrm{FUM}]_{\mathrm{i}}}{dt} = 0/W_{\mathrm{i}} \tag{2.39}$$
$$\frac{d[\mathrm{MAL}]_{\mathrm{i}}}{dt} = \left(-J_{\mathrm{MALPI}} + J_{\mathrm{MALt}} + J_{\mathrm{AKGMAL}} + J_{\mathrm{CITMAL}} + J_{\mathrm{SUCMAL}}\right)/W_{\mathrm{i}} \tag{2.40}$$
$$\frac{d[\mathrm{GLU}]_{\mathrm{i}}}{dt} = \left(-J_{\mathrm{GLUH}} + J_{\mathrm{ASPGLU}} + J_{\mathrm{GLUt}}\right)/W_{\mathrm{i}} \tag{2.41}$$
$$\frac{d[\mathrm{ASP}]_{\mathrm{i}}}{dt} = \left(-J_{\mathrm{ASPGLU}} + J_{\mathrm{ASPt}}\right)/W_{\mathrm{i}} \tag{2.42}$$

Our model covers two cases, in the first case, the outer compartment is the external space

in which the isolated mitochondria are found. This case is important for several experimental frameworks used for measuring the P/O ratio, oxygen consumption, and hydrogen leak:

$$\frac{d[ATP]_c}{dt} = -J_{ATPt}/W_c \tag{2.43}$$
$$\frac{d[ADP]_c}{dt} = -J_{ADPt}/W_c \tag{2.44}$$
$$\frac{d[\mathrm{AMP}]_\mathrm{c}}{dt} = 0/W_\mathrm{c} \tag{2.45}$$
$$\frac{d[\mathrm{PI}]_\mathrm{c}}{dt} = -J_{\mathrm{PIt}}/W_\mathrm{c} \tag{2.46}$$
$$\frac{d[\mathrm{PYR}]_\mathrm{c}}{dt} = -J_{\mathrm{PYRt}}/W_\mathrm{c} \tag{2.47}$$
$$\frac{d[\mathrm{CIT}]_\mathrm{c}}{dt} = -J_{\mathrm{CITt}}/W_\mathrm{c} \tag{2.48}$$
$$\frac{d[\mathrm{ICIT}]_\mathrm{c}}{dt} = -J_{\mathrm{ICITt}}/W_\mathrm{c} \tag{2.49}$$
$$\frac{d[\mathrm{AKG}]_\mathrm{c}}{dt} = -J_{\mathrm{AKGt}}/W_\mathrm{c} \tag{2.50}$$
$$\frac{d[\mathrm{SUC}]_\mathrm{c}}{dt} = -J_{\mathrm{SUCt}}/W_\mathrm{c} \tag{2.51}$$
$$\frac{d[\mathrm{FUM}]_\mathrm{c}}{dt} = 0/W_\mathrm{c} \tag{2.52}$$
$$\frac{d[\mathrm{MAL}]_\mathrm{c}}{dt} = -J_{\mathrm{MALt}}/W_\mathrm{c} \tag{2.53}$$
$$\frac{d[\mathrm{GLU}]_\mathrm{c}}{dt} = -J_{\mathrm{GLUt}}/W_\mathrm{c} \tag{2.54}$$
$$\frac{d[\mathrm{ASP}]_\mathrm{c}}{dt} = -J_{\mathrm{ASPt}}/W_\mathrm{c} \tag{2.55}$$
$$\frac{d[\mathrm{PCr}]_\mathrm{c}}{dt} = 0/W_\mathrm{c} \tag{2.56}$$

If the external space is the cytoplasm, then the system is forced to remain at its non-equilibrium steady state by clamping the concentration of pyruvate in the cytoplasm. This ensures that the mitochondrion will not exhaust its supply of pyruvate and that it will continue to produce ATP. Otherwise most compounds are determined by the diffusion across the outer mitochondrial membrane. The exceptions to this were the ATP consumption (J_{AtC}), in addition, ADP may phosphorylate ADP, producing ATP and AMP (J_{AKe}), and the creatine kinase reaction which consumes creatine and ADP to produce ATP and hydrogen ions (J_{CKe}).

$$\frac{d[\mathrm{ATP}]_\mathrm{c}}{dt} = \left(-\frac{V_\mathrm{cyto}}{V_\mathrm{mito}} J_\mathrm{ATPt} - Q_\mathrm{ATP} + J_\mathrm{CKe} + J_\mathrm{AKe}\right)/W_\mathrm{c} \tag{2.57}$$

$$\frac{d[\mathrm{ADP}]_\mathrm{c}}{dt} = \left(-\frac{V_\mathrm{cyto}}{V_\mathrm{mito}} J_\mathrm{ADPt} + Q_\mathrm{ATP} - J_\mathrm{CKe} - 2J_\mathrm{AKe}\right)/W_\mathrm{c} \tag{2.58}$$

$$\frac{d[\mathrm{AMP}]_\mathrm{c}}{dt} = \left(-\frac{V_\mathrm{cyto}}{V_\mathrm{mito}} J_\mathrm{AMPt} + J_\mathrm{AKc}\right)/W_\mathrm{c} \tag{2.59}$$

$$\frac{d[\mathrm{PI}]_\mathrm{c}}{dt} = \left(-\frac{V_\mathrm{cyto}}{V_\mathrm{mito}} J_\mathrm{PIt} + J_\mathrm{AKc}\right)/W_\mathrm{c} \tag{2.60}$$

$$\frac{d[\mathrm{PYR}]_\mathrm{c}}{dt} = 0/W_\mathrm{c} \tag{2.61}$$

$$\frac{d[\mathrm{CIT}]_\mathrm{c}}{dt} = -\frac{V_\mathrm{cyto}}{V_\mathrm{mito}} J_\mathrm{CITt}/W_\mathrm{c} \tag{2.62}$$

$$\frac{d[\mathrm{AKG}]_\mathrm{c}}{dt} = -\frac{V_\mathrm{cyto}}{V_\mathrm{mito}} J_\mathrm{AKGt}/W_\mathrm{c} \tag{2.63}$$

$$\frac{d[\mathrm{SUC}]_\mathrm{c}}{dt} = -\frac{V_\mathrm{cyto}}{V_\mathrm{mito}} J_\mathrm{SUCt}/W_\mathrm{c} \tag{2.64}$$

$$\frac{d[\mathrm{FUM}]_\mathrm{c}}{dt} = 0/W_\mathrm{c} \tag{2.65}$$

$$\frac{d[\mathrm{MAL}]_\mathrm{c}}{dt} = -\frac{V_\mathrm{cyto}}{V_\mathrm{mito}} J_\mathrm{MALt}/W_\mathrm{c} \tag{2.66}$$

$$\frac{d[\mathrm{GLU}]_\mathrm{c}}{dt} = -\frac{V_\mathrm{cyto}}{V_\mathrm{mito}} J_\mathrm{GLUt}/W_\mathrm{c} \tag{2.67}$$

$$\frac{d[\mathrm{ASP}]_\mathrm{c}}{dt} = -\frac{V_\mathrm{cyto}}{V_\mathrm{mito}} J_\mathrm{ASPt}/W_\mathrm{c} \tag{2.68}$$

$$\frac{d[\mathrm{PCr}]_\mathrm{c}}{dt} = -J_\mathrm{CKe}/W_\mathrm{c}. \tag{2.69}$$

Some quantities were calculated explicitly from the above differential equations, assuming that the sum of two concentrations were conserved. This required us to find the pooled concentration of NAD^+ and NADH, of ubiquinone (oxidized coenzyme Q) and ubiquinol (reduced coenzyme Q), and Cytochrome C in both its reduced & oxidized forms. This gives us the following additional equations:

$$[\mathrm{NAD}^+]_\mathrm{x} = \mathrm{NAD}_\mathrm{tot} - [\mathrm{NADH}]_\mathrm{x} \tag{2.70}$$

$$[\mathrm{COQ}]_\mathrm{x} = \mathrm{Q}_\mathrm{tot} - [\mathrm{QH}_2]_\mathrm{x} \tag{2.71}$$

$$[\mathrm{Cox}]_\mathrm{i} = \mathrm{cytC}_\mathrm{tot} - [\mathrm{Cred}]_\mathrm{i} \tag{2.72}$$

So far we have ignored the ion concentrations of hydrogen, magnesium, and potassium. These ion concentrations are fixed in the intermembrane space and cytosol. In the mitochondrial matrix these quantities are not fixed. Their kinetics are complex because there are binding sites that the ions compete for and the mitochondrial matrix is buffered. Here we provide the equations describing their kinetics, and several quantities to simplify the equations. This model is derived in Beard and Qian [10] in the chapter "Biochemical Reaction Networks". Starting with the big picture, we have the following expressions for the derivatives of the ion concentrations, whose terms we will write out explicitly below:

$$\begin{aligned}\frac{d\left[\mathrm{H}^{+}\right]_{\mathrm{x}}}{dt} &= \left[\left(\frac{\partial\left[\mathrm{K}_{\mathrm{bound}}\right]}{\partial\left[\mathrm{Mg}^{2+}\right]}\cdot\frac{\partial\left[\mathrm{Mg}_{\mathrm{bound}}\right]}{\partial\left[\mathrm{K}^{+}\right]}-\alpha_{Mg}\alpha_{K}\right)\Phi^{H}\right. \\ &+\left(\alpha_{K}\frac{\partial\left[\mathrm{H}_{\mathrm{bound}}\right]}{\partial\left[\mathrm{Mg}^{2+}\right]}-\frac{\partial\left[\mathrm{H}_{\mathrm{bound}}\right]}{\partial\left[\mathrm{K}^{+}\right]}\cdot\frac{\partial\left[\mathrm{K}_{\mathrm{bound}}\right]}{\partial\left[\mathrm{Mg}^{2+}\right]}\right)\Phi^{Mg} \\ &\left.+\left(\alpha_{Mg}\frac{\partial\left[\mathrm{H}_{\mathrm{bound}}\right]}{\partial\left[\mathrm{K}^{+}\right]}-\frac{\partial\left[\mathrm{H}_{\mathrm{bound}}\right]}{\partial\left[\mathrm{Mg}^{2+}\right]}\cdot\frac{\partial\left[\mathrm{Mg}_{\mathrm{bound}}\right]}{\partial\left[\mathrm{K}^{+}\right]}\right)\Phi^{K}\right]/D \end{aligned} \tag{2.73}$$

$$\begin{aligned}\frac{d\left[\mathrm{Mg}^{2+}\right]_{\mathrm{x}}}{dt} &= \left[\left(\alpha_{K}\frac{\partial\left[\mathrm{Mg}_{\mathrm{bound}}\right]}{\partial\left[\mathrm{H}^{+}\right]}-\frac{\partial\left[\mathrm{K}_{\mathrm{bound}}\right]}{\partial\left[\mathrm{H}^{+}\right]}\cdot\frac{\partial\left[\mathrm{Mg}_{\mathrm{bound}}\right]}{\partial\left[\mathrm{K}^{+}\right]}\right)\Phi^{H}\right. \\ &+\left(\alpha_{H}\frac{\partial\left[\mathrm{K}_{\mathrm{bound}}\right]}{\partial\left[\mathrm{Mg}^{2+}\right]}-\frac{\partial\left[\mathrm{K}_{\mathrm{bound}}\right]}{\partial\left[\mathrm{H}^{+}\right]}\cdot\frac{\partial\left[\mathrm{H}_{\mathrm{bound}}\right]}{\partial\left[\mathrm{Mg}^{2+}\right]}\right)\Phi^{Mg} \\ &\left.+\left(\frac{\partial\left[\mathrm{Mg}_{\mathrm{bound}}\right]}{\partial\left[\mathrm{H}^{+}\right]}\cdot\frac{\partial\left[\mathrm{H}_{\mathrm{bound}}\right]}{\partial\left[\mathrm{Mg}^{2+}\right]}-\alpha_{H}\alpha_{Mg}\right)\Phi^{K}\right]/D \end{aligned} \tag{2.74}$$

$$\begin{aligned}\frac{d\left[\ \mathrm{K}^{+}\right]_{\mathrm{x}}}{dt} &= \left[\left(\alpha_{Mg}\frac{\partial\left[\mathrm{K}_{\mathrm{bound}}\right]}{\partial\left[\mathrm{H}^{+}\right]}-\frac{\partial\left[\mathrm{K}_{\mathrm{bound}}\right]}{\partial\left[\mathrm{Mg}^{2+}\right]}\cdot\frac{\partial\left[\mathrm{Mg}_{\mathrm{bound}}\right]}{\partial\left[\mathrm{H}^{+}\right]}\right)\Phi^{H}\right. \\ &+\left(\alpha_{H}\frac{\partial\left[\mathrm{K}_{\mathrm{bound}}\right]}{\partial\left[\mathrm{Mg}^{2+}\right]}-\frac{\partial\left[\mathrm{K}_{\mathrm{bound}}\right]}{\partial\left[\mathrm{H}^{+}\right]}\cdot\frac{\partial\left[\mathrm{H}_{\mathrm{bound}}\right]}{\partial\left[\mathrm{Mg}^{2+}\right]}\right)\Phi^{Mg} \\ &\left.+\left(\frac{\partial\left[\mathrm{Mg}_{\mathrm{bound}}\right]}{\partial\left[\mathrm{H}^{+}\right]}\cdot\frac{\partial\left[\mathrm{H}_{\mathrm{bound}}\right]}{\partial\left[\mathrm{Mg}^{2+}\right]}-\alpha_{H}\alpha_{Mg}\right)\Phi^{K}\right]/D \end{aligned} \tag{2.75}$$

We'll start by unpacking the expressions that are not partial derivatives. These include the denominator, the expressions connecting the binding to the cross-membrane fluxes of the model (Φ^{H}, Φ^{Mg}, and Φ^{K}), and the buffer terms (α_{H}, α_{Mg}, and α_{K}). In what follows, $\mathrm{L_i}$ under a summation refers to a generic reactant with hydrogen or the two metal ions considered, the full list of such reactants includes ATP, ADP, AMP, GTP, phosphate, NADH/NAD^{+}, coenzyme Q, oxaloacetate, acetyl-CoA, citrate, isocitrate, alphaketogluterate, succinyl-CoA, coenzyme A, succinate, fumerate, malate, glutamate, aspartate, cytochrome C, oxygen, water, $\mathrm{FADH_2}$/FAD^{2+}, carbon dioxide, phosphocreatinine, creatinine, pyruvate, glucose, and

glucose-6-phosphate. These reactants will also appear in the partial derivative expressions below.

$$
\begin{aligned}
D =& \alpha_H \frac{\partial\left[\mathrm{K_{bound}}\right]}{\partial\left[\mathrm{Mg^{2+}}\right]} \cdot \frac{\partial\left[\mathrm{Mg_{bound}}\right]}{\partial\left[\mathrm{K^{+}}\right]} + \alpha_K \frac{\partial\left[\mathrm{H_{bound}}\right]}{\partial\left[\mathrm{Mg^{2+}}\right]} \cdot \frac{\partial\left[\mathrm{Mg_{bound}}\right]}{\partial\left[\mathrm{H^{+}}\right]} \\
&+ \alpha_{Mg} \frac{\partial\left[\mathrm{H_{bound}}\right]}{\partial\left[\mathrm{K^{+}}\right]} \cdot \frac{\partial\left[\mathrm{K_{bound}}\right]}{\partial\left[\mathrm{H^{+}}\right]} - \alpha_{Mg}\alpha_K\alpha_H \\
&- \frac{\partial\left[\mathrm{H_{bound}}\right]}{\partial\left[\mathrm{K^{+}}\right]} \cdot \frac{\partial\left[\mathrm{K_{bound}}\right]}{\partial\left[\mathrm{Mg^{2+}}\right]} \cdot \frac{\partial\left[\mathrm{Mg_{bound}}\right]}{\partial\left[\mathrm{H^{+}}\right]} \\
&- \frac{\partial\left[\mathrm{H_{bound}}\right]}{\partial\left[\mathrm{Mg^{2+}}\right]} \cdot \frac{\partial\left[\mathrm{Mg_{bound}}\right]}{\partial\left[\mathrm{K^{+}}\right]} \cdot \frac{\partial\left[\mathrm{K_{bound}}\right]}{\partial\left[\mathrm{H^{+}}\right]}
\end{aligned} \tag{2.76}
$$

$$
\alpha_H = 1 + \frac{\partial\left[\mathrm{H_{bound}}\right]}{\partial\left[\mathrm{H^{+}}\right]} + \frac{B_x}{K_{Bx}\left(1 + \left[\mathrm{H^{+}}\right]/K_{Bx}\right)^2} \tag{2.77}
$$

$$
\alpha_{Mg} = 1 + \frac{\partial\left[\mathrm{Mg_{bound}}\right]}{\partial\left[\mathrm{Mg^{2+}}\right]}, \tag{2.78}
$$

$$
\alpha_K = 1 + \frac{\partial\left[\mathrm{K_{bound}}\right]}{\partial\left[\mathrm{K^{+}}\right]} \tag{2.79}
$$

$$
\Phi^H = -\sum_{i=1}^{N_r} \frac{\partial\left[\mathrm{H_{bound}}\right]}{\partial\left[\mathrm{L}_i\right]} \frac{d\left[\mathrm{\ L}_i\right]}{dt} + \sum_{k=1}^{N_f} n_k J_k + J_t^H, \tag{2.80}
$$

$$
\Phi^{Mg} = -\sum_{i=1}^{N_r} \frac{\partial\left[\mathrm{Mg_{bound}}\right]}{\partial\left[\mathrm{L}_i\right]} \frac{d\left[\mathrm{\ L}_i\right]}{dt} + J_t^{Mg} \tag{2.81}
$$

$$
\Phi^K = -\sum_{i=1}^{N_r} \frac{\partial\left[\mathrm{K_{bound}}\right]}{\partial\left[\mathrm{L}_i\right]} \frac{d\left[\mathrm{\ L}_i\right]}{dt} + J_t^K \tag{2.82}
$$

$$
\sum_{k=1}^{N_f} n_k J_k = \left(-J_{\mathrm{pdh}} + 2J_{\mathrm{dits}} - J_{\mathrm{akgd}} + J_{\mathrm{scoas}} + J_{\mathrm{mdh}}\right)/W_{\mathrm{x}}, \tag{2.83}
$$

$$
\begin{aligned}
J_t^H =& \left(J_{\mathrm{PYRH}} + J_{\mathrm{GLUH}} + J_{\mathrm{CTTMAL}} - J_{\mathrm{ASPGLU}} - 5J_{\mathrm{C1}} - 2J_{\mathrm{C3}} - 4J_{\mathrm{C4}} + \left(n_A - 1\right) J_{\mathrm{F1}}\right. \\
&\left. + 2J_{\mathrm{PHt}} + J_{\mathrm{Hle}} - J_{\mathrm{KH}}\right)/W_{\mathrm{x}}
\end{aligned} \tag{2.84}
$$

$$
J_t^{Mg} = 0 \tag{2.85}
$$

$$
J_t^K = J_{\mathrm{KH}}/W_{\mathrm{x}} \tag{2.86}
$$

The remaining terms to define are partial derivatives of bound ions relative to the free concentration of each of the other above ions. These establish the extent to which an increase in the concentration of one ion will impact the binding opportunities for another ion.

$$\frac{\partial\left[\mathrm{H_{bound}}\right]}{\partial\left[\mathrm{Mg^{2+}}\right]} = -\sum_{i=1}^{N_r} \frac{\left[\mathrm{L}_i\right]\left[\mathrm{H^+}\right]/K_i^H}{K_i^{Mg}\left(P_i\left(\left[\mathrm{H^+}\right],\left[\mathrm{Mg^{2+}}\right],\left[\mathrm{K^+}\right]\right)\right)^2} \tag{2.87}$$

$$\frac{\partial\left[\mathrm{H_{bound}}\right]}{\partial\left[\mathrm{K^+}\right]} = -\sum_{i=1}^{N_r} \frac{\left[\mathrm{L}_i\right]\left[\mathrm{H^+}\right]/K_i^H}{K_i^{K}\left(P_i\left(\left[\mathrm{H^+}\right],\left[\mathrm{Mg^{2+}}\right],\left[\mathrm{K^+}\right]\right)\right)^2} \tag{2.88}$$

$$\frac{\partial\left[\mathrm{H_{bound}}\right]}{\partial\left[\mathrm{H^+}\right]} = \sum_{i=1}^{N_r} \frac{\left[\mathrm{L}_i\right]\left(1+\left[\mathrm{Mg^{2+}}\right]/K_i^{Mg}+\left[\mathrm{K^+}\right]/K_i^{K}\right)}{K_i^{H}\left(P_i\left(\left[\mathrm{H^+}\right],\left[\mathrm{Mg^{2+}}\right],\left[\mathrm{K^+}\right]\right)\right)^2}, \tag{2.89}$$

$$\frac{\partial\left[\mathrm{Mg_{bound}}\right]}{\partial\left[\mathrm{H^+}\right]} = -\sum_{i=1}^{N_r} \frac{\left[\mathrm{L}_i\right]\left[\mathrm{Mg^{2+}}\right]/K_i^{Mg}}{K_i^{H}\left(P_i\left[\left[\mathrm{H^+}\right],\left[\mathrm{Mg^{2+}}\right],\left[\mathrm{K^+}\right]\right)\right)^2}, \tag{2.90}$$

$$\frac{\partial\left[\mathrm{Mg_{bound}}\right]}{\partial\left[\mathrm{K^+}\right]} = -\sum_{i=1}^{N_r} \frac{\left[\mathrm{L}_i\right]\left[\mathrm{Mg^{2+}}\right]/K_i^{\mathrm{Mg}}}{K_i^{K}\left(P_i\left(\left[\mathrm{H^+}\right],\left[\mathrm{Mg^{2+}}\right],\left[\mathrm{K^+}\right]\right)\right)^2}, \tag{2.91}$$

$$\frac{\partial\left[\mathrm{Mg_{bound}}\right]}{\partial\left[\mathrm{Mg^{2+}}\right]} = \sum_{i=1}^{N_r} \frac{\left[\mathrm{L}_i\right]\left(1+\left[\mathrm{H^+}\right]/K_i^{H}+\left[\mathrm{K^+}\right]/K_i^{K}\right)}{K_i^{Mg}\left(P_i\left(\left[\mathrm{H^+}\right],\left[\mathrm{Mg^{2+}}\right],\left[\mathrm{K^+}\right]\right)\right)^2}, \tag{2.92}$$

$$\frac{\partial\left[\mathrm{K_{bound}}\right]}{\partial\left[\mathrm{H^+}\right]} = -\sum_{i=1}^{N_r} \frac{\left[\mathrm{L}_i\right]\left[\mathrm{K^+}\right]/K_i^{K}}{K_i^{H}\left(P_i\left(\left[\mathrm{H^+}\right],\left[\mathrm{Mg^{2+}}\right],\left[\mathrm{K^+}\right]\right)\right)^2}, \tag{2.93}$$

$$\frac{\partial\left[\mathrm{K_{bound}}\right]}{\partial\left[\mathrm{Mg^{2+}}\right]} = -\sum_{i=1}^{N_r} \frac{\left[\mathrm{L}_i\right]\left[\mathrm{K^+}\right]/K_i^{K}}{K_i^{Mg}\left(P_i\left(\left[\mathrm{H^+}\right],\left[\mathrm{Mg^{2+}}\right],\left[\mathrm{K^+}\right]\right)\right)^2} \tag{2.94}$$

$$\frac{\partial\left[\mathrm{K_{bound}}\right]}{\partial\left[\mathrm{K^+}\right]} = \sum_{i=1}^{N_r} \frac{\left[\mathrm{L}_i\right]\left(1+\left[\mathrm{H^+}\right]/K_i^{H}+\left[\mathrm{Mg^{2+}}\right]/K_i^{Mg}\right)}{K_i^{K}\left(P_i\left(\left[\mathrm{H^+}\right],\left[\mathrm{Mg^{2+}}\right],\left[\mathrm{K^+}\right]\right)\right)^2} \tag{2.95}$$

where $P_i\left(\left[\mathrm{H^+}\right],\left[\mathrm{Mg^{2+}}\right],\left[\mathrm{K^+}\right]\right)$ is the reaction polynomial which may be expressed as follows:

$$P_i\left(\left[\mathrm{H^+}\right],\left[\mathrm{Mg^{2+}}\right],\left[\mathrm{K^+}\right]\right) = 1+\frac{[H^+]}{K_i^H}+\frac{[Mg^{2+}]}{K_i^{Mg}}+\frac{[K^+]}{K_i^K} \tag{2.96}$$

The complexity of ion binding is due to the many charged particles in the mitochondrial matrix to which these metal ions and protons may bind, and the complex buffering of ions in the cell.

Parameter	Model Value (μM)
K_{mA}	38.3
K_{mB}	9.9
K_{mC}	60.7
K_{iNADH}	40.2
K_{iACCOA}	40.0

Table 2.1: Kinetic parameters for pyruvate dehydrogenase.

2.1 Matrix Reactions

In this section we deal with reactions happening in the mitochondrial matrix, the majority of these reactions are directly related to the TCA cycle or pyruvate oxidation. Both biochemical pathways are subject to significant regulatory complexities, we will point it out where it occurs and where it is important we will indicate where the kinetics of the enzymes involved are discussed more at-length.

Pyruvate in the mitochondrial matrix is consumed by pyruvate dehydrogenase alongside coenzyme A and NAD^+ to produce acetyl-CoA, NADH, and carbon dioxide. Pyruvate dehydrogenase may be phosphorylated by pyruvate dehydrogenase kinase, inhibiting pyruvate dehydrogenase. Pyruvate dehydrogenase kinase itself is activated by NADH and acetyl-CoA, and thus pyruvate dehydrogenase activity is inhibited by both. The kinetics of pyruvate dehydrogenase are as follows:

$$J_{\text{pdh}} = \frac{V_{mf}\left(1 - \frac{1}{K_{eq,\text{pdh}}}\frac{[\text{CO}_2]_\text{x}[\text{ACCOA}]_\text{x}[\text{NADH}]_\text{x}}{[\text{PYR}]_\text{x}[\text{COASH}]_\text{x}[\text{NAD}]_\text{x}}\right)}{K_{mC}\alpha_{i2}[\text{PYR}]_\text{x}[\text{COASH}]_\text{x} + K_{mB}\alpha_{i1}[\text{PYR}]_\text{x}[\text{NAD}]_\text{x} + K_{mA}[\text{COASH}]_\text{x}[\text{NAD}]_\text{x} + [\text{PYR}]_\text{x}[\text{COASH}]_\text{x}[\text{NAD}]_\text{x}} \tag{2.97}$$

The inhibition is represented in the terms α_{i1} and α_{i2}, which are as follows:

$$\alpha_{i1} = 1 + \frac{[\text{ACCOA}]_\text{x}}{K_{i\text{ACCOA}}} \tag{2.98}$$

$$\alpha_{i2} = 1 + \frac{[\text{NADH}]_\text{x}}{K_{i\text{NADH}}} \tag{2.99}$$

Pyruvate dehydrogenase kinetics are described at length in Cox & Nelson [33], and the reaction mechanism used to arrive at these kinetics are found in the appendix of Wu et al [193]. The parameters for J_{pdh} are summarized in Table 2.1. The form of the equilibrium constant here and below are discussed in the supplementary material for Wu et al. [193].

Acetyl-CoA produced by pyruvate dehydrogenase is consumed by citrate synthase along with oxaloacetate to produce citrate. Citrate synthase is also subject to complex regulation, including competitive inhibition by unchelated citrate of the oxaloacetate binding site,

Parameter	Model Value (μM)
K_{mA}	4
K_{mB}	14
K_{ia}	3.33
K_{iCIT}	1600
K_{iATP}	900
K_{iADP}	1800
K_{iAMP}	6000
K_{iCOASH}	67
K_{iSCOA}	140

Table 2.2: Kinetic parameters for citrate synthase.

and uncompetitive inhibition by unchelated adenine nucleotides, unchelated coenzyme A, unchelated acetyl-CoA, and unchelated succinyl-CoA against the enzyme-acetyl-CoA complex, this gives us:

$$J_{\text{cits}} = \frac{V_{mf}\left([\text{OAA}]_x[\text{ACCOA}]_x - \frac{[\text{COASH}]_x[\text{CIT}]_x}{K_{eq,\text{cits}}}\right)}{K_{ia}K_{mB}\alpha_{i1} + K_{mA}\alpha_{i1}[\text{ACCOA}]_x + K_{mB}\alpha_{i2}[\text{OAA}]_x + [\text{OAA}]_x[\text{ACCOA}]_x} \tag{2.100}$$

where α_{i1} and α_{i2} are as follows:

$$\alpha_{i1} = 1 + \frac{[\text{uCIT}]_x}{K_{i\text{CIT}}} \tag{2.101}$$

$$\alpha_{i2} = 1 + \frac{[\text{uATP}]_x}{K_{i\text{ATP}}} + \frac{[\text{uADP}]_x}{K_{i\text{ADP}}} + \frac{[\text{uAMP}]_x}{K_{i\text{AMP}}} + \frac{[\text{uCOASH}]_x}{K_{i\text{COASH}}} + \frac{[\text{uSCOA}]_x}{K_{i\text{SCOA}}} \tag{2.102}$$

Here the prefix indicates that the compounds are unchelated. The mechanism underlying this model of citrate synthase is a mechanism described by Wu et al [193]. We give a list of parameters in Table 2.2.

Acontinase converts citrate to isocitrate, and has a simple reaction mechanism. Naturally, its kinetics reflect this simplicity. It may be expressed as follows:

$$J_{\text{acon}} = \frac{V_{mf}V_{mr}\left([\text{CIT}]_x - \frac{[\text{ICIT}]_x}{K_{eq,\text{acon}}}\right)}{K_{mA}V_{mr} + V_{mr}[\text{CIT}]_x + \frac{V_{mf}}{K_{eq,\ \text{acon}}}[\text{ICIT}]_x} \tag{2.103}$$

The parameters are catalogued in Table 2.3. V_{mr} may be calculated as $V_{mf}K_{mA}K_{mP}^{-1}K_{eq,acon}^{-1}$.

Isocitrate is then converted by isocitrate dehydrogenase to alpha-ketogluterate. In the process NAD^+ is reduced to NADH, and carbon dioxide is produced. Free ATP acts as an allosteric inhibitor and free ADP may bind to the same site to prevent ATP-dependent

Parameter	Model Value (μM)
K_{mA}	1161
K_{mP}	434

Table 2.3: Kinetic parameters for acontinase.

Parameter	Model Value (μM)
K_{mA}	74
K_{mB}	183
n_H	3 (unitless)
K_{ib}	23.8
K_{iq}	29
K_{iATP}	91
K_{aADP}	50

Table 2.4: Kinetic parameters for isocitrate dehydrogenase.

inhibition (below we denote free ATP/ADP with a prefix f). NADH also competes for the binding site of NAD^+. The reaction mechanism is discussed in the appendix of Wu et al. [193], and the regulation of the reaction is discussed at length in Kohn and Garfinkel [91]. Altogether we get the following expression for the flux via isocitrate dehydrogenase:

$$J_{\text{isod}} = \frac{V_{mf}\left(1 - \frac{1}{K_{eq,\text{isod}}}\frac{[\text{AKG}]_x[\text{NADH}]_x[\text{CO}_2]_x}{[\text{NAD}]_x[\text{ICIT}]_x}\right)}{1 + \left(\frac{K_{mB}}{[\text{ICIT}]_x}\right)^{n_H}\alpha_i + \frac{K_{mA}}{[\text{NAD}]_x}\left(1 + \left(\frac{K_{ib}}{[\text{ICIT}]_x}\right)^{n_H}\alpha_i + \frac{[\text{NADH}]_x}{K_{iq}}\alpha_i\right)} \tag{2.104}$$

For the unitless exponent n_H, we use the value 3 like in Wu et al [193]. Where the regulatory term α_i may be expressed as follows:

$$\alpha_i = 1 + \frac{K_{a,\text{ADP}}}{[\text{fADP}]_x}\frac{[\text{fATP}]_x}{K_{i\text{ATP}}} \tag{2.105}$$

The kinetic parameters included are listed in Table 2.4.

Alpha-ketogluterate is used and produced by multiple reactions including the above reaction, in our exposition we will first introduce how it may be consumed to continue the TCA cycle. However we will return to alpha-ketogluterate again. Alpha-ketogluterate dehydrogenase consumes alpha-ketogluterate and continues the progression of intermediates through the TCA cycle. The reaction mechanism is discussed in the appendix of Wu et al. [193], and the inhibition-activation by adenine nucleotides is discussed by Kohn and Garfinkel [91]. The kinetics may be expressed as follows:

$$J_{\text{akgd}} = \frac{V_{mf}\left(1 - \frac{1}{K_{eq,\text{akgd}}}\frac{[\text{CO}_2]_x[\text{SCOA}]_x[\text{NADH}]_x}{[\text{AKG}]_x[\text{COASH}]_x[\text{NAD}]_x}\right)}{\left(1 + \frac{K_{mA}}{[\text{AKG}]_x}\alpha_i + \frac{K_{mB}}{[\text{COASH}]_x}\left(1 + \frac{[\text{SCOA}]_x}{K_{iq}}\right) + \frac{K_{mC}}{[\text{NAD}]_x}\left(1 + \frac{[\text{NADH}]_x}{K_{ir}}\right)\right)} \tag{2.106}$$

Parameter	Model Value (μM)
K_{mA}	80
K_{mB}	55
K_{mC}	21
K_{iq}	6.9
K_{ir}	0.6
K_{iATP}	50
K_{aADP}	100

Table 2.5: Kinetic parameters for alphaketogluterate dehydrogenase.

Where the regulatory term α_1 may be expressed as follows:

$$\alpha_i = 1 + \frac{K_{a,\mathrm{ADP}}}{[\mathrm{fADP}]_\mathrm{x}} \frac{[\mathrm{fATP}]_\mathrm{x}}{K_{i\mathrm{ATP}}} \tag{2.107}$$

The kinetic parameters included are listed in Table 2.5.

Alpha-ketogluterate is oxidized by the above reaction to succinyl-CoA, and in the process NAD^+ is reduced to NADH. Succinyl-CoA is consumed by succinyl-CoA synthetase to produce succinate, in the process GDP is phosphorylated to GTP. Coenzyme A is also produced as a side product. While the reaction is not subject to serious regulation, the reaction catalysed by succinyl-CoA synthetase is quite complex and the expression for succinyl-CoA synthetase activity is as follows:

$$J_{\mathrm{scoas}} = \frac{V_{mf}V_{mr}\left([\mathrm{GDP}]_\mathrm{x}[\mathrm{SCOA}]_\mathrm{x}[\mathrm{PI}]_\mathrm{x} - \frac{[\mathrm{COASH}]_\mathrm{x}[\mathrm{SUC}]_\mathrm{x}[\mathrm{GTP}]_\mathrm{x}}{K_{eq,\mathrm{scoas}}}\right)}{V_{mr}K_{ia}K_{ib}K_{mC} + V_{mr}K_{ib}K_{mc}[\mathrm{GDP}]_\mathrm{x} + V_{mr}K_{ia}K_{mB}[\mathrm{PI}]_\mathrm{x} + V_{mr}K_{mC}[\mathrm{GDP}]_\mathrm{x}[\mathrm{SCOA}]_\mathrm{x}} \tag{2.108}$$

$$\begin{aligned}
&+ V_{mr}K_{mB}[\mathrm{GDP}]_\mathrm{x}[\mathrm{PI}]_\mathrm{x} + V_{mr}K_{mA}[\mathrm{SCOA}]_\mathrm{x}[\mathrm{PI}]_\mathrm{x} + V_{mr}[\mathrm{GDP}]_\mathrm{x}[\mathrm{SCOA}]_\mathrm{x}[\mathrm{PI}]_\mathrm{x} \\
&+ \frac{V_{mf}K_{ir}K_{mQ}[\mathrm{COASH}]_\mathrm{x}}{K_{eq,\mathrm{scoas}}} + \frac{V_{mf}K_{iq}K_{mP}[\mathrm{GTP}]_\mathrm{x}}{K_{eq,\mathrm{scoas}}} + \frac{V_{mf}K_{mR}[\mathrm{COASH}]_\mathrm{x}[\mathrm{SUC}]_\mathrm{x}}{K_{eq,\mathrm{scoas}}} \\
&+ \frac{V_{mf}K_{mQ}[\mathrm{COASH}]_\mathrm{x}[\mathrm{GTP}]_\mathrm{x}}{K_{eq,\mathrm{scoas}}} + \frac{V_{mf}K_{mP}[\mathrm{SUC}]_\mathrm{x}[\mathrm{GTP}]_\mathrm{x}}{K_{eq,\mathrm{scoas}}} + \frac{V_{mf}[\mathrm{COASH}]_\mathrm{x}[\mathrm{SUC}]_\mathrm{x}[\mathrm{GTP}]_\mathrm{x}}{K_{eq,\mathrm{scoas}}} \\
&+ \frac{V_{mf}K_{mQ}K_{ir}[\mathrm{GDP}]_\mathrm{x}[\mathrm{COASH}]_\mathrm{x}}{K_{ia}K_{eq,\mathrm{scoas}}} + \frac{V_{mr}K_{ia}K_{mB}[\mathrm{PI}]_\mathrm{x}[\mathrm{GTP}]_\mathrm{x}}{K_{ir}} + \frac{V_{mf}K_{mQ}K_{ir}[\mathrm{GDP}]_\mathrm{x}[\mathrm{SCOA}]_\mathrm{x}[\mathrm{SUC}]_\mathrm{x}}{K_{ia}K_{ib}K_{eq,\mathrm{scoas}}} \\
&+ \frac{V_{mr}K_{mA}[\mathrm{SCOA}]_\mathrm{x}[\mathrm{PI}]_\mathrm{x}[\mathrm{GTP}]_\mathrm{x}}{K_{ir}} + \frac{V_{mf}K_{mR}[\mathrm{GDP}]_\mathrm{x}[\mathrm{COASH}]_\mathrm{x}[\mathrm{SUC}]_\mathrm{x}}{K_{ia}K_{eq,\mathrm{scoas}}} \\
&+ \frac{V_{mr}K_{ia}K_{mB}[\mathrm{PI}]_\mathrm{x}[\mathrm{SUC}]_\mathrm{x}[\mathrm{GTP}]_\mathrm{x}}{K_{iq}K_{ir}} + \frac{V_{mf}K_{ir}K_{mQ}[\mathrm{GDP}]_\mathrm{x}[\mathrm{SCOA}]_\mathrm{x}[\mathrm{PI}]_\mathrm{x}[\mathrm{COASH}]_\mathrm{x}}{K_{ia}K_{ib}K_{ic}K_{eq,\mathrm{scoas}}} \\
&+ \frac{V_{mf}K_{ip}K_{mR}[\mathrm{GDP}]_\mathrm{x}[\mathrm{SCOA}]_\mathrm{x}[\mathrm{PI}]_\mathrm{x}[\mathrm{SUC}]_\mathrm{x}}{K_{ia}K_{ib}K_{ic}K_{eq,\mathrm{scoas}}} + \frac{V_{mf}K_{mR}[\mathrm{GDP}]_\mathrm{x}[\mathrm{SCOA}]_\mathrm{x}[\mathrm{COASH}]_\mathrm{x}[\mathrm{SUC}]_\mathrm{x}}{K_{ia}K_{ib}K_{eq,\mathrm{scoas}}}
\end{aligned}$$

$$+\frac{V_{mf}K_{mA}[\text{SCOA}]_\text{x}[\text{PI}]_\text{x}[\text{SUC}]_\text{x}[\text{GTP}]_\text{x}}{K_{iq}K_{ir}}+\frac{V_{mr}K_{mA}K_{ic}[\text{SCOA}]_\text{x}[\text{COASH}]_\text{x}[\text{SUC}]_\text{x}[\text{GTP}]_\text{x}}{K_{ip}K_{iq}K_{ir}}$$
$$+\frac{V_{mr}K_{ia}K_{mB}[\text{PI}]_\text{x}[\text{COASH}]_\text{x}[\text{SUC}]_\text{x}[\text{GTP}]_\text{x}}{K_{ip}K_{iq}K_{ir}}+\frac{V_{mf}K_{mR}[\text{GDP}]_\text{x}[\text{SCOA}]_\text{x}[\text{PI}]_\text{x}[\text{COASH}]_\text{x}[\text{SUC}]_\text{x}}{K_{ia}K_{ib}K_{ic}K_{eq,\text{scoas}}}$$
$$+\frac{V_{mf}K_{mA}[\text{SCOA}]_\text{x}[\text{PI}]_\text{x}[\text{COASH}]_\text{x}[\text{SUC}]_\text{x}[\text{GTP}]_\text{x}}{K_{ip}K_{iq}K_{ir}}$$

The parameters for this reaction are included in Table : The kinetic parameters included are listed in Table 2.6. V_{mr} may be calculated as $V_{mf}K_{eq,scoas}^{-1}K_{mP}^{-1}K_{iq}^{-1}K_{ir}^{-1}K_{ia}^{-1}K_{ib}^{-1}K_{mC}^{-1}$.

Parameter	Model Value (μM)
K_{mA}	16
K_{mB}	55
K_{mC}	660
K_{mP}	20
K_{mQ}	880
K_{mR}	11.1
K_{ia}	5.5
K_{ib}	100
K_{ic}	2000
K_{ip}	20
K_{iq}	3000
K_{ir}	11.1

Table 2.6: Kinetic parameters for succinyl-CoA synthetase.

Succinate dehydrogenase, as well as being an enzyme involved in oxidative phosphorylation, directly catalyzes a step of the TCA cycle. Succinate from the above reaction is consumed by Complex II, allowing Complex II to donate an electron to coenzyme Q, an intermediate in oxidative phosphorylation, and producing fumarate in the process. The reaction mechanism assumed by the Kohn-Garfinkel model and used in Wu et al. [193] doesn't explicitly include the implicit reduction and then oxidation of FAD/$FADH_2$ that occurs in this process. The reaction is represented with the following kinetics:

$$J_\text{sdh}=\frac{V_{mf}V_{mr}\left([\text{SUC}]_\text{x}[\text{COQ}]_\text{x}-\frac{[\text{QH}_2]_\text{x}[\text{FUM}]_\text{x}}{K_{eq,\text{sdh}}}\right)}{V_{mr}K_{ia}K_{mB}\alpha_i+V_{mr}K_{mB}[\text{SUC}]_\text{x}+V_{mr}K_{mA}\alpha_i[\text{COQ}]_\text{x}+\frac{V_{mf}K_{mQ}\alpha_i}{K_{eq,\text{sdh}}}[\text{QH}_2]_\text{x}+\frac{V_{mf}K_{mP}}{K_{eq,\text{sdh}}}[\text{FUM}]_\text{x}}$$
$$+V_{mr}[\text{SUC}]_\text{x}[\text{COQ}]_\text{x}+\frac{V_{mf}K_{mQ}}{K_{eq,\text{sdh}}K_{ia}}[\text{SUC}]_\text{x}[\text{QH}_2]_\text{x}+\frac{V_{mr}K_{mA}}{K_{iq}}[\text{COQ}]_\text{x}[\text{FUM}]_\text{x}$$
$$+\frac{V_{mf}}{K_{eq,\text{sdh}}}[\text{QH}_2]_\text{x}[\text{FUM}]_\text{x} \tag{2.109}$$

Parameter	Model Value (μM)
K_{mA}	467
K_{mB}	480
K_{mP}	2.45
K_{mQ}	1200
K_{ia}	120
K_{iq}	1275
K_{iOAA}	1.5
K_{aSUC}	450
K_{aFUM}	375

Table 2.7: Kinetic parameters for succinate dehydrogenase.

Where α_i is an inhibition-activation term, with activation by succinate and fumarate, and competitive inhibition of that activation by oxaloacetate. Altogether that gives us the following regulatory term α_i:

$$\alpha_i = \frac{\left(1 + \frac{[\text{OAA}]_\text{x}}{K_{i\text{OAA}}} + \frac{[\text{SUC}]_\text{x}}{K_{a\text{SUC}}} + \frac{[\text{FUM}]_\text{x}}{K_{a\text{FUM}}}\right)}{\left(1 + \frac{[\text{SUC}]_\text{x}}{K_{a\text{SUC}}} + \frac{[\text{FUM}]_\text{x}}{K_{a\text{FUM}}}\right)} \tag{2.110}$$

The parameters governing succinate dehydrogenase are found in Table 2.7. V_{mr} can be calculated as $V_{mf}K_{mP}K_{iq}K_{eq,sdh}^{-1}K_{ia}^{-1}K_{mB}^{-1}$

Fumarate is in-turn consumed by fumarase to produce malate. Fumarase also binds to citrate, free adenine nucleotides, GTP, and GDP competitively. The mechanism is discussed in Wu et al. [193]:

$$J_\text{fum} = \frac{V_{mf}V_{mr}\left([\text{FUM}]_\text{x} - \frac{[\text{MAL}]_\text{x}}{K_{eq,\text{fum}}}\right)}{K_{mA}V_{mr}\alpha_i + V_{mr}[\text{FUM}]_\text{x} + \frac{V_{mf}[\text{MAL}]_\text{x}}{K_{eq,\text{fum}}}} \tag{2.111}$$

Where α_i may be written as follows (as previously, the prefix f denotes that it is free, dissociated nucleotides):

$$\alpha_i = 1 + \frac{[\text{CIT}]_\text{x}}{K_{i\text{CIT}}} + \frac{[\text{fATP}]_\text{x}}{K_{i\text{ATP}}} + \frac{[\text{fADP}]_\text{x}}{K_{i\text{ADP}}} + \frac{[\text{fGTP}]_\text{x}}{K_{i\text{GTP}}} + \frac{[\text{fGDP}]_\text{x}}{K_{i\text{GDP}}} \tag{2.112}$$

The kinetic parameters included are listed in Table 2.8. V_{mr} is calculated as $V_{mf}K_{mP}K_{eq,fum}^{-1}K_{mA}^{-1}$.

Malate from the previous reaction is consumed by malate dehydrogenase, generating oxaloacetate, which will be used to generate citrate, completing the TCA cycle. Malate

Parameter	Model Value (μM)
K_{mA}	44.7
K_{mP}	197.7
K_{iCIT}	3500
K_{iATP}	40
K_{iADP}	400
K_{iGTP}	80
K_{iGDP}	330

Table 2.8: Kinetic parameters for fumarase.

dehydrogenase reduces NAD^+ to NADH during the process. Malate dehydrogenase is competitively inhibited at the NAD^+/NADH site by adenine nucleotides. Malate dehydrogenase's kinetics may be described as follows:

$$J_{\mathrm{mdh}} = \frac{V_{mf}V_{mr}\left([\mathrm{NAD}]_{\mathrm{x}}[\mathrm{MAL}]_{\mathrm{x}} - \frac{[\mathrm{OAA}]_{\mathrm{x}}[\mathrm{NADH}]_{\mathrm{x}}}{K_{eq,\mathrm{mdh}}}\right)}{V_{mr}K_{ia}K_{mB}\alpha_i + V_{mr}K_{mB}[\mathrm{NAD}]_{\mathrm{x}} + V_{mr}K_{mA}\alpha_i[\mathrm{MAL}]_{\mathrm{x}} + \frac{V_{mf}K_{mQ}\alpha_i[\mathrm{OAA}]_{\mathrm{x}}}{K_{eq,\mathrm{mdh}}} + \frac{V_{mf}K_{mP}[\mathrm{NADH}]_{\mathrm{x}}}{K_{eq,\mathrm{mdh}}}} \tag{2.113}$$
$$+ V_{mr}[\mathrm{NAD}]_{\mathrm{x}}[\mathrm{MAL}]_{\mathrm{x}} + \frac{V_{mf}K_{mQ}[\mathrm{NAD}]_{\mathrm{x}}[\mathrm{OAA}]_{\mathrm{x}}}{K_{eq,\mathrm{mdh}}K_{ia}} + \frac{V_{mf}[\mathrm{OAA}]_{\mathrm{x}}[\mathrm{NADH}]_{\mathrm{x}}}{K_{eq,\mathrm{mdh}}}$$
$$+ \frac{V_{mr}K_{mA}[\mathrm{MAL}]_{\mathrm{x}}[\mathrm{NADH}]_{\mathrm{x}}}{K_{iq}} + \frac{V_{mr}[\mathrm{NAD}]_{\mathrm{x}}[\mathrm{MAL}]_{\mathrm{x}}[\mathrm{OAA}]_{\mathrm{x}}}{K_{ip}} + \frac{V_{mf}[\mathrm{MAL}]_{\mathrm{x}}[\mathrm{OAA}]_{\mathrm{x}}[\mathrm{NADH}]_{\mathrm{x}}}{K_{ib}K_{eq,\mathrm{mdh}}}$$

The competitive inhibition by adenine nucleotides is included in the above expression in the α_i term. It is written as follows:

$$\alpha_i = 1 + \frac{[\mathrm{fATP}]_{\mathrm{x}}}{K_{i\mathrm{ATP}}} + \frac{[\mathrm{fADP}]_{\mathrm{x}}}{K_{i\mathrm{ADP}}} + \frac{[\mathrm{fAMP}]_{\mathrm{x}}}{K_{i\mathrm{AMP}}} \tag{2.114}$$

Malate dehydrogenase completes the essential components of the TCA cycle, the reaction mechanism is noted in Wu et al [193]. The kinetic parameters included are listed in Table 2.9. V_{mr} may be calculated as $V_{mf}K_{iq}K_{mP}K_{eq,mdh}^{-1}K_{ia}^{-1}K_{mB}^{-1}$.

We include multiple other reactions, we start with nucleoside diphosphokinase. Nucleoside disphosphokinase transfers a phosphate group from magnesium-bound GTP to a magnesium-bound ADP to produce ATP, we represent its kinetics as follows (see Wu et al. [193] for the reaction mechanism):

$$J_{\mathrm{ndk}} = \frac{V_{mf}V_{mr}\left([\mathrm{GTP}]_{\mathrm{x}}[\mathrm{ADP}]_{\mathrm{x}} - \frac{[\mathrm{GDP}]_{\mathrm{x}}[\mathrm{ATP}]_{\mathrm{x}}}{K_{eq,\mathrm{ndk}}}\right)/\alpha_i}{V_{mr}K_{mB}[\mathrm{GTP}]_{\mathrm{x}} + V_{mr}K_{mA}[\mathrm{ADP}]_{\mathrm{x}} + \frac{V_{mf}K_{mQ}[\mathrm{GDP}]_{\mathrm{x}}}{K_{eq,\mathrm{ndk}}} + \frac{V_{mf}K_{mP}[\mathrm{ATP}]_{\mathrm{x}}}{K_{eq,\mathrm{ndk}}} + V_{mr}[\mathrm{GTP}]_{\mathrm{x}}[\mathrm{ADP}]_{\mathrm{x}}} \tag{2.115}$$

Parameter	Model Value (μM)
K_{mA}	90.55
K_{mB}	250
K_{mP}	6.128
K_{mQ}	2.58
K_{ia}	279
K_{ib}	360
K_{ip}	5.5
K_{iq}	3.18
K_{iATP}	183.2
K_{iADP}	394.4
K_{iAMP}	420.0

Table 2.9: Kinetic parameters for malate dehydrogenase.

$$+\frac{V_{mf}K_{mQ}[\mathrm{GTP}]_{\mathrm{x}}[\mathrm{GDP}]_{\mathrm{x}}}{K_{eq,\mathrm{ndk}}K_{ia}}+\frac{V_{mf}[\mathrm{GDP}]_{\mathrm{x}}[\mathrm{ATP}]_{\mathrm{x}}}{K_{eq,\mathrm{ndk}}}+\frac{V_{mr}K_{mA}[\mathrm{ADP}]_{\mathrm{x}}[\mathrm{ATP}]_{\mathrm{x}}}{K_{iq}}$$

Nucleoside disphosphokinase is regulated by free AMP, leading to the α_i in the above equation, which may be written as follows:

$$\alpha_i = 1+\frac{[\mathrm{fAMP}]_{\mathrm{x}}}{K_{i\mathrm{AMP}}} \tag{2.116}$$

The kinetic parameters included are listed in Table 2.10. V_{mr} may be calculated as $V_{mf}K_{mQ}K_{ip}K_{eq,ndk}^{-1}K_{ia}^{-1}K_{mB}^{-1}$.

Parameter	Model Value (μM)
K_{mA}	111
K_{mB}	100
K_{mP}	260
K_{mQ}	278
K_{ia}	170
K_{ib}	143.6
K_{ip}	146.6
K_{iq}	156.5
K_{iAMP}	650

Table 2.10: Kinetic parameters for nucleoside disphosphokinase.

There are only two matrix compounds included in our model that we have not yet discussed, glutamate and aspartate. Glutamate and aspartate are both amino acids, and are both used to a limited extent as a metabolic intermediate. Additionally, glutamate is a

Parameter	Model Value (μM)
K_{mA}	3900
K_{mB}	430
K_{mP}	88
K_{mQ}	8900
K_{ia}	3480
K_{ib}	710
K_{ip}	50
K_{iq}	8400
K_{iAKG}	16600

Table 2.11: Kinetic parameters for glutamate oxaloacetate transaminase.

neurotransmitter. Glutamate oxaloacetate transaminase (also known as aspartate transaminase) converts aspartate to glutamate, and in the process produces alpha-ketogluterate from oxaloacetate. Glutamate oxaloacetate transaminase's aspartate binding site is competitively inhibited by alpha-ketogluterate. The reaction mechanism is discussed further in Wu et al [193]:

$$J_{\text{got}} = \frac{V_{mf}V_{mr}\left([\text{ASP}]_\text{x}[\text{AKG}]_\text{x} - \frac{[\text{OAA}]_\text{x}[\text{GLU}]_\text{x}}{K_{eq,\text{got}}}\right)}{V_{mr}K_{mB}[\text{ASP}]_\text{x} + V_{mr}K_{mA}\alpha_i[\text{AKG}]_\text{x} + \frac{V_{mf}K_{mQ}\alpha_i[\text{OAA}]_\text{x}}{K_{eq,\text{got}}} + \frac{V_{mf}K_{mP}[\text{GLU}]_\text{x}}{K_{eq,\text{got}}} + V_{mr}[\text{ASP}]_\text{x}[\text{AKG}]_\text{x}} \tag{2.117}$$
$$+ \frac{V_{mf}K_{mQ}[\text{ASP}]_\text{x}[\text{OAA}]_\text{x}}{K_{eq,\text{got}}K_{ia}} + \frac{V_{mf}[\text{OAA}]_\text{x}[\text{GLU}]_\text{x}}{K_{eq,\text{got}}} + \frac{V_{mr}K_{mA}[\text{AKG}]_\text{x}[\text{GLU}]_\text{x}}{K_{iq}}$$

Where α_i may be expressed as follows:

$$\alpha_i = 1 + \frac{[\text{AKG}]_\text{x}}{K_{i\text{AKG}}} \tag{2.118}$$

The kinetic parameters included are listed in Table 2.11. V_{mr} may be calculated as $V_{mf}K_{mQ}K_{ip}K_{eq,got}^{-1}K_{ia}^{-1}K_{mB}^{-1}$.

Glutamate may also be consumed directly to produce alpha-ketogluterate by glutamate dehydrogenase. Glutamate dehydrogenase activity is particularly relevant to hepatocytes in the liver [84]. We use a simple kinetic description of glutamate dehydrogenase because the only measurements we could find of glutamate dehydrogenase kinetics, based on the kinetic model used in the experiments we relied on [84]. We represent glutamate dehydrogenase activity as follows:

$$J_{\text{gdh}} = X_{\text{GDH}}\frac{[\text{GLU}]_\text{x}[\text{NAD}^+]_\text{x}}{K_{\text{M, GLU}} + [\text{GLU}]_\text{x}} \tag{2.119}$$

In Jonker et al. [84], they use an even simpler model that did not depend on NAD^+. We chose X_{GDH} so that $V_{\mathrm{GDH}}[\mathrm{NAD}^+]$ was what Jonker et al. measured to be the $V_{\max}$ of their simpler equation. This change was introduced in order to avoid failures of non-negativity in our model.

Adenylate kinase acts both in the mitochondria and in the cytosol. Adenylate kinase regulates the quantity of AMP in the cell by converting two ADP into AMP and ATP, and is fast enough to be maintained at equilibrium. AMP plays an important regulatory role for cellular metabolism. The kinetics of adenylate kinase are as follows:

$$J_{\mathrm{AKi}} = X_{\mathrm{AK}} \left(K_{\mathrm{AK}} [\mathrm{ADP}]_{\mathrm{i}} [\mathrm{ADP}]_{\mathrm{i}} - [\mathrm{AMP}]_{\mathrm{i}} [\mathrm{ATP}]_{\mathrm{i}} \right) \tag{2.120}$$

2.2 Oxidative Phosphorylation

We will go through the process of oxidative phosphorylation in order, which is particularly crucial to the work that follows. The flux through Complex I depends both on chemical kinetics and the thermodynamic dependence of Complex I activity on the electrical potential gradient:

$$J_{\mathrm{C1}} = X_{\mathrm{CI}} \left(\exp(-(\Delta_r G^0_{\mathrm{C1}} - 4F\Delta\Psi)/RT) \frac{[\mathrm{H}^+]^5_{\mathrm{x}}}{[\mathrm{H}^+]^4_i} [\mathrm{NADH}]_{\mathrm{x}} [\mathrm{COQ}]_{\mathrm{x}} - [\mathrm{NAD}^+]_{\mathrm{x}} [\mathrm{QH_2}]_{\mathrm{x}} \right) \tag{2.121}$$

We see that the thermodynamic term gives an exponential dependence of the flux on the electrical potential gradient. The reaction is written so that there is proportional dependence of the forward and backward reactions on their reactants.

Complex III flux has similar kinetics, including exponential dependence on the electrical potential gradient. It primarily differs in the stoichiometry of proton movement via Complex III:

$$J_{\mathrm{C3}} = X_{\mathrm{C3}} \left(\frac{1 + [\mathrm{PI}]_{\mathrm{x}}/k_{\mathrm{Pi,1}}}{1 + [\mathrm{PI}]_{\mathrm{x}}/k_{\mathrm{Pi,2}}} \right) \left(\left(\exp(-(\Delta_r G^0_{\mathrm{C3}} - 2F\Delta\Psi)/RT) \frac{[\mathrm{H}^+]^2_{\mathrm{x}}}{[\mathrm{H}^+]^4_i} \right)^{1/2} [\mathrm{Cox}]_{\mathrm{i}} [\mathrm{QH_2}]^{1/2}_{\mathrm{x}} - [\mathrm{Cred}]_{\mathrm{i}} [\mathrm{COQ}]^{1/2}_{\mathrm{x}} \right) \tag{2.122}$$

The flux via Complex IV is different because it is not transferring an electron from one intermediate to another, rather it is transferring an electron to its final resting place: an oxygen molecule, in the process producing water. Once again the reaction exhibits exponential dependence on the electrical potential gradient.

$$J_{\mathrm{C4}} = X_{\mathrm{C4}} \left(\frac{1}{1 + k_{\mathrm{o_2}}/[\mathrm{O_2}]} \right) \exp\left(\frac{F\Delta\Psi}{RT} \right) \left(\frac{[\mathrm{Cred}]_{\mathrm{i}}}{\mathrm{cytC_{tot}}} \right) \left(\left(\frac{[\mathrm{H}^+]^4_{\mathrm{x}}}{[\mathrm{H}^+]^2_i} \exp(-(\Delta_r G^0_{\mathrm{C4}} - 4F\Delta\Psi)/RT) \right)^{1/2} \right.$$

$$[\mathrm{Cred}]_\mathrm{i}\,[\mathrm{O_2}]_\mathrm{x}^{1/4} - [\mathrm{Cox}]_\mathrm{i}\Big) \tag{2.123}$$

The final step of oxidative phosphorylation is ATP synthase (also known as Complex V or $\mathrm{F_0F_1}$-ATPase). ATP Synthase generates a significant portion of the total ATP produced by mitochondrial respiration and consumes the majority of the oxygen used in aerobic respiration:

$$J_\mathrm{F1} = X_\mathrm{F1}\left(\exp(-(\Delta_r G^0_\mathrm{F1} - 4F\Delta\Psi)/RT)\frac{[\mathrm{H^+}]_i^{n_A}}{[\mathrm{H^+}]_x^{n_A-1}}\frac{P_\mathrm{ATP}}{P_\mathrm{ADP}P_\mathrm{PI}}[\mathrm{ADP}]_\mathrm{x}[\mathrm{PI}]_\mathrm{x} - [\mathrm{ATP}]_\mathrm{x}\right) \tag{2.124}$$

where P_ATP, P_ADP, and P_PI are the reaction polynomials associated with ATP, ADP, and phosphate respectively. The reaction polynomials may be written explicitly as follows (they're also discussed above in relation to ion concentrations):

$$P_\mathrm{ATP} = 1 + \frac{[\mathrm{H^+}]_\mathrm{x}}{K_\mathrm{H,ATP}} + \frac{[\mathrm{K^+}]_\mathrm{x}}{K_\mathrm{K,ATP}} + \frac{[\mathrm{Mg^{2+}}]_\mathrm{x}}{K_\mathrm{Mg,ATP}} \tag{2.125}$$

$$P_\mathrm{ADP} = 1 + \frac{[\mathrm{H^+}]_\mathrm{x}}{K_\mathrm{H,ADP}} + \frac{[\mathrm{K^+}]_\mathrm{x}}{K_\mathrm{K,ADP}} + \frac{[\mathrm{Mg^{2+}}]_\mathrm{x}}{K_\mathrm{Mg,ADP}} \tag{2.126}$$

$$P_\mathrm{PI} = 1 + \frac{[\mathrm{H^+}]_\mathrm{x}}{K_\mathrm{H,PI}} + \frac{[\mathrm{K^+}]_\mathrm{x}}{K_\mathrm{K,PI}} + \frac{[\mathrm{Mg^{2+}}]_\mathrm{x}}{K_\mathrm{Mg,PI}} \tag{2.127}$$

2.3 Other Membrane Fluxes

The mitochondrion is composed of two compartments that allow for the reactions involved in cellular respiration to be performed more efficiently as discussed above. The inner membrane is highly impermeable and so relies heavily on transporters to regulate crucial concentrations in the mitochondrion. We will begin our discussion of membrane fluxes with those transporters.

A key transporter for understanding the behaviour of mitochondria is adenine nucleotide translocase. Adenine nucleotide translocase swaps ATP and ADP across the inner mitochondrial membrane. Since ATP synthase converts ADP into ATP in the mitochondrial matrix, the mitochondrial matrix needs a constant supply of ADP and a means of exporting its ATP. More importantly however, adenine nucleotide translocase is a limiting flux for aerobic respiration, meaning that the cell is highly sensitive to the activity of adenine nucleotide translocase. We represent the kinetics of this crucial transporter as follows:

$$J_\mathrm{ANT} = \left(\frac{X_\mathrm{ANT}}{1 + k_{m,\mathrm{ADP}}/\left[\mathrm{ADP^{3-}}\right]_\mathrm{i}}\right)\left(\frac{\left[\mathrm{ADP^{3-}}\right]_\mathrm{i}}{\left[\mathrm{ADP^{3-}}\right]_\mathrm{i} + \left[\mathrm{ATP^{4-}}\right]_\mathrm{i}\exp\left((\theta-1)F\Delta\Psi/RT\right)} - \right. \tag{2.128}$$

$$\frac{\left[\mathrm{ADP}^{3-}\right]_{\mathrm{x}}}{\left[\mathrm{ADP}^{3-}\right]_{\mathrm{x}} + \left[\mathrm{ATP}^{4-}\right]_{\mathrm{x}} \exp\left(\theta F \Delta\Psi / RT\right)}\Bigg)$$

Adenine nucleotide translocase is dependent on the electrical potential gradient because ATP and ADP are both charged, but their exchange is not electroneutral.

Dihydrogen phosphate and a proton are co-transported across the inner membrane of the mitochondrion. This supplies inorganic phosphate ions that may be used in ATP synthesis:

$$J_{\mathrm{PIHt}} = X_{\mathrm{PIHt}} \cdot \frac{\left[\mathrm{H_2PO_4^-}\right]_{\mathrm{i}} \left[\mathrm{H^+}\right]_{\mathrm{i}} - \left[\mathrm{H_2PO_4^-}\right]_{\mathrm{x}} \left[\mathrm{H^+}\right]_{\mathrm{x}}}{k_{\mathrm{PIHt}} \left(1 + \left[\mathrm{H_2PO_4^-}\right]_{\mathrm{i}} / k_{\mathrm{PIHt}}\right) \left(1 + \left[\mathrm{H_2PO_4^-}\right]_{\mathrm{x}} / k_{\mathrm{PIHt}}\right)} \tag{2.129}$$

Another crucial transporter is the potassium-hydrogen antiporter. The potassium-hydrogen antiporter exchanges potassium ions for hydrogen ions according to simple mass-action kinetics. Typically hydrogen ions move into the mitochondrial matrix and potassium ions into the intermembrane space. Once again, this flux is electoneutral. This gives us the following kinetics:

$$J_{\mathrm{KH}} = X_{\mathrm{KH}} \left(\left[\mathrm{K^+}\right]_{\mathrm{i}} \left[\mathrm{H^+}\right]_{\mathrm{x}} - \left[\mathrm{K^+}\right]_{\mathrm{x}} \left[\mathrm{H^+}\right]_{\mathrm{i}}\right) \tag{2.130}$$

Pyruvate and hydrogen ions are co-transported across the inner membrane of the mitochondrion. Since pyruvate is consumed by pyruvate dehydrogenase inside the cell, the pyruvate-hydrogen co-transporter preferably transports pyruvate and hydrogen into the mitochondrial matrix. Pyruvate-hydrogen co-transporter also follows mass-action kinetics and is electroneutral, giving us the following kinetics:

$$J_{\mathrm{PYRH}} = X_{\mathrm{PYRH}} \left(\left[\mathrm{PYR^-}\right]_{\mathrm{i}} \left[\mathrm{H^+}\right]_{\mathrm{i}} - \left[\mathrm{PYR^-}\right]_{\mathrm{x}} \left[\mathrm{H^+}\right]_{\mathrm{x}}\right) \tag{2.131}$$

Glutamate and hydrogen ions are also co-transported across the inner membrane of the mitochondrion. When glutamate dehydrogenase activity is high, glutamate will be consumed in the mitochondrial matrix. Otherwise it may not be so clear what flux to expect through the glutamate-hydrogen co-transporter.

$$J_{\mathrm{GLUH}} = X_{\mathrm{GLUH}} \left(\left[\mathrm{GLU^-}\right]_{\mathrm{i}} \left[\mathrm{H^+}\right]_{\mathrm{i}} - \left[\mathrm{GLU^-}\right]_{\mathrm{x}} \left[\mathrm{H^+}\right]_{\mathrm{x}}\right) \tag{2.132}$$

The above two transporters are examples of co-transporters of elemental ions and important metabolites. They provide essential metabolites that the mitochondrion will use. On the other hand, antiporting mechanisms for pairs of metabolites help to maintain appropriate mixes of those pairs of metabolites. Our model includes four examples of this form: citrate-malate antiporter which follows simple mass-action kinetics, alphaketogluterate-malate antiporter, aspartate-glutamate antiporter, and succinate-malate antiporter. The latter three follow more complex kinetics discussed in Wu et al [193]:

$$J_{\mathrm{CITMAL}} = X_{\mathrm{CITMAL}} \left(\left[\mathrm{HCIT^{2-}}\right]_{\mathrm{i}} \left[\mathrm{MAL^{2-}}\right]_{\mathrm{x}} - \left[\mathrm{HCIT^{2-}}\right]_{\mathrm{x}} \left[\mathrm{MAL^{2-}}\right]_{\mathrm{i}}\right) \tag{2.133}$$

$$J_{\mathrm{AKGMAL}} = \frac{X_{\mathrm{AKGMAL}}\left([\mathrm{AKG}]_{\mathrm{i}}[\mathrm{MAL}]_{\mathrm{x}} - [\mathrm{AKG}]_{\mathrm{x}}[\mathrm{MAL}]_{\mathrm{i}}\right)}{K_{m\mathrm{AKGi}}K_{m\mathrm{MALx}}\left(2 + \frac{[\mathrm{MAL}]_{\mathrm{i}}}{K_{m\mathrm{MALi}}} + \frac{[\mathrm{MAL}]_{\mathrm{x}}}{K_{m\mathrm{MALx}}} + \frac{[\mathrm{AKG}]_{\mathrm{i}}}{K_{m\mathrm{AKGi}}} + \frac{[\mathrm{AKG}]_{\mathrm{x}}}{K_{\mathrm{mAKGx}}}\right.} \tag{2.134}$$
$$\left. + \frac{[\mathrm{MAL}]_{\mathrm{i}}[\mathrm{AKG}]_{\mathrm{x}}}{K_{m\mathrm{MALi}}K_{m\mathrm{AKGx}}} + \frac{[\mathrm{MAL}]_{\mathrm{x}}[\mathrm{AKG}]_{\mathrm{i}}}{K_{m\mathrm{MALx}}K_{m\mathrm{AKGi}}}\right)$$

$$J_{\mathrm{ASPGLU}} = \frac{X_{\mathrm{ASPGLU}}\ \left(K_{\mathrm{eq\ ,\ ASPGLU}}\,[\mathrm{ASP}]_i[\mathrm{GLU}]_{\mathrm{x}}\,[\mathrm{H}^+]_{\mathrm{x}} - [\mathrm{ASP}]_{\mathrm{x}}[\mathrm{GLU}]_{\mathrm{i}}\,[\mathrm{H}^+]_{\mathrm{i}}\right)}{K_{eq,\mathrm{ASPGLU}}K_{i\mathrm{ASP}}K_{i\mathrm{GLUX}}K_{h,\mathrm{ASPGLU}}\left(2m + m\frac{[\mathrm{ASP}]_{\mathrm{i}}}{Ki\mathrm{ASPc}} + \frac{[\mathrm{ASP}]_{\mathrm{i}}[\mathrm{GLU}]_{\mathrm{x}}[\mathrm{H}^+]_{\mathrm{x}}}{K_{i\mathrm{ASP}}K_{i\mathrm{GLU}}K_{h,\mathrm{ASPGLU}}}\right.}$$
$$+ m\frac{[\mathrm{ASP}]_{\mathrm{x}}\,[\mathrm{H}^+]_{\mathrm{i}}}{K_{i\mathrm{ASP}}K_{h,\mathrm{ASPGLU}}} + \frac{[\mathrm{ASP}]_{\mathrm{x}}[\mathrm{GLU}]_{\mathrm{i}}\,[\mathrm{H}^+]_{\mathrm{i}}}{K_{i\mathrm{SSP}}K_{i\mathrm{GLUi}}K_{h,\mathrm{ASPGLU}}} + m\frac{[\mathrm{ASP}]_{\mathrm{x}}}{K_{i\mathrm{ASPx}}} + m\frac{[\mathrm{ASP}]_{\mathrm{i}}\,[\mathrm{H}^+]_{\mathrm{x}}}{K_{i\mathrm{ASPi}}K_{h,\mathrm{ASPGLU}}}$$
$$\left. + m\frac{[\mathrm{H}^+]_{\mathrm{x}}}{K_{h,\mathrm{ASPGLU}}} + m\frac{[\mathrm{GLU}]_{\mathrm{i}}\,[\mathrm{H}^+]_{\mathrm{i}}}{K_{i\mathrm{GLUi}}K_{h,\mathrm{ASPGLU}}} + m\frac{[\mathrm{H}^+]_{\mathrm{i}}}{K_{h,\mathrm{ASPGLU}}} + m\frac{[\mathrm{GLU}]_{\mathrm{x}}\,[\mathrm{H}^+]_{\mathrm{x}}}{K_{i\mathrm{GLUx}}}\right) \tag{2.135}$$

$$J_{\mathrm{SUCMAL}} = X_{\mathrm{SUCMAL}}\ \left(\left[\mathrm{SUC}^{2-}\right]_{\mathrm{i}}\left[\mathrm{MAL}^{2-}\right]_{\mathrm{x}} - \left[\mathrm{SUC}^{2-}\right]_{\mathrm{x}}\left[\mathrm{MAL}^{2-}\right]_{\mathrm{i}}\right) \tag{2.136}$$

Another regulator of malate concentrations in the mitochondrial matrix is the Malate-Phosphate antiporter. This antiporter follows simple mass-action kinetics, like the citrate-malate antiporter, and it exchanges inorganic phosphate for malate.

$$J_{\mathrm{MALPI}} = X_{\mathrm{MALPI}}\ \left(\left[\mathrm{MAL}^{2-}\right]_{\mathrm{i}}\left[\mathrm{PI}^{2-}\right]_{\mathrm{x}} - \left[\mathrm{MAL}^{2-}\right]_{\mathrm{x}}\left[\mathrm{PI}^{2-}\right]_{\mathrm{i}}\right) \tag{2.137}$$

The last pair of fluxes between the mitochondrial matrix and the cell are particularly important, they are the hydrogen and potassium leaks. These effects it is important to mention are not electroneutral, they lead to a net flow of hydrogen and potassium ions into the mitochondrial matrix. The mitochondrial electrical potential gradient will always favour leak into the matrix for the same reason. As noted above in Section 1.3, these leak fluxes were adjusted for Edwards, Palm, and Layton's model [44] to match more recent kinetic data on ion leakage across the mitochondria's inner membrane.

$$J_{\mathrm{HLe}} = P_{\mathrm{H,leak}}\left(\left[\mathrm{H}^+\right]_{\mathrm{i}}\exp\left(\frac{\mathrm{F}\Delta\Psi}{2\mathrm{RT}}\right) - \left[\mathrm{H}^+\right]_{\mathrm{x}}\exp\left(\frac{-\mathrm{F}\Delta\Psi}{2\mathrm{RT}}\right)\right) \tag{2.138}$$

$$J_{\mathrm{KLe}} = P_{\mathrm{K,leak}}\left(\left[\mathrm{K}^+\right]_{\mathrm{i}}\exp\left(\frac{\mathrm{F}\Delta\Psi}{2\mathrm{RT}}\right) - \left[\mathrm{K}^+\right]_{\mathrm{x}}\exp\left(\frac{-\mathrm{F}\Delta\Psi}{2\mathrm{RT}}\right)\right) \tag{2.139}$$

The remaining membrane fluxes of interest connect the cytosol and the intermembrane space. These fluxes represent passive diffusion because the outer mitochondrial membrane is highly permeable and doesn't for the most part depend on transporters to control the flux in the quantities we include. The passive diffusion fluxes we include are as follows:

$$J_{\mathrm{ATPt}} = \gamma p_A\left([\mathrm{ATP}]_{\mathrm{c}} - [\mathrm{ATP}]_{\mathrm{i}}\right) \tag{2.140}$$
$$J_{\mathrm{ADPt}} = \gamma p_A\left([\mathrm{ADP}]_{\mathrm{c}} - [\mathrm{ADP}]_{\mathrm{i}}\right) \tag{2.141}$$
$$J_{\mathrm{AMPt}} = \gamma p_A\left([\mathrm{AMP}]_{\mathrm{c}} - [\mathrm{AMP}]_{\mathrm{i}}\right) \tag{2.142}$$
$$J_{\mathrm{PIt}} = \gamma p_{\mathrm{PI}}([\mathrm{PI}]_{\mathrm{c}} - [\mathrm{PI}]_{\mathrm{i}}) \tag{2.143}$$
$$J_{\mathrm{PYRt}} = \gamma p_{\mathrm{TI}}\left([\mathrm{PYR}]_{\mathrm{c}} - [\mathrm{PYR}]_{\mathrm{i}}\right) \tag{2.144}$$

$$J_{\mathrm{CITt}} = \gamma p_{\mathrm{TI}} \left([\mathrm{CIT}]_{\mathrm{c}} - [\mathrm{CIT}]_{\mathrm{i}} \right) \tag{2.145}$$
$$J_{\mathrm{MALt}} = \gamma p_{\mathrm{TI}} \left([\mathrm{MAL}]_{\mathrm{c}} - [\mathrm{MAL}]_{\mathrm{i}} \right) \tag{2.146}$$
$$J_{\mathrm{AKGt}} = \gamma p_{\mathrm{TI}} \left([\mathrm{AKG}]_{\mathrm{c}} - [\mathrm{AKG}]_{\mathrm{i}} \right) \tag{2.147}$$
$$J_{\mathrm{SUCt}} = \gamma p_{\mathrm{TI}} \left([\mathrm{SUC}]_{\mathrm{c}} - [\mathrm{SUC}]_{\mathrm{i}} \right) \tag{2.148}$$
$$J_{\mathrm{GLUt}} = \gamma p_{\mathrm{TI}} \left([\mathrm{GLU}]_{\mathrm{c}} - [\mathrm{GLU}]_{\mathrm{i}} \right) \tag{2.149}$$
$$J_{\mathrm{ASPt}} = \gamma p_{\mathrm{TI}} \left([\mathrm{ASP}]_{\mathrm{c}} - [\mathrm{ASP}]_{\mathrm{i}} \right) \tag{2.150}$$

The outer membrane is highly permeable and so the cytosol and intermembrane space typically have very similar concentrations of all the above compounds.

2.4 Other Reactions in the Cytosol

ATP consumption is the most important remaining flux in the model. ATP consumption is treated as independent of the system's state by the previous model [44]. However we use Michaelis-Menten dynamics for the cell's ATP consumption (Q_{ATP}), i.e.

$$Q_{\mathrm{ATP}} = Q_{\mathrm{ATP,\ max}} \frac{[ATP]_c}{K_m + [ATP]_c} \tag{2.151}$$

The parameterization of this equation is discussed in Section 3.2.1.

We also include glycolysis in some tissues (the liver by default, the mTAL optionally) as follows (with K_{mGlyc} chosen to be so small that it only serves to ensure non-negativity of ADP levels for an otherwise relatively constant source term):

$$J_{\mathrm{Glyc}} = V_{\mathrm{Glyc}} \frac{[\mathrm{ADP}]_c}{K_{\mathrm{mGlyc}} + [\mathrm{ADP}]_c} \tag{2.152}$$

In the cytosol, adenylate kinase (represented in our model by J_{AKc}) and creatine kinase (represented in our model by J_{CKc}) impact adenine nucleotide homeostasis by controlling AMP concentrations. Aside from being an adenine nucleotide, AMP plays an important regulatory role in the cell. These reactions have a high capacity in our model and are kept near equilibrium:

$$J_{\mathrm{AKc}} = X_{\mathrm{AK}} \left(K_{\mathrm{AK}} \left[\mathrm{ADP}^{3-}\right]_{\mathrm{c}}^{2} - \left[\mathrm{AMP}^{2-}\right]_{\mathrm{c}} \left[\mathrm{ATP}^{4-}\right]_{\mathrm{c}} \right) \tag{2.153}$$
$$J_{\mathrm{CKc}} = X_{\mathrm{CK}} \left(K_{\mathrm{CK}} \left[\mathrm{ADP}^{3-}\right]_{\mathrm{c}} \left[\mathrm{PCr}^{2-}\right]_{\mathrm{c}} \left[\mathrm{H}^{+}\right]_{\mathrm{c}} - \left[\mathrm{ATP}^{4-}\right]_{\mathrm{c}} \left[\mathrm{Cr}^{0}\right]_{\mathrm{c}} \right) \tag{2.154}$$

These reactions exhaust the fluxes included in our model.

2.5 Full List of State Variables

State Variable	Brief Description
Electrical Potential Gradient ($\Delta\Psi$)	The gradient of ion activity across the inner membrane, the only quantity in our model that is not a molar concentration, measured in millivolts
Matrix Adenosine Triphosphate ($[ATP]_x$)	A crucial cellular energy source produced primarily in the mitochondrial matrix and transported to the cytosol for consumption
Matrix Adenosine Diphosphate ($[ADP]_x$)	An adenine nucleoside transported into the matrix to be phosphorylated to ATP
Matrix Adenosine Monophosphate ($[AMP]_x$)	An adenine nucleoside with one less phosphate group than adenine disphosphate
Matrix Gunanosine Triphosphate ($[GTP]_x$)	A guanine nucleoside used to produce ATP in our model
Matrix Guanosine Diphosphate ($[GDP]_x$)	A gunanine nucleoside phosphorylated to GTP by nucleoside disphosphokinase
Matrix Inorganic Phosphate ($[PI]_x$)	Used to produce nucleosides that the cell uses for energy
Matrix Nicotinamide Adenosine Nucleoside ($[NADH]_x$)	An electron carrier produced during the TCA cycle that reduces Complex I and III
Matrix Reduced Coenzyme Q ($[QH_2]_x$)	An electron carrier and cofactor produced by Complex I and II
Matrix Pyruvate ($[PYR]_x$)	An energy source & biproduct of glycolysis that is broken down by pyruvate oxidation to be fed into the TCA cycle
Matrix acetyl-Coenzyme A ($[ACCOA]_x$)	An energized form of coenzyme A which may with oxaloacetate produce citrate, the 'first step' of the TCA cycle
Matrix Citrate ($[CIT]_x$)	An intermediate in the TCA cycle
Matrix Isocitrate ($[ICIT]_x$)	An intermediate in the TCA cycle
Matrix Alphaketogluterate ($[AKG]_x$)	An intermediate in the TCA cycle
Matrix succinyl-Coenzyme A ($[SCOA]_x$)	An intermediate in the TCA cycle, that again uses the cofactor coenyme A
Matrix coenzyme A ($[COASH]_x$)	Unbound coenzyme A that may be used in multiple processes previously mentioned
Matrix Succinate ($[SUC]_x$)	An intermediate in the TCA cycle that will be discussed at length in Chapter 4
Matrix Fumerate ($[FUM]_x$)	An intermediate in the TCA cycle
Matrix Malate ($[MAL]_x$)	An intermediate in the TCA cycle

Matrix Oxaloacetate ($[OAA]_x$)	An intermediate in the TCA cycle
Matrix Glutamate ($[GLU]_x$)	An amino acid that may contribute to the TCA cycle
Matrix Aspartate ($[ASP]_x$)	An amino acid that may contribute to the TCA cycle
Matrix Oxygen ($[O_2]_x$)	Oxygen, which is consumed at several points in mitochondrial respiration
Matrix Carbon Dioxide ($[CO_2tot]_x$)	A biproduct of oxygen consumption
Intermembrane Reduced Cytochrome C ($[Cred]_i$)	An electron carrier that is reduced by Complex III and oxidized by Complex IV
Intermembrane Adenosine Triphosphate ($[ATP]_i$)	An adenosine nucleoside that is being transported to the cytosol for consumption
Intermembrane Adenosine Diphosphate ($[ADP]_i$)	An adenosine nucleoside that is being transported to the matrix for the production of ATP
Intermembrane Adenosine Monophosphate ($[AMP]_i$)	An adenosine nucleoside found in the intermembrane space
Intermembrane Inorganic Phosphate ($[PI]_i$)	Phosphate used in reactions involving nucleosides
Intermembrane Pyruvate ($[PYR]_i$)	Pyruvate from the cytosol that is transported for consumption in the matrix
Intermembrane Citrate ($[CIT]_i$	External citrate that may be used by the mitochondrion
Intermembrane Isocitrate ($[ICIT]_i$)	External isocitrate that may be used by the mitochondrion
Intermembrane Alphaketogluterate ($[AKG]_i$)	External alphaketogluterate that may be used by the mitochondrion
Intermembrane Succinate ($[SUC]_i$)	External succinate that may be used by the mitochondrion
Intermembrane Fumerate ($[FUM]_i$)	External fumerate that may be used by the mitochondrion
Intermembrane Malate ($[MAL]_i$)	External malate that may be used by the mitochondrion
Intermembrane Glutamate ($[GLU]_i$)	External glutamate, an amino acid, that may be used by the mitochondrion
Intermembrane Aspartate ($[ASP]_i$)	External aspartate, an amino acid, that may be used by the mitochondrion
Cytosolic Adenine Triphosphate ($[ATP]_c$)	An adenosine nucleoside that is used as a fuel by the cell in the cytosol
Cytosolic Adenine Diphosphate ($[ADP]_c$)	An adenosine nucleoside that may be turned into ATP in the mitochondrion

Cytosolic Adenine Monophosphate ($[AMP]_c$)	An adenosine nucleoside that may be phosphorylated to ADP
Cytosolic Inorganic Phosphate ($[PI]_c$)	Phosphate that may be used in reactions involving adenine nucleosides
Cytosolic Pyruvate ($[PYR]_c$)	Pyruvate that is transported for consumption in the mitochondrial matrix
Cytosolic Citrate ($[CIT]_c$)	Extramitochondrial citrate that may be used by the mitochondrion
Cytosolic Isocitrate ($[ICIT]_c$)	Extramitochondrial isocitrate that may be used by the mitochondrion
Cytosolic Alphaketogluterate ($[AKG]_c$)	Extramitochondrial alphaketogluterate that may be used by the mitochondrion
Cytosolic Succinate ($[SUC]_c$)	Extramitochondrial succinate that may be used by the mitochondrion
Cytosolic Fumerate ($[FUM]_c$)	Extramitochondrial fumerate that may be used by the mitochondrion
Cytosolic Malate ($[MAL]_c$)	Extramitochondrial malate that may be used by the mitochondrion
Cytosolic Glutamate ($[GLU]_c$)	Extramitochondrial glutamate, an amino acid, that may be used by the mitochondrion
Cytosolic Aspartate ($[ASP]_c$)	Extramitochondrial aspartate, an amino acid, that may be used by the mitochondrion
Phosphocreatine ($[PCr]_c$)	An extra reserve of energy that may be converted into ATP during periods of high metabolic demand

Table 2.12: State variables included in our model.

2.6 List of Significant Parameters

Parameter	Units	Brief Description
X_{PDH}	M^4/s	Pyruvate dehydrogenase activity
X_{CITS}	M/s	Citrate synthase activity
X_{ACON}	M/s	Acontinase activity
X_{ISOD}	M/s	Isocitrate dehydrogenase activity
X_{AKGD}	M/s	Alphaketogluterate dehydrogenase activity
X_{SCOAS}	M/s	Succinyl-CoA synthetase activity
X_{SDH}	M/s	Succinate dehydrogenase activity
X_{FUM}	M/s	Fumarase activity
X_{MDH}	M/s	Malate dehydrogenase activity
X_{NDK}	M/s	Nucleoside diphosphokinase activity
X_{GOT}	M/s	Glutamaete oxaloacetate transaminase activity
X_{GDH}	s^{-1}	Glutamate dehydrogenase activity
X_{PYRH}	M/s	Pyruvate-hydrogen cotransporter activity
X_{GLUH}	M/s	Glutamate-hydrogen cotransporter activity
X_{CITMAL}	M/s	Citrate-Malate exchange transporter activity
X_{AKGMAL}	M/s	Alphaketogluterate-Malate exchange transporter activity
X_{MALPI}	M/s	Malate-Phosphate exchange transporter activity
X_{ASPGLU}	M/s	Aspartate-Glutamate exchange transporter activity
X_{SUCMAL}	M/s	Succinate-Malate exchange transporter activity
X_{HK}	M/s	Hexokinase activity
X_{CI}	M/s	Complex I activity
X_{CIII}	M/s	Complex III activity
X_{CIV}	M/s	Complex IV activity
X_{ATP}	M/s	Complex V/ATPase/ATP Synthase activity
X_{ANT}	M/s	Adenine nucleotide translocase activity
X_{PIHt}	M/s	Phosphate-hydrogen co-transporter activity
k_{PiH}	M	Phosphate-hydrogen regulative parameter
X_{KH}	M/s	Potassium-hydrogen antiport activity
$P_{H,\ leak}$	s^{-1}	Hydrogen leak permeability
$k_{Pi,1}$	M	Determines the dependence of Complex III on phosphate, producing a more sensitive dependence
$k_{Pi,2}$	M	Determines the dependence of Complex III on phosphate, producing a less sensitive dependence
W_x	(L water)/(L matrix)	Mitochondrial matrix water fraction

W_i	(L water)/(L intermembrane space)	Mitochondrial intermembrane space water fraction
W_c	(L water)/(L cytoplasm)	Cytosolic water fraction
Ctot	M	Total concentration of reduced and oxidized cytochrome C in intermembrane space
Qtot	M	Total concentration of reduced and oxidized coenzyme Q in mitochondrial matrix
NADtot	M	Total concentration of reduced and oxidized NAD^+/NADH in mitochondrial matrix
FADtot	M	Total concentration of reduced and oxidized FAD^{2+}/$FADH_2$
k_{O2}	M	Oxygen affinity of Complex V
k_{mADP}	M	ADP affinity of Complex V
$P_{K,\ leak}$	s^{-1}	Potassium leak permeability
$Q_{ATP,\ max}$	M/s	Maximal ATP consumption
K_{mATP}	M	K_m for ATP consumption
V_{Glyc}	M/s	Maximal Glycolytic ATP production
K_{mGlyc}	M	K_m for glycolytic ATP production
K_{CK}	M^{-1}	Creatine kinase equilibrium constant
γ	μm^2	Outer membrane area per mitochondrial volume
ρ_m	(mg prot) / (L mito)	Protein density of mitochondria
V_{mito}	(L mito)/(L cell)	Mitochondrial volume fraction
V_{cyto}	(L cyto)/(L cell)	Cytoplasmic volume fraction
n_A	Unitless	Stoichiometry for hydrogen ion transport by Complex V
p_{PI}	μm/s	Permeability of outer membrane to inorganic phosphate
p_A	μm/s	Permeability of outer membrane to nucleotides
$k_{m,\ ADP}$	M	ANT Michaelis-Menten constant
θ	Unitless	ANT kinetic parameter
β	M	Matrix buffering capacity
C_{IM}	mol/(L mito mV)	Capacitance of inner membrane for electrical potential gradient

B_x	M	Matrix buffering parameter
K_{Bx}	M	Matrix buffering parameter

Table 2.13: Adjustable parameters of the model that are fitted in previous work or estimated below [193]. In each reaction expression where there is a V_{mf} and V_{mr} term, the V_{mf} (or forward reaction) term is the associated activity, and V_{mr} may be calculated as explained in the relevant section above.

2.7 List of Physical Parameters

Physical Parameter	Value	Units	Brief Description
RT	2.5775	kJ/mol	Gas constant times temperature
F	0.096484	kJ/(mol mV)	Faraday's constant

Table 2.14: Non-adjustable physical constants used in our model.

Chapter 3

A Mathematical Model of Mitochondria in Proximal Tubule and Thick Ascending Limb Cells

3.1 Introduction

The choice to focus on the proximal tubule (PT) and medullary thick ascending limb (mTAL) in the nephron is motivated by the study of chronic kidney disease (CKD) and diabetic nephropathy. The large active transport requirements of the PT are a source of stress. The PT accounts for two thirds of sodium reabsorption by the kidney, done mostly via active transport [103]. The work of Edwards et al. [44] that we build on here suggests that the efficiency of cellular respiration in the kidney is reduced by diabetes, suggesting that could be a cause of diabetic nephropathy. Furthermore they suggest that a class of diabetes medications that target the kidney, SGLT-2 inhibitors, could worsen the nephropathic effects of diabetes. The model includes chemical kinetics for pyruvate oxidation, the Krebs cycle, and oxidative phosphorylation, as well as a phenomenological description of the consumption of ATP, an important fuel for the cell. We examine the robustness of the PT in the kidney in light of this large metabolic demand, in response to known stressors upon the PT.

The outer medullar part of the thick ascending limb of the loop of Henle (mTAL) is notable for its contribution to acute kidney injury (AKI) especially brought on by hypoxemia, such as is observed in septic shock [24, 47]. The medulla of the kidney has low tissue oxygen tension but plays a large role in active sodium transport [176], and hypoxemia is more likely to translate into hypoxia in the outer medulla of the kidney due to the inelasticity of its blood supply compared to the renal cortex [47]. Of the nephron segments that are largely in the outer medulla, the mTAL plays the largest role in active reabsorption, and so is at risk due to its high metabolic demand. For this reason, the best way to extend *in silico* methods for studying renal hypoxia to a wider range of cases is to extend them to cover the

thick ascending limb in the outer medulla. There is some modelling work on the mTAL, that suggests that the oxygen consumption is more efficient in the mTAL than its active sodium transport activity would suggest, and that this is why the mTAL is robust in the face of its lower baseline oxygen tension [201]. In that paper they hypothesize that this greater efficiency may be due to greater reliance on anaerobic respiration, which we will consider *in silico* using estimates of glycolysis activity in the mTAL. The manner in which the mTAL maintains its active sodium transport activity remains a matter of significant experimental interest with many partial explanations but none that seem conclusive [158].

There are three classes of question that we wish to address in this work. First, the comparative questions: a published *in silico* study on PT mitochondrial function has found that oxygen tension is not rate limiting in the renal cortex for ATP production [44], we compare this to the outer medulla, where lower baseline oxygen tension means that hypoxia may be more extreme. And relatedly, in line with the predictions of Zhang and Edwards [201] that ATP production should be more efficient in the mTAL, we wish to consider the ratios of ATP Synthase mediated ATP generation to Complex IV mediated oxygen consumption, i.e. the P/O ratios (Phosphate/Oxygen ratio), in the PT and mTAL in order to examine their relative efficiencies.

The second kind of question that we hope to answer in this work is about the mTAL itself. The mTAL is known to be subject to greater degrees of hypoxia *in vivo* in the rat under baseline conditions [158], and it is believed that this plays a role in the onset of AKI. Aside from comparative questions mentioned before about its relative robustness, we can directly predict the mitochondrial matrix oxygen tension threshold under which the mTAL will experience hypoxic injury. Evans et al. [47] and Calzavacca et al. [24] report tissue oxygen tensions for various states of hypoxemia and/or shock in the medulla and cortical regions of the kidney in sheep. They find that the kidney might maintain relatively consistent overall oxygenation under ordinary circumstances but during sepsis, renal blood flow was diverted to the cortex over the medulla, and that the outer medulla experienced hypoxia [24]. This accords well with Ma et al. [119] who suggest that septic AKI overall is a disease due to local tissue ischemia. Simulations of the mTAL could address what partial pressures of oxygen tension are required to actually produce pathological tissue hypoxia.

The third kind of question I'll point to is how the PT and mTAL respectively respond to pathological circumstances, in particular to diabetes, electrolyte or pH imbalance, ischemia-reperfusion cycles, drug-use, and mitochondrial disease, along with the aforementioned hypoxia. Some of this work has been done for the PT although not all; for instance uncoupling and pH imbalance were examined in Edwards et al. [44] for the PT. For this reason, this work is not just useful as an exercise in comparison, but also will break new ground in the study of the PT and the mTAL in diseased states.

Edwards et al. examine the effects of diabetes on mitochondria in the kidney by increasing the rate of mitochondrial uncoupling, or proton leak across the inner membrane of the mitochondria. Friederich-Persson et al. [55] suggests that the deletion of UCP-2 completely prevents uncoupling in the diabetic kidney, and eliminates hypoxia (although increasing

oxidative stress). This suggests that we should expect uncoupling to produce significant increases in oxygen consumption in the kidney, which we can test with our model. Since the mTAL is hypothesized by Zhang and Edwards [201] to compensate for low oxygen levels with high efficiency, and proton leak reduces this efficiency, it is possible that diabetic nephropathy could trigger hypoxia in the mTAL. To determine whether diabetes may produce hypoxia, it would be necessary to simulate comparable mitochondrial uncoupling in the PT (which is done already by Edwards et al. [44]) and mTAL.

Mitochondrial disease are understood to have a large role in numerous diseases [155] but have not been captured in previous work using the model adapted here. Key questions in the study of mitochondrial disease revolve around the interactions between dysfunctions of different complexes in the electron transport chain, because it is widely observed that epistatic effects play a large role in mitochondrial disease. A question we wish to address is how ATP production is impacted by different combinations of dysfunctions in the electron transport chain. *In vivo* work on mitochondrial disease mechanism is difficult and suffers from the substantial heterogeneity of mitochondrial disease that makes generalizations difficult [1]. Thus *in silico* work may serve as a welcome supplement to experimental work. For instance, it could identify potential therapeutic targets for therapies in the cases of different combinations of electron transport chain defects. This may be done by seeing which electron transport chain component's recovery would lead to the greatest recovery of ATP concentration. As a side question, since there is known to be substantial heterogeneity in how distinct tissues are impacted by mitochondrial disease [1], it is worthwhile to see if there are substantial differences between the impact of mitochondrial diseases in the PT and the mTAL.

Ischemia-reperfusion injury has been a major subject of research for those interested in mitochondrial dynamics in the kidney [71]. Transplantation often requires that the donor kidney is not perfused for an extended period of time, but in that case, the kidney may become injured upon reperfusion. More precisely, delayed graft function incidence among kidney transplant recipients is roughly 21% [180] and delayed graft function is understood to be the principle manifestation of ischemia-reperfusion injury. A frequently suggested explanation of this phenomenon is that reperfusion leads to the sudden generation of reactive oxygen species, which, arriving in a pulse, cause significant oxidative damage to the cell. These reactive oxygen species may also be produced before the cell can produce adequate antioxidants to respond to the generation of reactive oxygen species. A helpful starting point for testing these hypotheses is measuring the redox state of the electron transport chain and the proton motive force during reperfusion. Addressing this question would have implications beyond transplantation, because as discussed above, ischemia might be a hallmark of septic AKI as well [119].

3.2 Methods

3.2.1 Adjustments to the Model

ATP consumption is treated as independent of the system's state by the previous model [44]. This assumption was justified there by the necessity of reabsorbing a large portion of ions from the glomerular filtrate, the necessary level of reabsorption is relatively inelastic. But even if ion reabsorption is necessary, it is still sensitive to ATP levels in the cell, and so cannot be entirely inelastic. For this reason, it is reasonable to choose Michaelis-Menten dynamics for the cell's ATP consumption (Q_{ATP}), i.e.

$$Q_{\text{ATP}} = Q_{\text{ATP, max}} \frac{[ATP]_c}{K_m + [ATP]_c} \tag{3.1}$$

To make the model comparable to the previous model, $Q_{\text{ATP, max}}$ was chosen so that the ATP consumption was the same at the previous model's predicted equilibrium (1.57×10^{-3} M/s in the PT, 2.125×10^{-3} M/s in the mTAL). K_m was chosen to equal the K_m of Na-K-ATPase because of its major part in ATP consumption in PT and mTAL cells. The value for K_m is taken from Vrbhar, Javorkovam, and Pechanova [184], which models ATP consumption by Na-K-ATPase with Michaelis-Menten dynamics. The K_m is below baseline ATP concentrations at 1.49 mM. This equation is also discussed above in Section 2.4.

3.2.2 Model Parameters

Most parameters were chosen based on existing experimental estimates. Some were estimated in non-specific kidney tissue when more specific measurements were unavailable. The results are collected in Table 3.1.

The parameter estimates for the proximal tubule were taken from Edwards et al. [44]. The values for both the PT and mTAL of the fractional mitochondrial volume come from Pfaller and Rittinger [138]. Pfaller and Rittinger give estimates for the mTAL in both the inner and outer stripe of the outer medulla. For the former they estimate the mitochondrial volume fraction to be 0.32, and for the latter, 0.23. The same paper gave us cytoplasm volume fraction estimates for both the PT and mTAL [138]. While it was not possible to find cytoplasm water fraction estimates for the mTAL specifically, estimates from across organs, including in a kidney epithelial cell line, have found comparable estimates of roughly 0.77 [62]. This estimate is now a widely shared assumption in studies of cytoplasmic concentrations, including in the kidney [105, 172]. The cytoplasm water fraction may change under hyper/hypotonic conditions or when the cell is growing. Values for mitochondrial water fraction were not forthcoming for the mTAL, and the mitochondrial water fraction did vary significantly between tissues, and so we considered a range chosen to encompass known estimates in other tissues, including the PT [105, 172, 178]. We found that the cell's state

Parameter	Values for PT	Values for TAL
Fractional Mitochondrial Volume (L mito/L cell)	0.25	0.23-0.32*
Fractional Cytoplasmic Volume (L cyto/L cell)	0.72	0.59-0.66*
Cytoplasm Water Fraction (L water/L cyto)	0.77	0.77
Mitochondria Water Fraction (L water/L mito)	0.659	0.58-0.66**
Protein density of Mitochondria (mg protein/L mito)	3.274×10^{5}†	3.274×10^{5}†
Matrix NADH/NAD^{+} concentration (mmol/L matrix)	8.24×10^{-4}	8.24×10^{-5}‡
Matrix concentration of co-enzyme Q (mmol/L matrix)	2.15×10^{-3}†	2.15×10^{-3}†
Intermembrane concentration of Cytochrome C (mmol/L IM)	1.96×10^{-3}†	1.96×10^{-3}†
Kidney-to-heart Ratio Complex I	0.75†	0.75†
Kidney-to-heart Ratio Complex III	0.5†	0.5†
Kidney-to-heart Ratio Complex IV	0.25†	0.25†

Table 3.1: The parameters used in the model where we had to find parameter estimates. The single-starred ranges represent physiological ranges rather than parametric uncertainty. There are large differences between the inner and outer slice of the outer medulla (often much larger than the standard error interval). We use the higher end of the range for the mTAL's fractional mitochondrial volume and lower end of the range for the fractional cytoplasmic volume, representing the more hypoxic inner slice of the outer medulla. The double-starred ranges represent values chosen to deliberately cover a wide range. The daggers represent values estimated on non-specific kidney tissues. Value marked with a double dagger were fitted rather than chosen based on estimates from the literature. References and further discussion of parameter choices can be found in Section 3.2.2 and 3.2.3.

was not sensitive to the mitochondrial water fraction and so we used the same value as for the PT. The cytosolic magnesium, hydrogen, and potassium ion concentrations in the mTAL are chosen from experimental estimates, but they are the same as in the PT due to significant uniformity in the cytosolic concentrations of these ions [145, 188, 141, 142]. None of

our measurements of cytosolic free magnesium have been done in rats in the thick ascending limb, although the measurements found in other species all agree with 0.5 mM estimate that we use [141, 142].

The maximal mTAL ATP consumption was chosen so that at typical ATP concentrations (2.5 mM) the cell's cytoplasmic ATP consumption is comparable to mTAL ATP metabolic demand that is observed from experimental measurements of ATP consumption. Experimentalists have observed 0.64 pmol ATP consumption per second per mm of mTAL [181]. We can calculate the cytoplasmic ATP consumption using the epithelial cell volume per millimeter of tubule of 566 x 10^3 μm^3 per mm of tubule [18] and a cytoplasmic volume fraction of 0.60 in the epithelial cell [138]. Using these values, we find an ATP consumption of 1.70 mM/s in the cytoplasm. By considering the typical baseline cytosolic ATP concentration of roughly 2.5 mM, this allows us to estimate that the maximal ATP consumption should be 2.13 mM/s.

The remaining parameters taken from the literature were for non-specific kidney tissues, often studied for the purpose of studying physiological diversity across organ systems. These estimates are used for the PT and the mTAL. The protein density of mitochondria was estimated by Schmitt et al. [160] for the kidney. The ratio of the activity of Complex I between the kidney and heart is taken from Yu et al. [197]. Complex III and Complex IV ratios between the kidney and the heart, as well as matrix concentrations of co-enzyme Q and intermembrane concentrations of Cytochrome C in the kidney are taken from Benard et al. [13].

	Experimental Values	Predicted Values
State 3 O_2 Consumption (nmol O_2 mg^{-1} s^{-1})	4.08 ± 0.6	3.78
Respiratory Control Ratio	8.5 ± 0.9	7.36
Leak Respiration (nmol O_2 mg^{-1} s^{-1})	0.37 ± 0.06	0.52
P/O Ratio	1.8 ± 0.1	1.98
Fold Change in dPsi due to Nigericin	1.05	1.06

Table 3.2: Predictions from fitting experimental measurements in isolated mitochondria from the PT in Sciffer et al. [156] and perfused PT in Feldkamp et al [49].

	Experimental Values	Predicted Values
Respiratory Control Ratio	10.0±1.6	10.43
P/O Ratio	1.93±0.13	1.99

Table 3.3: Predictions from fitting experimental measurements in isolated mitochondria from the mTAL taken from Schiffer, Gustafsson, and Palm [158].

Fitted Parameter	Value in PT	Value in mTAL
$P_{H,leak}$ (s^{-1})	922	595
$P_{K,leak}$ (s^{-1})	5.35 x 10^{-4}	3.45 x 10^{-4}
k_{O2} (M)	1.32 x 10^{-4}	6 x 10^{-5}
X_{KH} (M/s)	412360	317200
X_{ANT} (M/s)	6.75 x 10^{-3}	5.06 x 10^{-3}

Table 3.4: Parameters fitted in the PT and mTAL.

3.2.3 Model Parameter Fitting

Our model fitting relied on several data sources, namely State 3 respiration, leak respiration, respiratory control ratio, and P/O ratio estimates for the PT [156], P/O ratio and respiratory control ratio for the mTAL [158], and measurements of the response in electrical potential gradient to nigericin in the PT [49]. We use the BFGS algorithm to find an appropriate parameter set (in a five-dimensional parameter space), penalizing divergence from the experimental measurements of the above parameters. We compute the difference between the average of the experimental measurements and our predicted value, divided by the standard deviation of the experimental measurements, squared. Then the objective function is the sum of these squares, plus an extra penalty if the P/O ratio was lower in the mTAL than in the PT (using the difference of the PT and mTAL P/O ratios multiplied by a constant of one hundred, chosen to give it comparable weight to other costs). We allowed the adenine nucleotide translocase (X_{ANT}, see Equation 2.128), potassium-hydrogen antiporter (X_{KH}, see Equation 2.130), hydrogen & potassium leak permeabilities ($P_{\mathrm{H,\,leak}}$ and $P_{\mathrm{K,\,leak}}$, see Equations 2.138 and 2.139), and Complex IV oxygen affinity (k_{O2}, see Equations 2.123) to vary. The most significant change to these parameters was to the potassium-hydrogen antiporter, which is an order of magnitude lower in our model relative to Edwards et al. [44]. The experimental and fitted values from the above fitting may be found in Tables 3.2 and 3.3. The $NADH/NAD^+$ pool size in the mTAL was also lowered in this model based on measurements of the $NADH/NAD^+$ ratio by Hall et al. [70] because we did not have direct experimental measurements of the $NADH/NAD^+$ ratio. The other experimental measurements considered are not sensitive to the $NADH/NAD^+$ pool size and so this does not affect our other results.

3.2.4 Simulations

All simulations discussed below consider an *in vivo* case for our model, the State 3 respiration, leak respiration, respiratory control ratio, and P/O ratio discussed in the previous section were predicted using a different model structure that nevertheless shares most model equations (see the discussion in Chapter 2).

Comparative Questions and Questions about the mTAL

We consider a range of values for several cytosolic ion concentrations, hydrogen & potassium leak permeabilities ($P_{\mathrm{H,\,leak}}$ and $P_{\mathrm{K,\,leak}}$, see Equations 2.138 and 2.139), and the maximal ATP consumption in the mTAL ($Q_{\mathrm{ATP,\,max}}$, see Section 2.4). This work serves as a counterpart to work already done for the PT [44], which we reproduce with our refitted model. A full list of considered cases for both the PT and mTAL may be found in Tables 3.6 and 3.7.

Pathological States

Three pathological states are noted above: mitochondrial disease, ischemia-reperfusion injury, and diabetes. Renal Fanconi Syndrome (PT-specific kidney injury) can be caused by mitochondrial disease, often related to a dysfunction of Complex I [3] and especially in pediatric patients. Mitochondrial diseases for the most part impact oxidative phosphorylation, exceptions include impaired mitochondrial biogenesis [2], and so may be represented by reduced activity in the complexes in the inner membrane of the mitochondrion. Specifically we reduce the activity of any combination of Complex I, III, IV, and F_0F_1-ATPase (that is, X_{CI}, X_{CIII}, X_{CIV}, and X_{F1}, see Section 2.2) by increments of a quarter to as low as a quarter of normal activity.

Ischemia-reperfusion injury is examined here by modelling an extended phase of hypoxia (0 mmHg oxygen tension) followed by reoxygenation, with an adenine nucleotide pool 30% of its typical size (that is the concentration of each adenine nucleotide is lowered by 30%), matching the results of Cunningham, Keaveny, and Fitzgerald [34].

Aside from OXPHOS dysfunction, we also consider hypoxia and uncoupling. For hypoxia, we consider reductions in the mitochondrial oxygen tension by tenths to as low as 10% of typical. In the PT the most extreme case considered was an oxygen tension of 5 mmHg and in the mTAL the most extreme case considered was 1 mmHg. For uncoupling (motivated by the study of diabetes, which will be discussed at length in Chapter 5), we consider by default a range of n-fold increases in hydrogen leak activity from twice normal to ten times normal.

Drug Actions

Many cancer drugs and antibiotics directly or indirectly affect cellular respiration. Where their mechanism is well-understood we may estimate the impact of those drugs on cellular respiration, which ultimately helps us better understand how to alleviate the side-effects of those drugs. In particular, drug-induced Fanconi syndrome is associated with mitochondrial dysfunction on both biochemical and histological evidence [69]. We systematize the understanding of these drug actions by a sensitivity analysis of the relevant parameters.

Here we discuss where known effects of different drugs, as recorded in Table 3.5, were found. The value for how ifosfamide affects Complex I activity is taken from Nissim et

Compound	Parameter(s) Affected	Known effect	Indications for Use
Ifosfamide	X_{CI}	55% reduction	Cancer
Gentamicin	X_{CI}, X_{CIII}, X_{CIV}, X_{F1}, $P_{H,leak}$	OXPHOS reductions like those described above (see Section 3.2.4), $P_{H,leak}$ increased 1.15-, 2-, 5-, or 10-fold	Antibiotic
Salicylate	$P_{H,leak}$	$P_{H,leak}$ increased 1.15-, 2-, 5-, or 10-fold	Analgesia, anti-inflammatory
NRTIs/NtRTIs	X_{CI}, X_{CIII}, X_{CIV}, X_{F1}	OXPHOS reductions like those described above (see Section 3.2.4)	Anti-virals
Dichloroacetate	K_{iNADH}	A 1.15- or 2-fold increase	Cancer

Table 3.5: The parameters that we studied to examine the effects of a drug on mitochondrial respiration. Unless otherwise noted, the parameters are the same as those noted in the appendix to Wu et al. [193]. Where the scale of the effect is not known, a range was considered. Indications for use are taken from Hall, Bass, and Unwin [69]. Dichloroacetate is not known to be nephrotoxic and was instead studied in combination with other drugs.

al. [132]. The mechanism for gentamicin is through an uncoupling effect and inhibition of magnesium-dependent components of oxidative phosphorylation, which is chiefly via F_0F_1-ATPase [140, 189]. Salicylate, a biproduct of aspirin, is a known uncoupler [122]. Nucleoside(/Nucleotide) reverse transcriptase inhibitors (NRTIs/NtRTIs) like tenofovir impact mitochondrial DNA replication by targetting mitochondria-specific DNA polymerases, this primarily causes general OXPHOS dysfunction like in mitochondrial disease [110].

Dichloroacetate is a cancer drug that is used to switch cells towards aerobic over anaerobic respiration, contrary to the Warburg effect which is cancer's natural tendency to prefer anaerobic respiration even in the presence of oxygen [174]. Dichloroacetate accomplishes this by preventing pyruvate dehydrogenase kinase from downregulating pyruvate dehydrogenase activity, a key step in pyruvate oxidation. Recent work has examined the possibility of dichloroacetate having renal protective effects in combination with mitotoxic agents such as the uncoupler 2,4-dinitrophenol, an illicit "slimming" drug, with encouraging results [58] and with cisplatin, a cancer drug known to cause Fanconi syndrome [59, 69]. We simulate the combination of dichloroacetate with the previously mentioned drugs to predict whether it may protect against their nephrotoxic effects.

	O_2 Consumption (nmol O_2 mg^{-1} s^{-1})	ATP Generation (nmol ATP mg^{-1} s^{-1})	P/O	Electrical Potential Gradient (mV)	Proton Motive Force (PMF, mV)	$[ATP]_c$ (mM)	$[ATP]_c/[ADP]_c$
Base Case							
P_{O2} = 50mmHg pH_c = 7.20	2.52	9.93	1.97	158.00	165.67	2.30	5.69
P_{O2} Variation							
P_{O2} = 60mmHg	2.53	9.96	1.97	158.23	166.03	2.31	5.89
P_{O2} = 40mmHg	2.51	9.89	1.97	157.67	165.17	2.28	5.40
P_{O2} = 20 mmHg	2.45	9.68	1.97	156.23	163.01	2.15	4.18
P_{O2} = 10mmHg	2.31	9.08	1.97	153.90	159.65	1.85	2.59
$Q_{ATP,max}$ Variation							
$Q_{ATP,max}$ x 0.75	2.00	7.61	1.90	157.73	166.63	2.45	8.89
$Q_{ATP,max}$ x 1.25	2.91	11.67	2.01	158.43	165.06	1.97	3.07
$Q_{ATP,max}$ x 1.50	3.12	12.59	2.02	158.78	164.79	1.56	1.79
pH_c Variations							
pH_c = 7.40	2.33	9.36	2.01	153.81	165.42	1.98	3.13
pH_c = 7.00	2.66	10.15	1.91	160.15	164.98	2.45	8.73
pH_c = 6.80	2.79	10.20	1.83	160.40	163.32	2.51	11.15
$[K^+]_c$ Variations							
$[K^+]_c$ = 60mM	2.55	10.09	1.98	174.77	167.37	2.39	7.33
$[K^+]_c$ = 140mM	2.50	9.78	1.96	151.38	164.69	2.21	4.68
$[Mg^{2+}]_c$ Variations							
$[Mg^{2+}]_c$ = 0.2mM	2.49	9.80	1.97	158.01	165.72	2.23	4.73
$[Mg^{2+}]_c$ = 0.8mM	2.55	10.07	1.97	157.99	165.62	2.38	7.16
Variations in H^+ and K^+ leak permeability							
No leaks	2.26	10.18	2.25	169.10	167.75	2.38	7.04
No H^+ leak	2.41	10.00	2.07	158.21	166.00	2.31	5.88
No H^+ leak, 10x K^+ leak	2.04	5.61	1.37	112.60	157.66	0.82	0.79
No K^+ leak, 10x H^+ leak	3.51	9.40	1.34	166.01	164.22	2.23	4.87
10x H^+ leak	3.44	9.31	1.35	156.41	163.19	2.17	4.28
10x K^+ leak	2.08	5.55	1.33	112.58	157.52	0.82	0.78
10x Leaks	2.44	5.06	1.04	112.42	156.40	0.75	0.72

Table 3.6: Several key intracellular quantities and their sensitivities to various parameter changes in the mitochondria in the proximal tubule.

3.3 Results

3.3.1 Baseline Results for the Proximal Tubule

Table 3.6 includes some baseline numbers and the sensitivity to changes in multiple quantities, both parameters and states for the PT. We consider several predicted values related to both fluxes in the mitochondria and states of the system. Oxygen consumption was predicted to be 2.52 nmol O_2 mg^{-1} s^{-1}, and at the same time there was ATP generated at a rate of 9.93 nmol (mg prot)$^{-1}$ s^{-1} by ATP Synthase. Together these numbers underlie the P/O ratio *in vivo* which was found to be 1.97. Known estimates of the P/O ratio for the kidney range from 1.7-2 *in vivo* [54] to 2.5 in the perfused kidney [53], while these are for the whole kidney, they include our estimate of 1.97. Further the concentration of ATP was predicted to be 2.30 mM, the ATP/ADP ratio was found to be 5.69, and the proton motive force across the inner membrane was predicted to be 166 mV, which together give an account of the cell's energetic state. These are key variables for which we have experimental results to which to compare, the typical range of proton motive force is from 170 to 200 mV [42]. The mitochondrial electrical potential gradient was predicted to be 158 mV, in the interior of known range from 150 to 180 mV [20]. Typical measured ranges for the concentration of ATP vary widely from 1.3 to 2.8 mM [40, 107]. The ATP/ADP ratio has been measured to be roughly 9 in mice renal cortex [198], however Zager notes that the ratio is extremely variable. Results from others for the rat renal cortex indicate the ratio may be as low as 3, based on independent calculation of the ATP/ADP ratio [76]. Thus a value of 5.69 is within a plausible range for the ATP/ADP ratio. We see that the proton motive force is close to our predicted value, the predicted ATP concentration is in the middle of the possible range, and measured ATP/ADP ratios and electrical potential gradient appear to allow for our prediction. These results for the PT are relatively similar to the values found by Edwards et al. [44]. The proton motive force and the ATP/ADP ratio predictions differ most from the predictions of Edwards et al. (Edwards et al. predict a proton motive force of 173 mV and an ATP/ADP ratio of 10.94), but the latter is very variable as previously mentioned. The latter was found to be sensitive to the parameter variations considered in Table 3.6. Unlike in Edwards et al. [44], we see that less cytosolic potassium leads to greater oxygen consumption, this is due in our model to a greater hydrogen gradient, with less of the proton motive force being shunted into electrical potential gradient. The combined lower potassium concentration and lower activity of the potassium-hydrogen antiport leaves the hydrogen gradient higher across the inner membrane, stimulating oxidative phosphorylation.

Across all simulations considered, the P/O ratio or efficiency of the cell was most sensitive to hydrogen and potassium leaks. These sensitivity cases were significant because the mitochondrion's ion leak activity was highly uncertain. Greater leak decreased efficiency, a tenfold increase in both leaks reduced the P/O ratio to 1.04 (see the last row of Table 3.6), the lowest predicted for the PT, primarily via decreased ATP generation. In the absence of any leak, the P/O ratio was 2.25 (see the first row of the last block of Table 3.6).

The greatest factors controlling oxygen consumption were maximal ATP consumption ($Q_{ATP,max}$) and hydrogen leak (the third and last blocks in Table 3.6 include these numbers). The greatest oxygen consumption predicted was 3.51 nmol mg^{-1} s^{-1} when potassium leak was zero and hydrogen leak was increased tenfold. At 3.12 nmol per milligram per second, we see that a 1.5 fold increase maximal ATP consumption also increases the oxygen consumption substantially.

The proton motive force was insensitive to most changes, aside from leak permeability changes. The largest proton motive force was found to be 166 mV in the absence of leak, and when both potassium and hydrogen leak were increased tenfold the proton motive force was found to be 156 mV.

The cytosolic potassium and potassium leak (see the fifth and last blocks of Table 3.6) are impactful on ATP generation, ATP concentration, and the ATP/ADP ratio as well. The lowest ATP generation is 5.06 nmol ATP per milligram per second, the lowest cytosolic ATP concentration is 0.75 mM, and the lowest ATP/ADP ratio is 0.69, all in the case where potassium and hydrogen leaks are both increased tenfold. Results for tenfold increased potassium leak alone are comparable. The maximal ATP generation grows with maximal ATP consumption, for a 1.5-fold increase in maximal ATP consumption, the ATP generation grows by 25% and for 75% of the typical ATP generation, we see ATP generation go down by roughly the same amount.

3.3.2 Baseline Results for the medullary Thick Ascending Limb of the Loop of Henle

Table 3.7 includes some key baseline predictions and the model sensitivity to changes in multiple quantities, both parameters and states for the mTAL, analogous to those for the PT above. The oxygen consumption was predicted to be 2.35 nmol O_2 mg^{-1} s^{-1}, compared to ATP generated at a rate of 9.59 nmol (mg prot)$^{-1}$ s^{-1} (or 1.0 mmol (L cell)$^{-1}$ s^{-1}) by ATP Synthase. Together these numbers get us the P/O ratio *in vivo* which was found to be 2.04. This is slightly below whole kidney P/O measurements noted before for the perfused kidney [53], but on the higher range of *in vivo* values, as expected for the medullary thick ascending limb [54]. On the other hand, in isolated mitochondria we predict a P/O ratio of 1.99, slightly above the experimentally measured ratio of 1.93 [158]. The concentration of ATP was predicted to be 2.45 mM, the ATP/ADP ratio was predicted to be 8.66, and the proton motive force was predicted to be 169 mV. The electrical potential gradient was predicted to be 162 mV. Once again these values compare favourably with measurements for the kidney. As previously mentioned previously, typical ranges for the concentration of ATP go from 1.3 to 2.8 mM [107, 40]. Once again our predicted ATP concentration is in the interior of that range. The proton motive force for the mTAL is within the 170-200 mV range mentioned before [42] and the electrical potential gradient is in the interior of the biologically reasonable 150-180 mV range [20].

	O_2 Consumption (nmol O_2 mg^{-1} s^{-1})	ATP Generation (nmol ATP mg^{-1} s^{-1})	P/O	Electrical Potential Gradient (mV)	Proton Motive Force (PMF, mV)	$[ATP]_c$ (mM)	$[ATP]_c/[ADP]_c$
Base Case							
P_{O2} = 10mmHg pH_c = 7.20	2.35	9.59	2.04	161.87	169.41	2.45	8.66
P_{O2} Variation							
P_{O2} = 20mmHg	2.37	9.65	2.03	164.37	172.34	2.49	10.07
P_{O2} = 7.5mmHg	2.33	9.51	2.04	160.7	167.21	2.39	7.24
P_{O2} = 5.0mmHg	2.26	9.24	2.05	157.89	163.23	2.22	4.8
P_{O2} = 2.5mmHg	1.9	7.7	2.03	152.46	155.97	1.48	1.64
$Q_{ATP,max}$ Variation							
$Q_{ATP,max}$ x 0.5	1.31	4.83	1.85	164.35	173.82	2.56	14.27
$Q_{ATP,max}$ x 1.25	2.79	11.55	2.07	161.65	167.46	2.22	4.73
$Q_{ATP,max}$ x 1.5	3.04	12.7	2.09	161.44	166.34	1.8	2.41
pH_c Variations							
pH_c = 7.40	2.23	9.24	2.07	157.93	181.01	2.21	4.72
pH_c = 7.00	2.43	9.67	1.99	162.82	154.6	2.52	11.4
pH_c = 6.80	2.49	9.65	1.94	160.46	137.84	2.52	11.45
$[K^+]_c$ Variations							
$[K^+]_c$ = 60mM	2.35	9.61	2.05	177.24	168.48	2.45	9.0
$[K^+]_c$ = 140mM	2.34	9.51	2.03	155.43	168.45	2.39	7.25
$[Mg^{2+}]_c$ Variations							
$[Mg^{2+}]_c$ = 0.2mM	2.33	9.49	2.04	162.31	169.5	2.38	6.93
$[Mg^{2+}]_c$ = 0.8mM	2.37	9.68	2.04	162.2	169.31	2.51	11.07
Variations in H^+ and K^+ leak permeability							
No leaks	2.16	9.72	2.25	172.24	170.87	2.48	9.64
No H^+ leak	2.27	9.63	2.12	162.61	169.91	2.45	8.8
No H^+ leak, 10x K^+ leak	1.89	6.01	1.59	116.51	159.23	0.99	0.95
No K^+ leak, 10x H^+ leak	3.01	9.16	1.52	167.49	165.61	2.35	6.43
10x H^+ leak	2.99	9.13	1.53	159.37	165.27	2.32	6.05
10x K^+ leak	1.92	5.95	1.55	116.48	159.04	0.98	0.94
10x Leaks	2.12	5.38	1.27	116.21	157.43	0.87	0.82

Table 3.7: Several key intracellular quantities and their sensitivities to various parameter changes in the mitochondria in the medullary thick ascending limb of the loop of Henle.

The P/O ratio is most sensitive to ATP consumption and the leak permeabilities. At the low end of simulated ranges for ATP consumption, the P/O ratio is 1.85, whereas at the high end of the considered range for ATP consumption, the P/O ratio was predicted to be 2.09. In response to changes in leak permeability we also see large changes in the P/O ratio. In the absence of hydrogen or potassium leak, the P/O ratio is 2.25, and in the worst case scenarios for the P/O ratio, when hydrogen leak was 10 times normal and the potassium leak was 10 times normal, the P/O ratio was 1.27.

In the mTAL, the proton motive force is sensitive to hypoxia, at 2.5 mmHg oxygen tension, we see a proton motive force of 156 mV. The mTAL's proton motive force is more sensitive to hypoxia because the degree of hypoxia considered leads to much lower electron transport flux for the mTAL than the hypoxia considered for the PT (see the oxygen consumption in the third block in Tables 3.6 and 3.7, which is a proxy for electron transport activity). We also see a strong sensitivity of the proton motive force to the cytosolic pH, for a slightly acidic cytosolic pH we see a proton motive force of 138 mV. A difference likely related to the lower hydrogen leak permeability in the mTAL allowing a significant negative hydrogen gradient to persist. Predictably, and like for the PT, we also observe that the proton motive force is sensitive to hydrogen and potassium leak, particularly the potassium leak. Under tenfold increased hydrogen and potassium leak capacity, we predict a proton motive force of 157 mV.

3.3.3 Local Sensitivity Analysis for the Proximal Tubule and Thick Ascending Limb

We consider the change in state variables in the PT under a change in each parameter of our model. The full local sensitivity analysis is reported in Figure 3.1. Here we focus on several key state variables and the parameters that are most impactful upon these state variables. In Figure 3.3 we show the derivative of each state variable against each of the most significant parameters, calculated using a central difference scheme with $\Delta p = 0.01p$ where p is the size of the parameter. The derivative is normalized relative to the baseline size of each state variable and the size of each parameter. We see that the concentrations of NADH and reduced coenzyme Q (QH_2) are most sensitive to the parameter changes we considered. The cytosolic ATP concentration is most sensitive to the maximal ATP consumption. The concentration of NADH in the cell is determined heavily by alphaketogluterate dehydrogenase, which is positively associated with increased NADH content, and pyruvate dehydrogenase, which is negatively associated with NADH content. Greater alphaketogluterate dehydrogenase activity allows for more production of NADH because in the proximal tubule it is predicted to be a limiting step for the TCA cycle. Alphaketogluterate concentrations are higher in our model than any other TCA cycle intermediate, and the concentration of the product of alphaketogluterate dehydrogenase, succinyl-CoA, is lower than any TCA cycle intermediate. Pyruvate dehydrogenase on the other hand reduces NADH concentrations because it competes with alphaketogluterate dehydrogenase for coenzyme A as a substrate. Pyruvate dehydrogenase

uses coenzyme A to produce acetyl-CoA whereas alphaketogluterate uses coenzyme A to produce succinyl-CoA. In the full sensitivity plot, Figure 3.1, we see that the TCA cycle intermediates from citrate to alphaketogluterate are present in greater concentrations when you increase pyruvate dehydrogenase activity, and intermediates downstream of alphaketogluterate dehydrogenase are present in lower quantities. Supplementary simulations found that for 1% or 10% increases in the activity of pyruvate dehydrogenase, we observe a consistent alphaketogluterate dehydrogenase flux, despite larger concentrations of alphaketogluterate. This observation further supports this proposed mechanism, since more alphaketogluterate is necessary to produce the same enzyme flux. Aside from the above mechanism and its downstream effects, we see unsurprisingly that the concentration of reduced coenzyme Q and reduced cytochrome C continues to increase with increased total quantities of coenzyme Q and cytochrome C. We also see that the passing of electrons from coenzyme Q to cytochrome C appears to be limited by the available cytochrome C, since the reduction state of coenzyme Q appears to be highly sensitive to the total cytochrome C concentration.

In the mTAL we find several differences and an overall greater robustness to small perturbations of key parameters. The full local sensitivity analysis is reported in Figure 3.2. In Figure 3.3 we show the sensitivity calculated in the same manner as for the PT. At the same threshold for a parameter to be significant, two more parameters are significantly sensitive in the PT than are sensitive in the mTAL. The concentrations of NADH, reduced coenzyme Q (QH_2), and reduced cytochrome C are particularly sensitive state variables for the mTAL. The most significant difference between the PT and mTAL is that in the mTAL, NADH concentrations are less sensitive to pyruvate dehydrogenase and alphaketogluterate dehydrogenase activities. Instead we see in the mTAL that the pooled concentration of NADH and NAD^+ is by far the most important factor impacting the concentration of NADH. This suggests that whereas in the PT there are limited amounts of coenzyme A and this limits the amount available to alphaketogluterate dehydrogenase (as illustrated by the sensitivity to pyruvate dehydrogenase activity), instead NAD^+ is in short supply in the mTAL, and so the way to provide more NADH to the cell is to increase the size of the NADH/NAD^+ pool. Given the higher NADH to NAD^+ ratio in the mTAL and its relative hypoxia (which can leave the electron transport chain in a more reduced state [78]), coenzyme Q is also in high demand, leading to a high sensitivity of multiple states to the pooled coenzyme Q concentration.

3.3.4 Global Sensitivity Analysis of the Model

For our global sensitivity analysis we used the Sobol method for uniformly exploring a high-dimensional parameter space and describing the observed variation in the state space as a function of the parameters. For local estimates, interactions are negligible, but in a global sensitivity analysis interactions may be very important. For this reason we report two sensitivity estimates, the first Sobol indices, which do not account for interactions and the total Sobol indices, which account for two-way interactions. First Sobol indices are non-negative

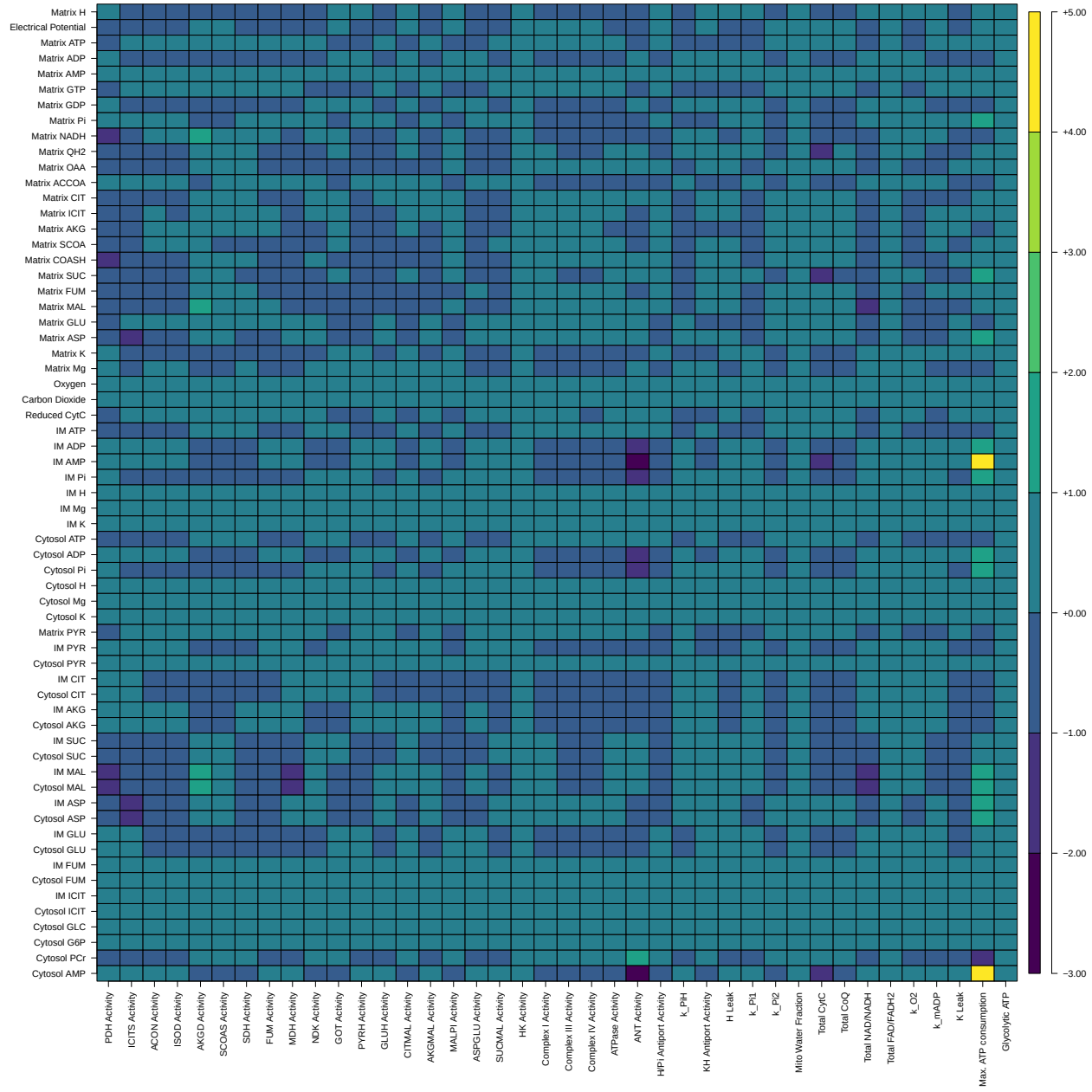

Figure 3.1: The full set of local sensitivities in the PT, for more information see section 3.3.3.

numbers between zero and one, whereas total Sobol indices may be greater than one. They represent the proportion of variance explained by a particular parameter in the case of the first Sobol index, and in the case of the total Sobol index, the variance explained by the parameter and the pair-wise interactions associated with it. In Figure 3.6 we present the first Sobol indices for several important state variables, and in Figure 3.7 we present the total Sobol indices for those state variables. The full results are found in Figures 3.4 and

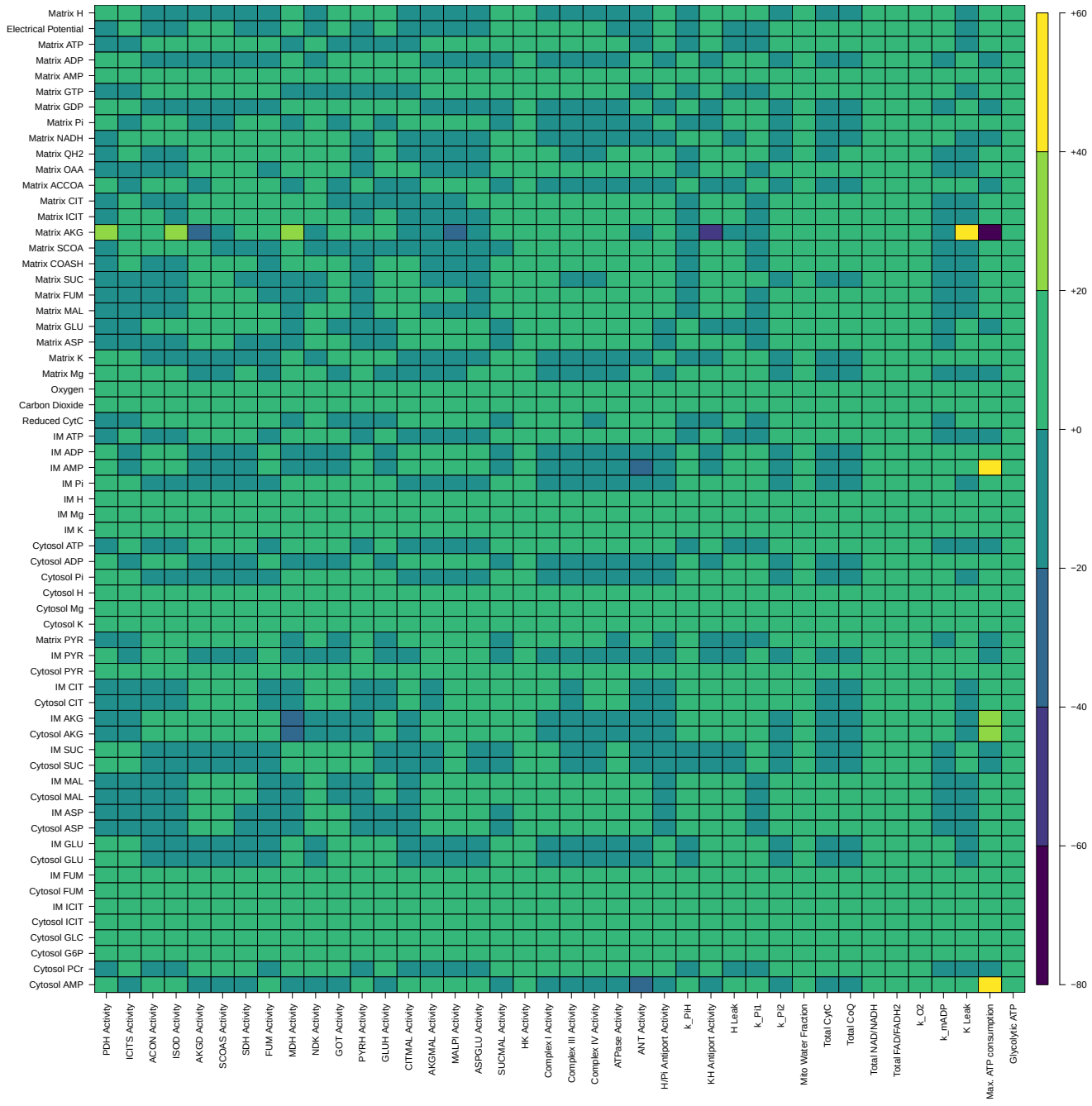

Figure 3.2: The full set of local sensitivities in the mTAL, for more information see section 3.3.3.

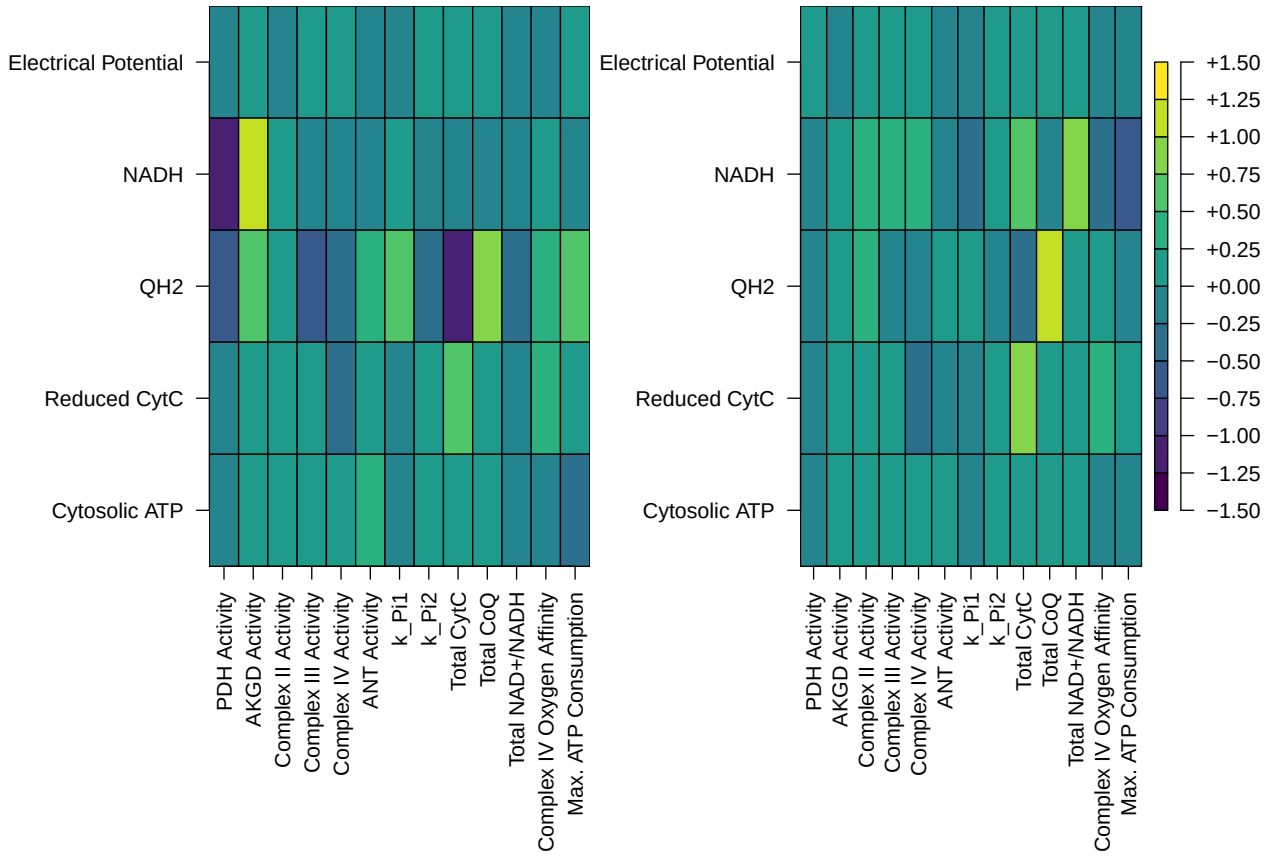

Figure 3.3: Local sensitivities of several important state variables in the PT (left panel) and mTAL (right panel) relative to certain parameters significant to either the PT or mTAL. The results are calculated as described in Section 3.3.3. CytC stands for cytochrome C, reduced cytochrome C refers to cytochrome C that has been donated an electron by Complex III. AKGD refers to alphaketogluterate dehydrogenase, PDH refers to pyruvate dehydrogenase, ANT refers to adenine nucleotide translocase, and QH_2 is the reduced form of coenzyme Q.

3.5. We see that the first Sobol index results share some features with the results above. We see that like for the local sensitivity analysis of the PT, pyruvate dehydrogenase features prominently, its importance is discussed above in our local sensitivity analysis. Succinyl-CoA synthetase *in vivo* catalyzes the conversion of succinyl-CoA into succinate and coenzyme A. This may increase the concentration of NADH by increasing the availability of coenzyme A, which in the PT and mTAL is found in lower concentrations than acetyl-CoA and succinyl-CoA. This could explain its effects on NADH concentrations in the mitochondrion. The next-most important parameter for influencing the state variables is the maximal ATP consumption, which plays a large role in determining the reduced cytochrome C concentration. ATP consumption frees ADP for phosphorylation. This relieves the proton gradient across the inner membrane. Complex IV requires protons in the mitochondrial matrix in order

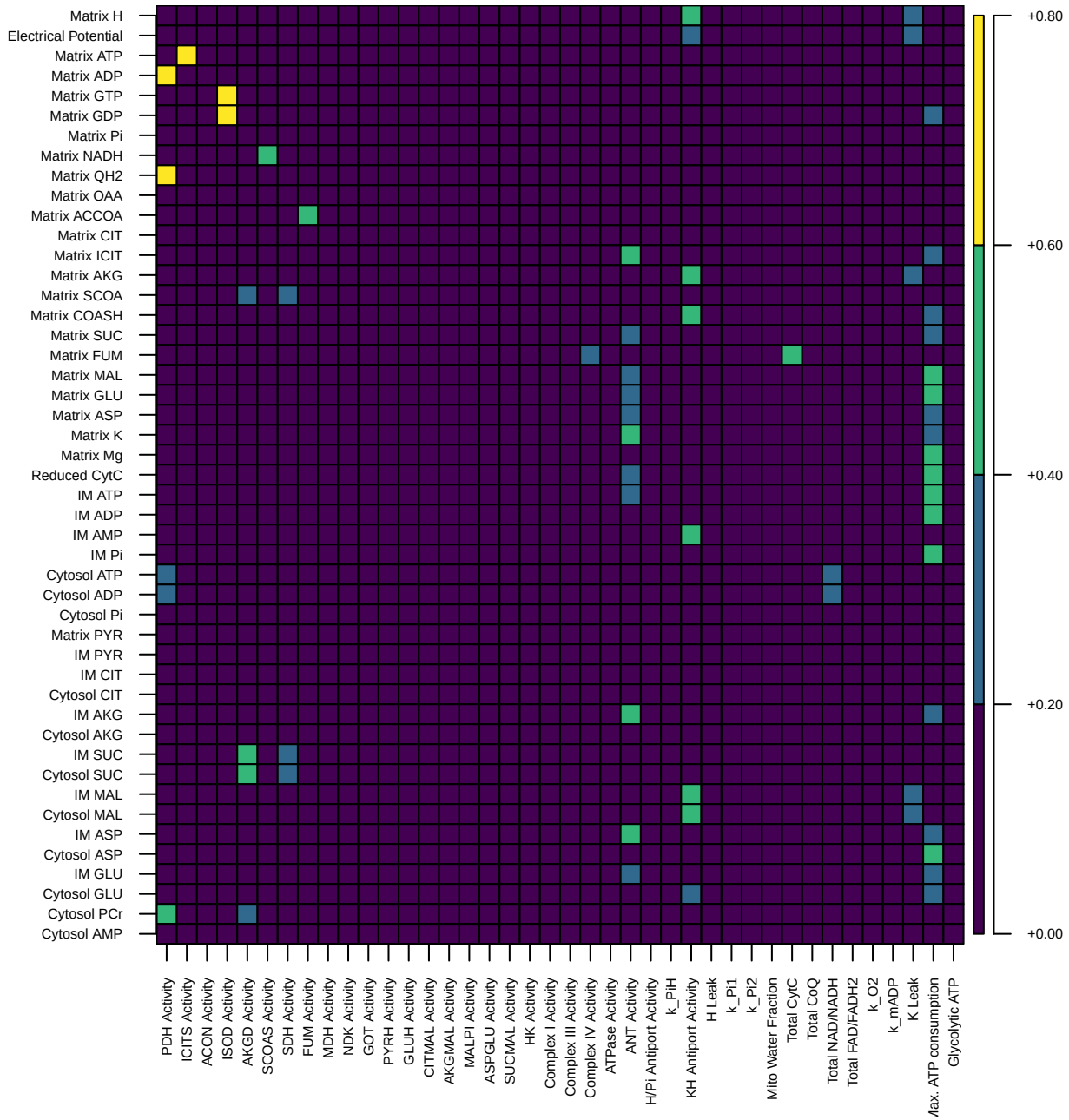

Figure 3.4: The sensitivity of all state variables to the parameters as calculated according to the Sobol method, without interactions.

to oxidize cytochrome C. When we consider pairwise interactions via the total Sobol index we see differences in which parameters stand out. Pyruvate dehydrogenase and succinyl-CoA synthetase still impact coenzyme Q and NADH concentrations. Most notably the total

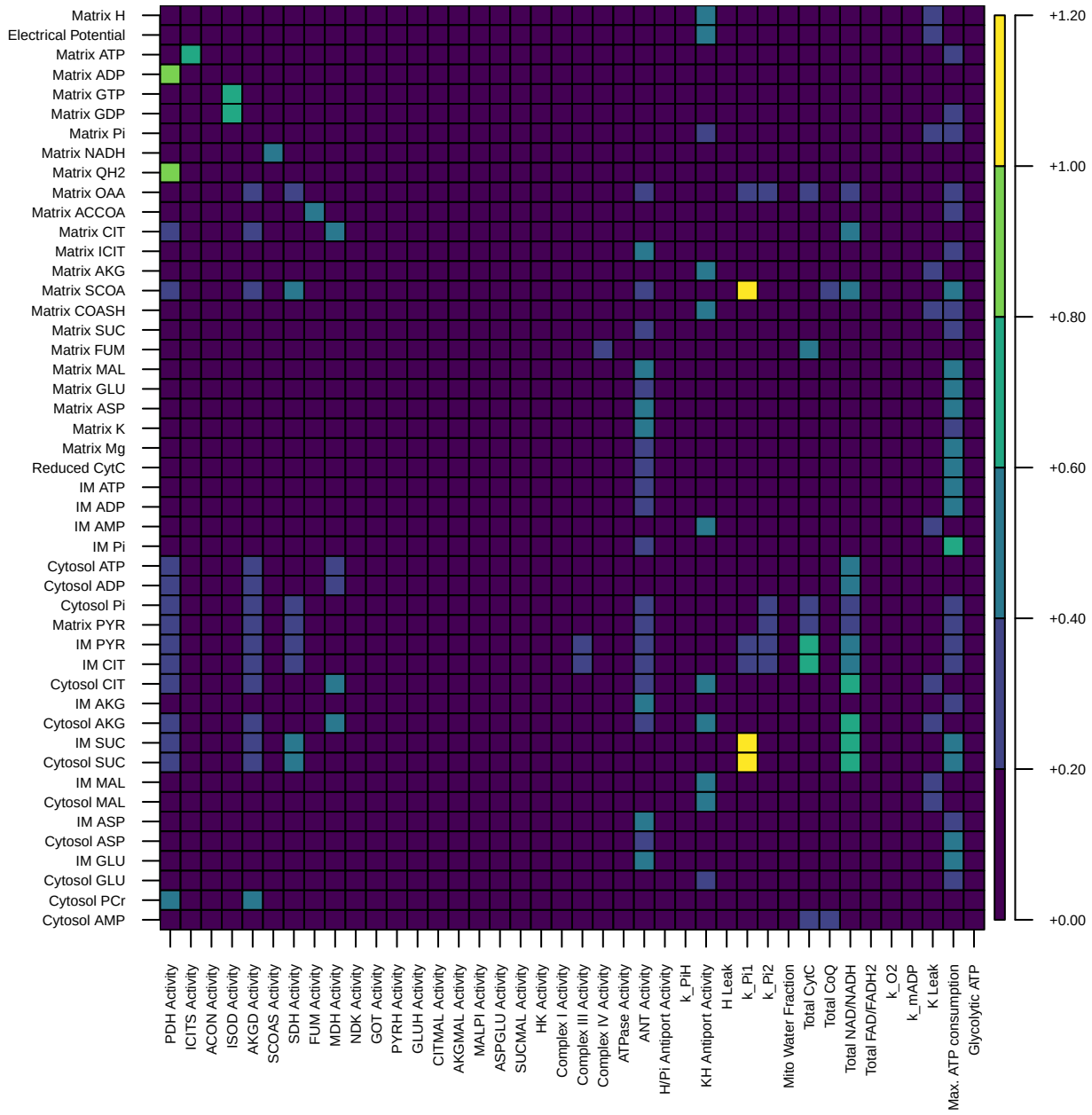

Figure 3.5: The sensitivity of all state variables to the parameters as calculated according to the Sobol method, taking into account two-way interactions.

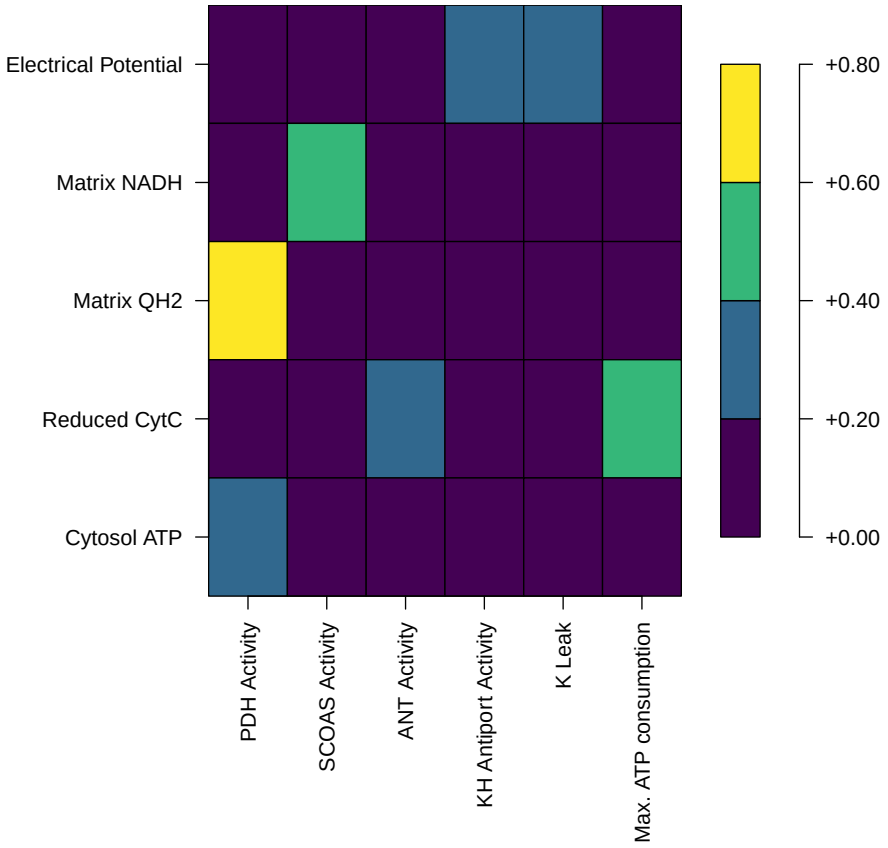

Figure 3.6: The sensitivity of important state variables to the most important parameters as calculated according to the Sobol method, not including interactions. CytC stands for cytochrome C, reduced cytochrome C refers to cytochrome C that has been donated an electron by Complex III.

$NADH/NAD^+$ and potassium-hydrogen antiport activity were all more significant when we consider interactions. Aside from this the results are fairly similar, and we don't see large changes in the influence of the most impactful parameters on the important state variables.

3.3.5 Response to Nigericin

Nigericin is a potassium-hydrogen antiporter [23] that in the quantities administered experimentally is known to remove entirely the proton gradient across the inner membrane of the mitochondria [96]. Feldkamp et al. [49] take advantage of this to measure the ΔpH, upon adding nigericin, the ΔpH decreases and the electrical potential gradient increases by the same amount. For this reason the addition of nigericin was modelled as an increase in potassium-hydrogen antiport activity, enough to force the ΔpH to zero, we use a twenty-fold

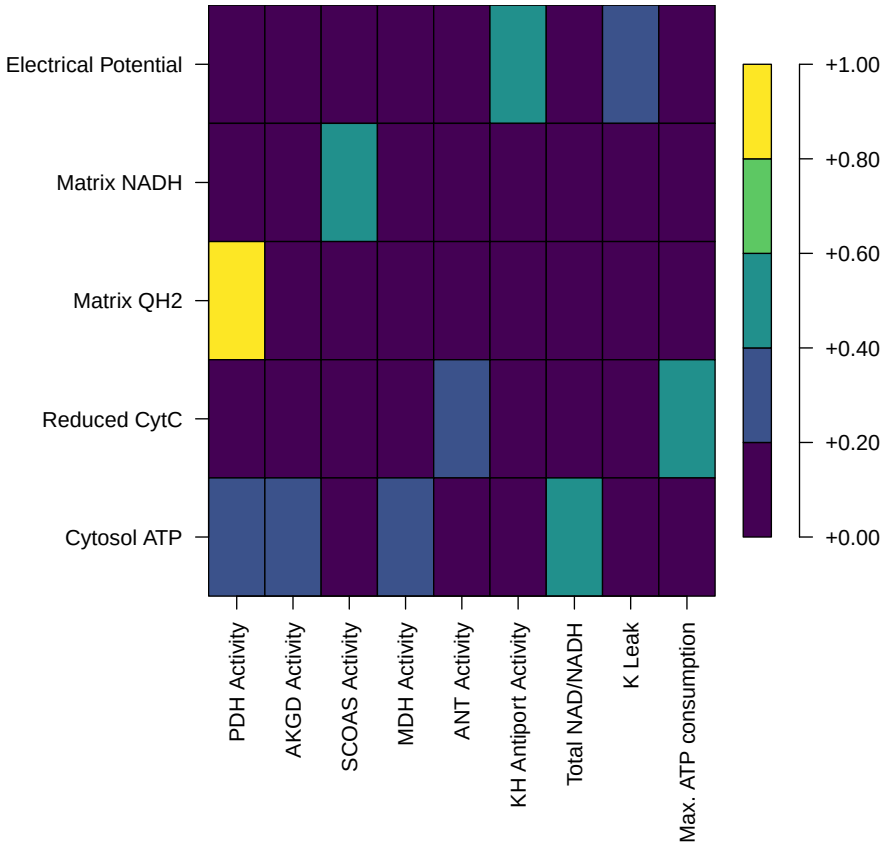

Figure 3.7: The sensitivity of important state variables to the most important parameters as calculated according to the Sobol method, taking into account two-way interactions. CytC stands for cytochrome C, reduced cytochrome C refers to cytochrome C that has been donated an electron by Complex III.

increase in antiport activity. We see that this saturates the corresponding increase in electrical potential gradient in Figure 3.8 (the baseline curve is green). The impact of nigericin on the electrical potential gradient, which goes up as hydrogen gradient is turned into electrical potential gradient, is predicted to go from 158 mV to 167 mV. While the results in Feldkamp et al. [49] are not numerically recorded and are no longer obtainable (Feldkamp, personal communication), based on careful measurement of Figure 4 found in Feldkamp et al. [49], a 5% increase in potential gradient was found to be the approximate effect of nigericin on the electrical potential gradient, after model fitting using this estimate, we see a 6% increase in our model.

For increased potassium leak, we predict a lower baseline electrical potential gradient. The electrical potential gradient increases under larger potassium-hydrogen antiporter activity, and it increases more (11%) for higher levels of potassium leak (in Figure 3.8 we see a

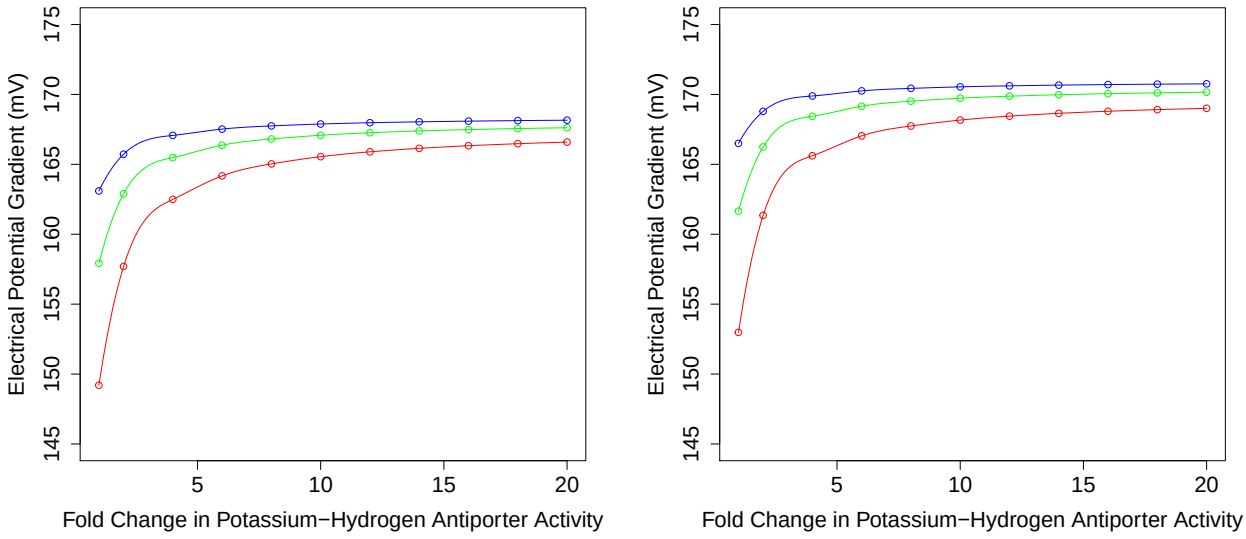

Figure 3.8: The associated increases in electrical potential gradient in the PT (left) and mTAL (right) for changes in the potassium-hydrogen antiporter activity. The green curve is for baseline potassium leak activity, red is for doubled potassium leak, and blue is for halved potassium leak. The green curve shows a roughly 6% increase in electrical potential gradient from left to right. The curve is a standard cubic spline.

electrical potential gradient curve in antiporter activity for doubled potassium leak activity in red, and for halved potassium leak in blue). With a large potassium-hydrogen antiporter activity, the electrical potential gradient is less sensitive to potassium leak. This suggests nigericin is more impactful when the potassium leak activity is greater.

Unlike the PT, we did not have experimental data for the use of nigericin in the mTAL. However, using the same procedure as for the PT (a twentyfold increase in potassium-hydrogen antiport activity), we predict the electrical potential gradient increases from 162 mV to 169 mV (4%) in the presence of nigericin for baseline potassium leak activity.

Nigericin is frequently used in studies on mitochondria [49, 93, 205] and so it is valuable that the model correctly captures the response to nigericin. Under previous versions of this model [44], the model did not correctly predict the response found in Feldkamp et al. [49] because the predicted ΔpH was too low. As discussed above in Section 3.2.2, we use a lower potassium-hydrogen antiporter activity. The potassium-hydrogen antiporter impacts the robustness of the electrical potential gradient to ion leakage.

3.3.6 Uncoupling Effects in Proximal Tubule Mitochondria

Uncoupling or increased hydrogen leak is another mechanism that impacts cell function by reducing the efficiency of respiration. Uncoupling may be caused by diabetes in which there's an upregulation of UCP-2 [55], or by salicylate, also known as aspirin, a known uncoupler and occasional cause of Fanconi Syndrome [69]. The cases considered here are of uncoupling without any other effects. These cases give a baseline expectation for what might happen during uncoupling. The exact simulation procedure used is outlined in Section 3.2.4. We find that the effect on cytosolic ATP concentration (<0.1 mM in the worst case), proton motive force (∼3.5 mV in the worst case) and electrical potential gradient (∼2 mV in the worst case) was minimal. The worst case hydrogen leak (tenfold increased hydrogen leak activity) considered is included in Table 3.6. The minimal effects of hydrogen leak on ATP generation (only a 10% reduction in ATP generation, see the third-last row of Table 3.6) and mitochondrial polarization are explained by compensatory increases in the flux through Complex I, III, and IV in our model. These electron transport chain components pump protons across the inner membrane into the intermembrane space, and so with increased hydrogen leak, they have more substrate to do their work. This is compatible with the hypothesis that uncoupling can perform an adaptive function by providing an outlet for over-reduced oxidative phosphorylation complexes [55]. This would not be possible if electrical potential gradient was significantly lost during mild uncoupling [193]. As noted in Section 3.3.1, under increased hydrogen leak, the oxygen consumption by the proximal tubule may be as much as 36% higher, this could be enough to trigger hypoxia, possibly causing progression of diabetic nephropathy [55]. This is an unfortunate consequence of the previously mentioned increases in Complex I, III, and IV activity. The oxygen consumption included in Table 3.6 is directly proportional to Complex IV activity.

3.3.7 Uncoupling Effects in the medullary Thick Ascending Limb Mitochondria

Uncoupling can also happen in the mTAL, and the effects were studied similarly. The effects on the cytosolic ATP concentration (∼0.2 mM in the worst case) and proton motive force (∼4 mV in the worst case) were significant. We also observe the corresponding effects, as noted in Section 3.3.2, on oxygen consumption. As noted before, oxygen consumption which is reported in uncoupling in Table 3.7 is directly proportional to Complex IV activity. The maximal Complex IV flux is lower in the mTAL than in the PT due to the lower baseline oxygen tension, not allowing the same growth in oxygen consumption in the mTAL compared to the PT. The oxygen consumption is still 27% higher despite that.

3.3.8 Oxidative Phosphorylation and Mitochondrial Disease in the Proximal Tubule

Mitochondrial diseases, as well as the consequences of certain drugs like NRTIs, do not have a single universal effect on oxidative phosphorylation. For instance, oxidative stress can cause any combination of OXPHOS dysfunctions, and that is a key pathway for NRTI-induced mitochondrial dysfunction. We considered combinations of reductions by quarters in the activity of Complex I, Complex III, Complex IV, and ATP Synthase, which are the components of oxidative phosphorylation encoded by the mtDNA (and thus most at risk). We examined the steady state electrical potential gradient and cytoplasmic ATP concentration because the former maintains hydrogen flux through the electron transport chain and the latter is predictive of downstream loss of cell viability [115]. When noteworthy, ATP generation and oxygen consumption are also reported. Importantly, the P/O ratio remains highly consistent under OXPHOS dysfunction alone, and so a decrease in ATP generation is typically accompanied by a nearly proportionate decrease in oxygen consumption. This is due to the coupling of Complex IV (which determines oxygen consumption) and ATP Synthase (which determines ATP generation). The P/O ratio is in some sense a measure of the stoichiometry of the two reactions combined, and so it is usually significantly impacted only when intermediate products are lost (protons crossing the inner membrane by other means than ATP Synthase, i.e. hydrogen leakage).

Univariate Parameter Changes

Examining one parameter at a time yields insights of the relative importance of the activities of each of the four components considered. The full set of univariate results for ATP concentration in the cytoplasm can be found in Figure 3.9. We see Complex III is much more important than the rest, likely due to which step is rate-limiting. There's almost no discernable consequences of varying the activity of ATP Synthase for example, whereas ATP concentrations are reduced by 26% and the electrical potential gradient is reduced by 5 mV when Complex III activity is reduced to one quarter of typical enzymatic activity. That there may be no direct impact of ATP Synthase on ATP concentrations is not altogether unexpected. Across all cases where cytosolic ATP is greater than 90% of baseline, the flux through ATP Synthase remains within 4% of typical. ATP Synthase activity doesn't significantly impact the ATP Synthase flux because ATP Synthase is not limiting for mitochondrial respiration. This is illustrated by results for ATP Synthase inhibition in mice neurons [52]. In that experimental model while there are indirect effects of ATP Synthase inhibition on murine neuronal aerobic respiration, the likely mechanism is via increased reactive oxygen species production, which leads to the downregulation of aerobic respiration as a whole, unrelated to the reduction in activity of ATP Synthase. A similar mechanism likely underlies Complex I-mediated mitochondrial dysfunction, it is well-known that it is a site of enhanced reactive oxygen species production during Complex I inhibition and that Complex I inhibition must be very strong before cellular respiration is inhibited [8, 163]. Low sensitivity to

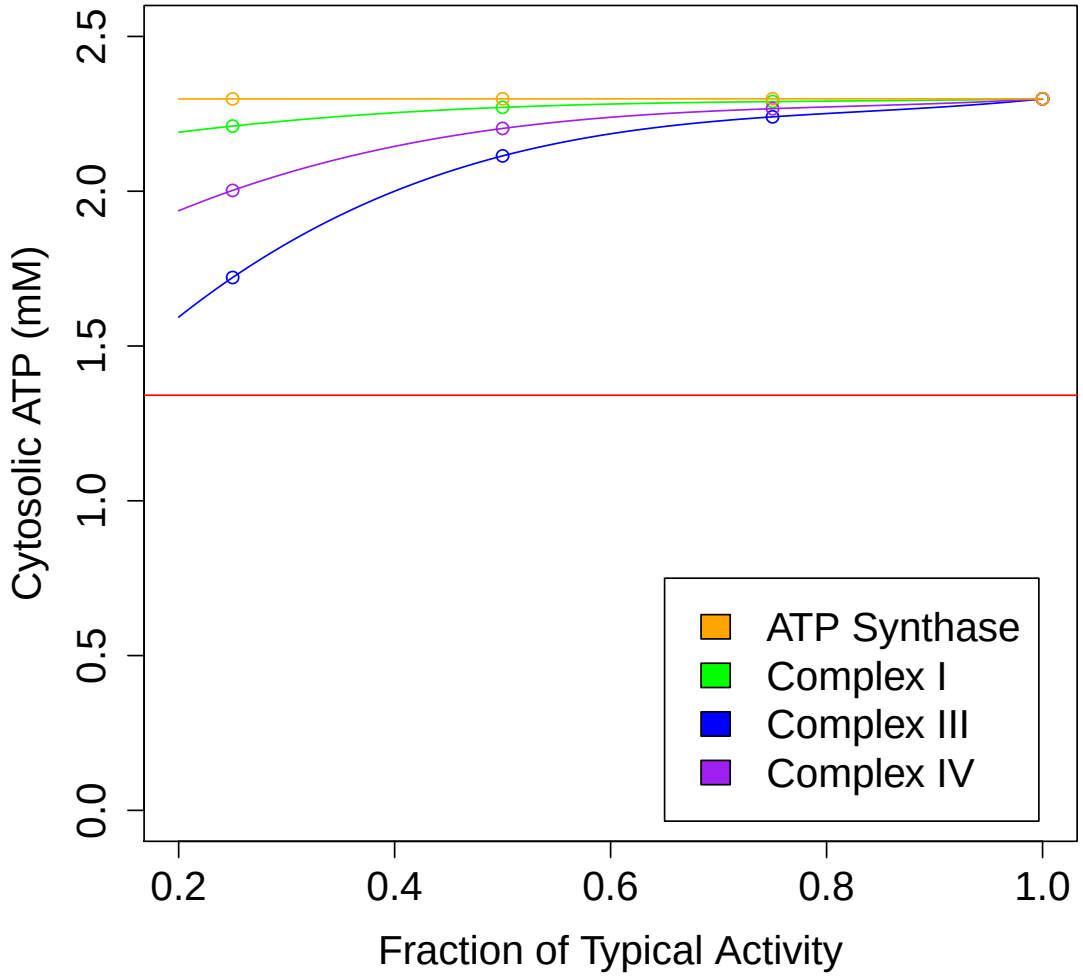

Figure 3.9: The effects on the cytoplasmic ATP concentration of changes to the activity of the four oxidative phosphorylation components considered in the PT. The red line represents the lowest ATP concentration found in any of the mitochondrial disease simulations performed.

Complex I inhibition has in fact been observed in proximal tubule cell lines specifically [164]. Respiration has been shown to have similarly weak sensitivity to Complex IV activity in the rat kidney [108]. Theoreticians have long believed that the majority of respiratory enzymes are abundant far beyond what is necessary to maintain oxidative phosphorylation activity [108], and our predictions for ATP Synthase, Complex I, and Complex IV are compatible with that. Complex III inhibition was the largest exception in our model as noted above. Cytosolic ATP concentrations were predicted to be the most sensitive to Complex III inhibition by our model. The numbers for Complex III do not diverge too strongly from the literature however, in a study on a cell line of myoblasts, Schirris et al. observed that a roughly 75% reduction in Complex III activity produced a roughly 20% reduction in ATP generation [159]. In our model on the other hand there is a 10% reduction in ATP generation, which given the fact that we are working in a different tissue, and the heart has been observed to be more sensitive to inhibition of other OXPHOS enzymes [108] is not surprising.

Multivariate Parameter Changes

We consider multivariate changes to oxidative phosphorylation due to the broad effects of Mitochondrial diseases on oxidative phosphorylation, as discussed later in Section 3.4. In considering these we wished to answer two questions: how much do multivariate changes extend the range of possible outcomes, and are there non-additive effects of interactions on the outcomes of interest? The first can be answered by comparing the range of outcomes from the univariate case to the multivariate case, using Figures 3.10. We see that Complex III still produces the most significant effects, explaining more of the variation in ATP concentration, as would be expected from the univariate case. What we see as well is that the added effect of combining activity reductions doesn't significantly impact the electrical potential gradient, although the ATP concentration seems more sensitive.

Tubule	Predicted Quantity	R^2 of Basic Model	R^2 of Model with All Interactions
PT	$[ATP_c]$	0.88	0.88
PT	$\Delta\Psi$	0.88	0.88
mTAL	$[ATP_c]$	0.85	0.85
mTAL	$\Delta\Psi$	0.90	0.92

Table 3.8: Models of cytosolic ATP concentrations and electrical potential gradients in the PT and mTAL, and the models' R^2 value. In the basic model, the only effects were additive in the relative change in the activity of each of the included OXPHOS components, in the interaction model, all combinations of multiplicative two-, three-, and four-way interactions were considered, which produced no meaningful difference in the model's explanatory power.

To determine if there are non-additive interactions between the activities that were varied, a linear regression was used. Using least squares fitting, an affine plane was chosen as a function either of the univariate activities (our first model) or of the univariate activities

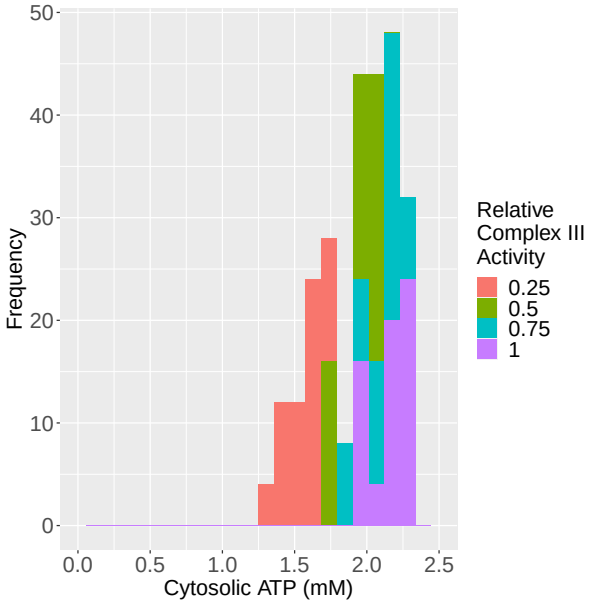

Figure 3.10: The cytosolic ATP concentration in each of the 256 cases considered, coloured by the activity of Complex III, after considering all the activities in the same manner as this graph we find that Complex III remains by far the most important determinant of the cytosolic ATP concentration.

combined with all the multiplicative interactions between them (our second model), in order to predict the cytosolic ATP concentration and the electrical potential gradient. The non-additive model performed no better than the univariate linear model. The R^2 was almost the same for the two models, or in other words they fit the results almost equally well. The results of this analysis are found in Table 3.8.

Ifosfamide and Dichloroacetate

Ifosfamide reduces Complex I activity by half, and dichloroacetate has the capacity to prevent allosteric inhibition of pyruvate dehydrogenase in a manner that might compensate for respiratory dysfunction [58, 59]. The results for these cases, with the strongest considered case for the effect of dichloroacetate shown (a doubling of $K_{i\mathrm{NADH}}$ as defined in equation 2.99), are in Figure 3.11 for cytosolic ATP concentration. Ifosfamide is nephrotoxic, and is specifically known to cause Fanconi syndrome. What the results suggest, compatible with our discussion above of Complex I existing in excess [8], is that the mechanism of nephrotoxicity may involve more than a direct loss of respiratory capacity. For instance, when Complex I is dysfunctional it may produce more reactive oxygen species, causing oxidative stress. Dichloroacetate shows little useful effect in these results, a result that matches the outcomes from experimental studies on dichloroacetate use with ifosfamide [132].

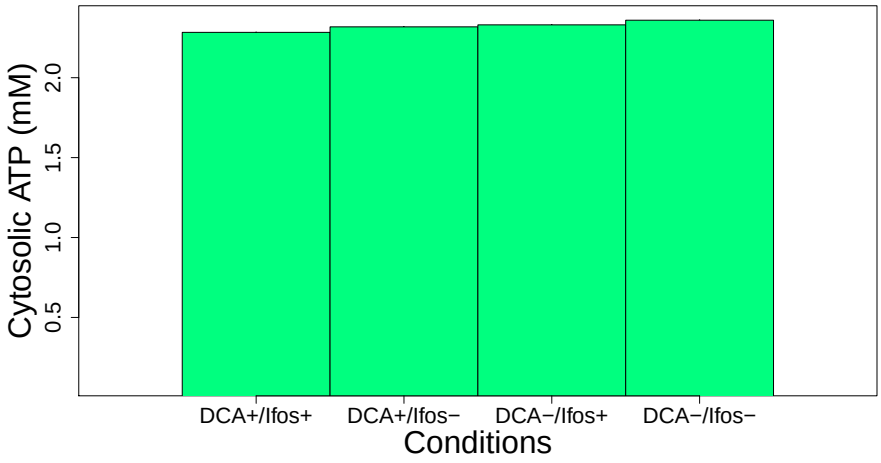

Figure 3.11: The effects of ifosfamide and dichloroacetate on cytosolic ATP concentration (mM) are shown.

More General Drug Simulations of Nephrotoxic Drugs in the PT Mitochondria

Many drugs impact the general regulation of mitochondria in the cell and cause mitochondrial fragmentation. This tends to produce a generalized OXPHOS dysfunction and uncoupling. We represent this through combinations of uncoupling and OXPHOS dysfunction effects. This represents a more general set of combinations of the effects observed in mitochondrial disease, and as noted in Table 3.5. For instance Gentamicin, which acts as an uncoupler and generates reactive oxygen species that subsequently reduce OXPHOS activity [133, 140, 189].

Considering this set of cases essentially means adding another dimension of uncoupling (increased hydrogen leak activity) to the already considered OXPHOS parameter variations. The results for all such cases, with a maximum increased activity of hydrogen leak of 10 times normal, are shown in Figure 3.12 for the cytosolic ATP concentration. Another factor of interest to us is oxygen consumption, however while uncoupling appeared to increase oxygen consumption, OXPHOS dysfunction typically decreased oxygen consumption and so the effects never exceeded the effect on oxygen consumption of uncoupling alone.

The results seen here show that the effect of Complex III is still extremely significant, but unlike in some previous cases, the lowest-activity case for Complex III is no longer disjoint from the other simulated cases. We now see that in some cases the combined effects on other activities can have as large of an effect on the ATP concentration and electrical potential gradient. This is evident from a linear model fit which predicts that the combined effects of the other variables will together have a comparable effect to that of Complex III activity reductions on their own.

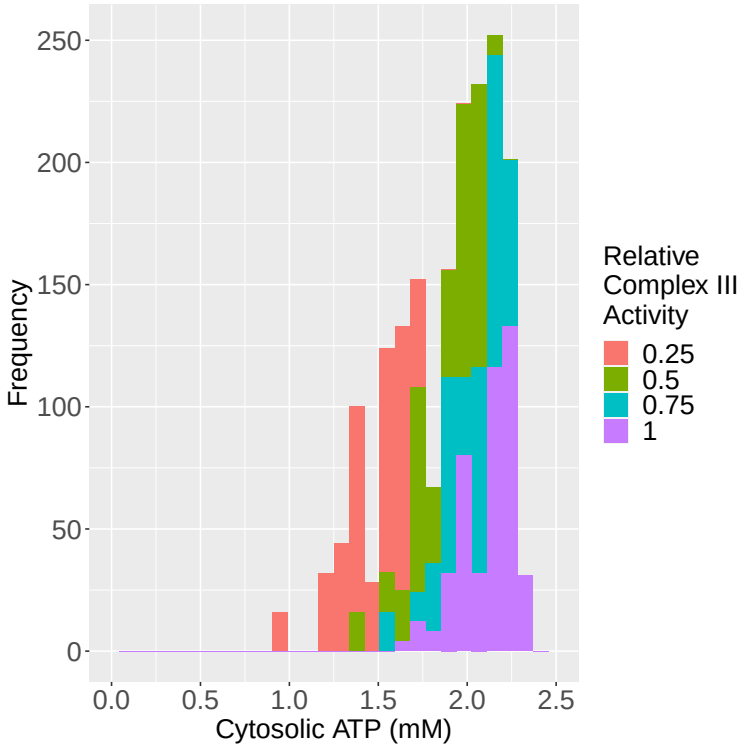

Figure 3.12: The ATP concentration in each of the cases considered of both OXPHOS dysfunction and increased uncoupling, coloured by the relative activity of Complex III, after considering all of the activities we find that Complex III remains the most important determinant of the ATP concentration.

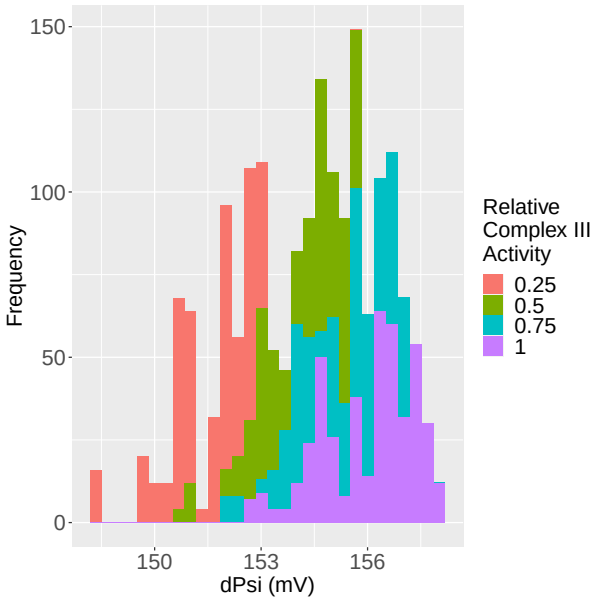

Figure 3.13: The electrical potential gradient in each of the cases considered of both oxidative phosphorylation dysfunction and increased uncoupling, coloured by the activity of Complex III, after considering all of the activities in the same manner as this graph we find that Complex III remains the most important determinant of the electrical potential gradient.

3.3.9 Oxidative Phosphorylation and Mitochondrial Disease in the medullary Thick Ascending Limb

Here we followed the same procedure as in the PT and considered cases of combinations of OXPHOS activity reductions in the mTAL.

Univariate Parameter Changes

The univariate cases for ATP concentration show large changes in the cytosolic ATP concentration under OXPHOS dysfunction, relatively comparable to the sensitivity predicted above in the PT. The mTAL appears to be most sensitive to dysfunction of Complex IV, unlike the PT which is most sensitive to Complex III dysfunction. The mTAL is also sensitive to Complex III dysfunction like the PT. We see that the mTAL is more sensitive to Complex IV dysfunction than the PT is. This different prediction can be explained simply: the activity of Complex IV is limited by the far lower oxygen tension in the mTAL. When we consider comparable Complex IV dysfunction (75% lower Complex IV activity) in the mTAL, but now with a PT-like 50 mmHg oxygen tension, we do not see the same sensitivity to Complex IV dysfunction (no change in cytosolic ATP concentrations in the 50 mmHg oxygen tension case, compared to a 37% change in cytosolic ATP concentrations in our baseline 10 mmHg oxygen tension case). Otherwise the results strongly resemble the PT case.

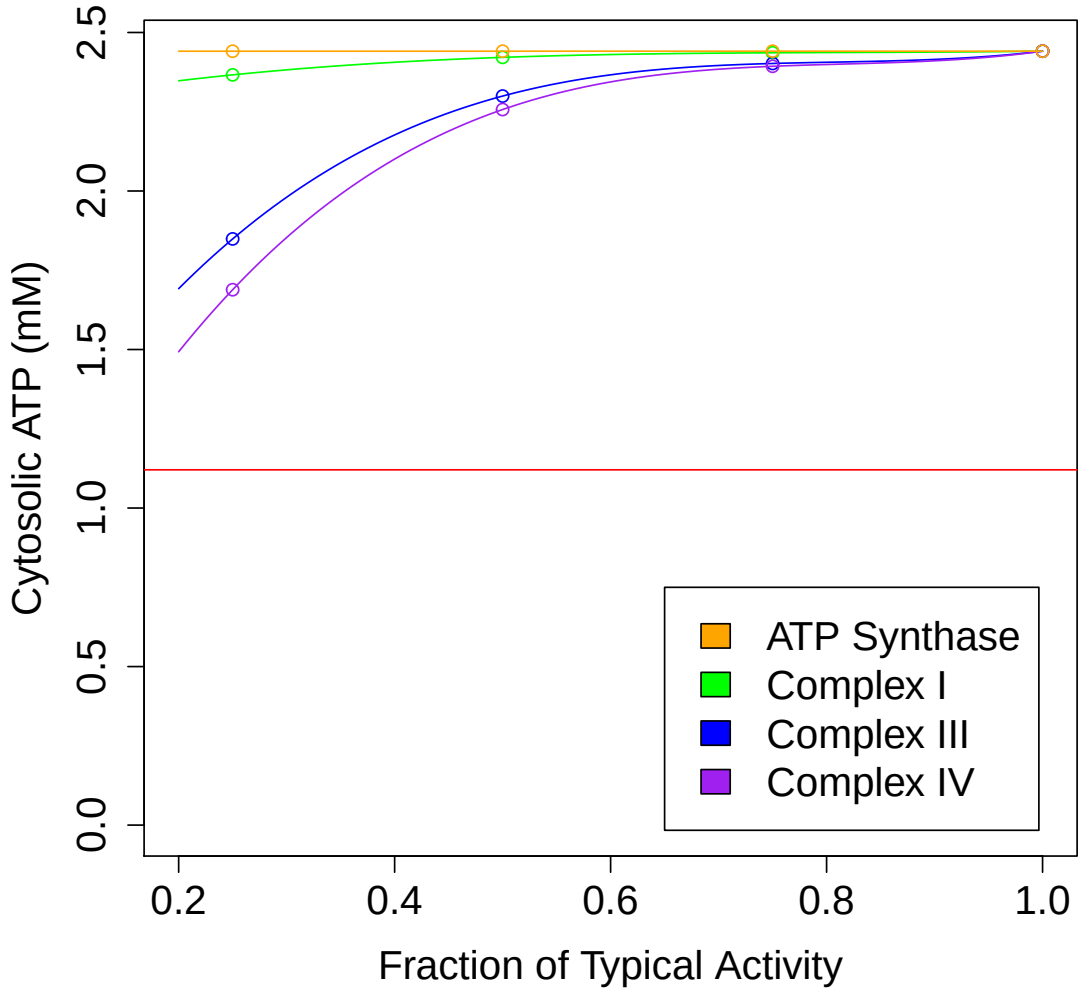

Figure 3.14: The effects on the cytoplasmic ATP concentration of changes to the activity of the four oxidative phosphorylation components considered in the mTAL. The red line represents the lowest ATP concentration found in any of the mitochondrial disease simulations performed.

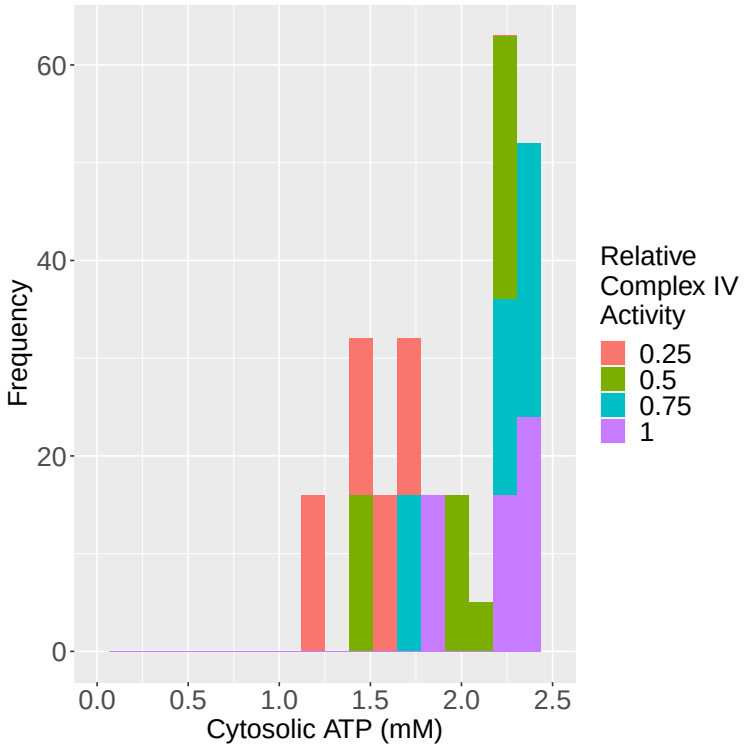

Figure 3.15: Cytosolic ATP levels in the mTAL in our mitochondrial disease simulations (various combinations of OXPHOS dysfunction), coloured by the level of Complex IV activity relative to typical Complex IV activity.

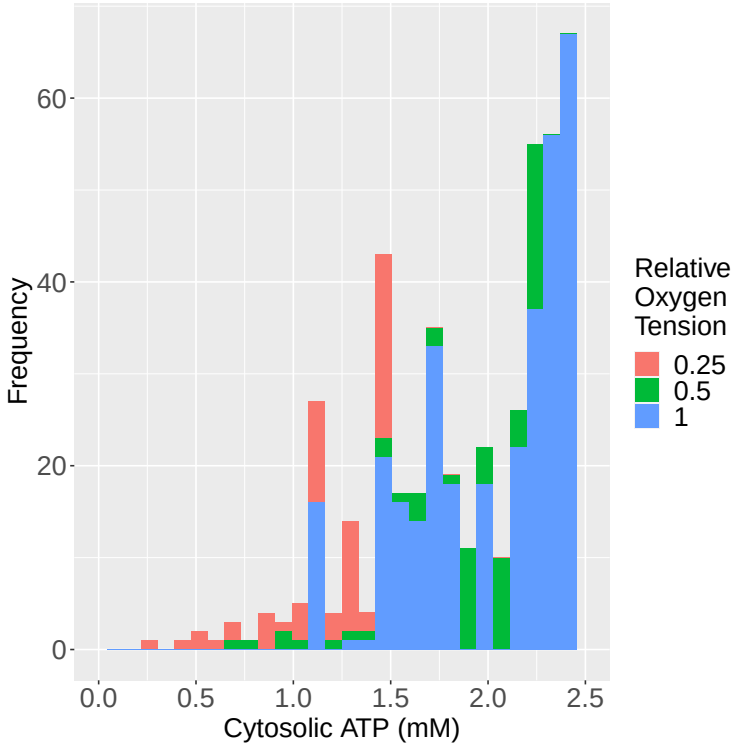

Figure 3.16: The cytosolic ATP levels for varied OXPHOS dysfunction, uncoupling, and oxygenation, coloured by oxygen tension levels. We only consider at most one kind of oxidative dysfunction at a time (meaning that a given simulation includes only Complex I dysfunction or only Complex III dysfunction or only Complex IV dysfunction or only ATP Synthase dysfunction) in order to reduce the number of cases. Some cases exceed baseline ATP levels due to the effects of glycolysis.

Multivariate Parameter Changes

Like for the PT we wish to address whether there are non-additive effects, and the total range of possible outcomes under multiple OXPHOS complex deficiencies for the mTAL, thereby capturing many mitochondrial diseases which often include these combined effects. In Figure 3.15 we show the range of cytosolic ATP concentrations for various combinations of OXPHOS dysfunction. Once again we fit a linear model and a model with multiplicative interaction terms, and like for the PT, the R^2 is above 0.8 for the linear models and the improvement from including interactions is marginal. The results can once again be found in Table 3.8.

OXPHOS Deficiencies Combined with Other Effects

OXPHOS dysfunction as previously discussed, is often concurrent with uncoupling, such as in diabetes, and we know the mTAL to be especially prone to hypoxic injury due to low

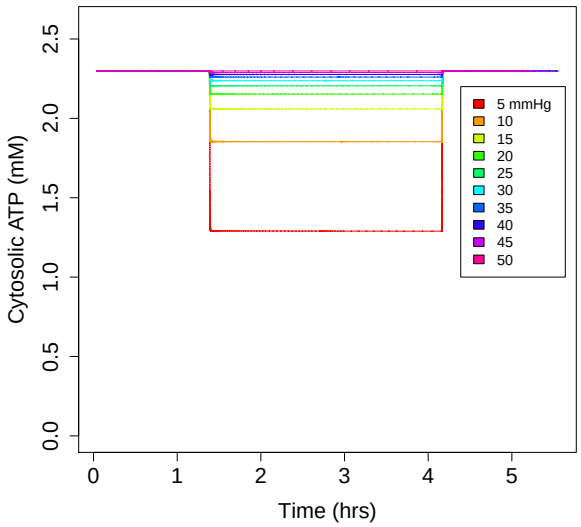

Figure 3.17: Cytosolic ATP concentration in the PT for a range of reductions by tenths of oxygen partial pressure (starting at 5000 s), to a lowest of one tenth of baseline oxygen partial pressure (or 5 mmHg) from a maximum of 50 mmHg. This is followed by reoxygenation at time 15,000 s.

tissue oxygen tension. Thus we considered these two factors as well to see their effect in combination with OXPHOS deficiency. We find that significant drops in oxygen tension lead to the largest effect in these combined cases. Under these combined effects, as shown in Figure 3.16, we still predict that oxygen tension is a particularly significant parameter for the maintenance of cytosolic ATP levels.

3.3.10 Hypoxia in Proximal Tubule Mitochondria

The kidney is sensitive to reductions in tissue oxygen partial pressure, and understanding the associated threshold for injury is both medically and physiologically significant. Micro- and macrovasculature problems may produce local hypoxia, often both are involved. The effects of macrovascular hypoxia though are more easily measurable, and we can rule out their sufficiency for hypoxic injury by determining whether the macroscale oxygen partial pressure is low enough to cause hypoxic injury, if it isn't then microvasculature problems must be contributing on a smaller scale than is measured [24, 119]. The results of a gradation of oxygen partial pressure reductions are shown in Figure 3.17. From this we see a degree of insensitivity of cytosolic ATP concentrations to oxygen partial pressure dropping in the renal cortex until 5-10 mmHg, where we see a much greater drop in ATP concentrations.

Reoxygenation is also considered in the simulation shown in Figure 3.17, in our model, the predicted response is immediate and returns to the previous equilibrium.

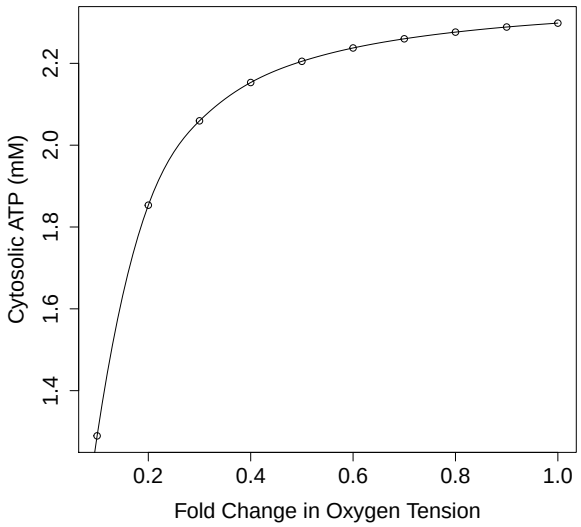

Figure 3.18: Cytosolic ATP concentration in the PT for a range of reductions by tenths of oxygen partial pressure, to a lowest of one tenth of baseline oxygen partial pressure (or 5 mmHg) from a maximum of 50 mmHg. Connected by a cubic spline.

The strong robustness to hypoxia, down to 10 mmHg in the proximal tubule (with significant changes in cell behaviour between 5 and 10 mmHg), agrees with measurements of a 'critical' P_{O2} found in experimental work of 10 mmHg [47]. This robustness is due to a sustained capacity to consume the necessary amount of oxygen until that point. For instance, at normoxic oxygen tensions (50 mmHg) we see an oxygen consumption of 2.52 nmol O_2 per milligram per second in our model, and at 10 mmHg, the cell still consumes 2.31 nmol O_2 per milligram per second in our model.

3.3.11 Hypoxia in medullary Thick Ascending Limb Mitochondria

A much smaller absolute change is required in order to produce an extremely low oxygen tension in the mTAL, because the baseline tissue oxygen tension of the mTAL is much lower than that of the PT (10-20 mmHg in the mTAL compared to 50 mmHg for the PT). However as noted by Schiffer, Gustafsson, and Palm [158], there are multiple adaptations that mTAL mitochondria have to address this problem, most notably: they are more densely packed in the mTAL, they have greater efficiency, and they have greater oxygen affinity [158]. These features are included in our model, and produce a partial robustness. The cytosolic ATP levels are still close to 2 mM until around 4 mmHg, whereas at 5 mmHg the PT's cytosolic ATP levels are much worse than necessary to kill the PT cell. Thus, the mTAL can survive much absolutely smaller oxygen tensions. However since the baseline oxygen tension is lower, it is not robust to comparably extreme variations of the oxygen tension, the PT's oxygen

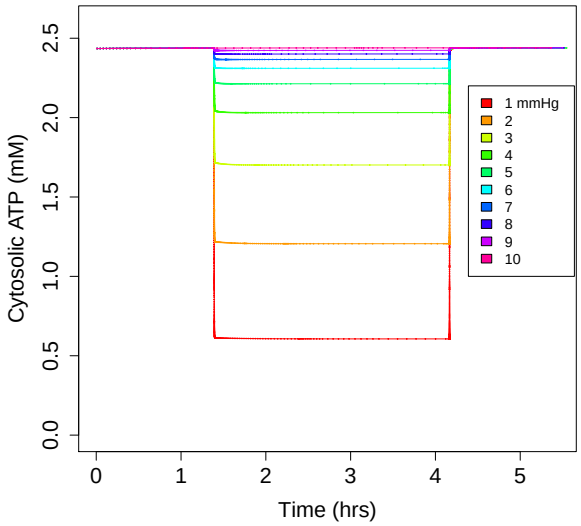

Figure 3.19: Cytosolic ATP concentration in the mTAL with high ATP consumption for a range of reductions by tenths of oxygen partial pressure (starting at 5,000 s), to a lowest of one tenth of baseline oxygen partial pressure (or 1 mmHg) from a maximum of 10 mmHg. This is followed by reoxygenation at time 15,000 s.

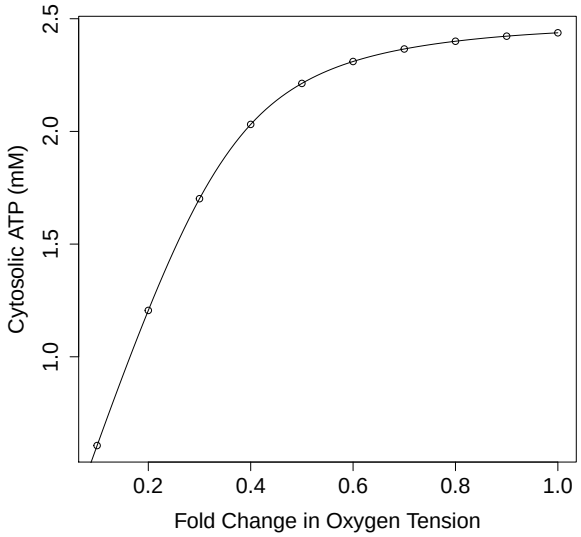

Figure 3.20: Cytosolic ATP concentration in the mTAL for a range of reductions by tenths of oxygen partial pressure, to a lowest of one tenth of baseline oxygen partial pressure (or 1 mmHg) from a maximum of 10 mmHg. Connected by a cubic spline.

Conditions	$[ATP]_c$ (mM)
mTAL at 1 mmHg	0.61
Hypoxic mTAL with PT-like V_{mito}	0.33
Hypoxic mTAL with PT-like k_{O2}	0.61
Hypoxic mTAL with both PT-like conditions	0.19
PT at 1 mmHg	0.26

Table 3.9: Variations in mTAL conditions and the consequences for cytosolic ATP concentrations under significant hypoxia.

Condition	Electrical Potential Gradient (mV)	Proton Motive Force (PMF, mV)	$[ATP]_c/[ADP]_c$	NADH/ NAD^+ Pool Reduced Proportion	CoQ Pool Reduced Proportion	CytC Reduced Proportion
PT	158.89	168.26	16.12	0.08	0.1	0.28
mTAL	164.55	174.13	20.22	0.85	0.52	0.49

Table 3.10: Key predictions after post-reperfusion equilibration in the PT and mTAL.

tension may be as low as 20% of typical before being in major danger. The mTAL's cytosolic ATP levels are much lower than baseline at oxygen tensions below 40% of typical. In Figure 3.19 we see the effects of adjusting the oxygen tension in the mTAL.

Like with OXPHOS dysfunction, we wished to identify the factors contributing to the robustness of the mTAL under hypoxia. To do this we consider 1 mmHg normal oxygen tension in the mTAL (1 mmHg) but with PT-like mitochondrial volume fraction or Complex IV oxygen affinity (and combinations thereof), see Table 3.9. We compare these cases with the PT's response to 1 mmHg oxygen tension. We find that while a PT-like mitochondrial volume fraction or Complex IV oxygen affinity makes the mTAL cell perform worse as expected, it is necessary and sufficient that you change both to PT-like values in order to produce comparable drops in the cytosolic ATP content in the mTAL.

3.3.12 Ischemia-Reperfusion Injury in the Proximal Tubule

During ischemia, the cell suffers a severe decline in oxygen concentration. As a consequence of ischemia, the adenine nucleotide (AMP/ADP/ATP) pool becomes smaller, an effect we include. For our model of reperfusion, the oxygen concentration returns to normal and the combined adenine nucleotide pool is 30% of its typical size, based on the results of Cunningham, Keaveny, and Fitzgerald [34]. In the post-reperfusion steady state with this model (see Table 3.10), we predict the proton motive force is only somewhat higher at 168 mV (compared to 166 mV typically). The NADH/NAD^+, coenzyme Q and cytochrome C pools are

not predicted to be left in a highly reduced state. Until the adenine nucleotide pool recovers the cell may be susceptible to reperfusion injury on these grounds. Adding dichloroacetate, which increases the flux through pyruvate dehydrogenase, did not significantly impact the redox state of the cell following reperfusion. Tripling the cytosolic pyruvate concentration, which also increases the flux through pyruvate dehydrogenase, similarly had no effect.

3.3.13 Ischemia-Reperfusion Injury in the medullary Thick Ascending Limb

Ischemia is represented in the same way for the mTAL as for the PT. Due to the small $NADH/NAD^+$ pool in the mTAL, we have a highly reduced $NADH/NAD^+$ pool and an elevated proton motive force at steady state. 85% of the $NADH/NAD^+$ pool is NADH and the proton motive force is 174 mV (relative to the typical value of 169 mV). The coenzyme Q and cytochrome C pools are left in a somewhat reduced state. Dichloroacetate and cytosolic pyruvate had small effects on the redox state of electron carriers and proton motive force.

3.4 Discussion

The goal of the present study was to develop a new model of mitochondria in the mTAL, to improve a model of mitochondria in the PT, and to examine both in several pathological conditions. Our model is able to predict several important cellular quantities, including ATP generation, P/O (Phosphate/Oxygen) ratio, proton motive force, electrical potential gradient, oxygen consumption, the redox state of important electron carriers, and ATP consumption. As noted above, for many of these quantities our predictions were within the range of known measurements both for *in vivo* and *in vitro* cases.

Schiffer et al. notes a lower P/O ratio in the PT than the mTAL, indicating that the mTAL is more metabolically efficient [158]. The P/O ratio is the ratio of ATP synthase phosphorylation of ATP to the Complex IV oxygen consumption. The ratio *in vitro* has been measured to be 1.93±0.13 in the mTAL, and 1.81±0.10 in the PT [158]. Our model predicts a similar *in vitro* P/O ratios between the PT and mTAL, but lower in the PT (see Table 3.2), like we see in Schiffer et al. The predicted P/O ratios *in vivo* are found in Tables 3.6 and 3.7 respectively, and we see that *in vivo* the mTAL has a marginally higher P/O ratio. This is driven *in vivo* by higher metabolic demand and lower oxygen consumption due to the mTAL's comparatively hypoxic state.

Before we get into the details of the dysfunctional cases, we define certain well-understood adverse outcomes. ATP depletion is a significant drop in the cytosolic ATP concentration. ATP depletion is one pathway by which cells die. In mice, there is significant risk of apoptosis from ATP depletion below 70% of typical cytosolic ATP concentrations, and necrosis is assured below 15% [115]. These benchmarks help us to understand the severity of the ATP

depletion observed under the conditions we simulate. Depolarization is a significant loss of either electrical potential gradient, pH difference, or both across the inner membrane of the mitochondria. Remaining polarized is a necessary prerequisite for ATP generation by the mitochondria in a way that is included in our model (see Section 2.2 for the model equations surrounding the electron transport chain). At equilibrium, ATP generation matches consumption. Reduced ATP generation will limit how much ATP may be consumed, leading to poor reabsorption on the part of the kidney. Finally, overproduction of reactive oxygen species is understood to be a major problem for instance in ischemia-reperfusion injury. We capture this in our model by examining the reduction state of the NADH, Cytochrome C, and co-enzyme Q pools in the cell. For instance, if there is much more NADH than NAD^+, then Complex I will be in a more reduced state, and if simultaneously there is more of the reduced form of coenzyme Q than its oxidized form, then Complex I may create reactive oxygen species. Similarly Complex III may do the same if the pools of co-enzyme Q and Cytochrome C are both in a reduced state.

Model simulations indicate that the PT and mTAL are sensitive to different metabolic perturbations, we deal with these pathological questions first. Both are predicted to be susceptible to a lowered activity of Complex III, but the mTAL is more susceptible to Complex IV deficiency. This result is unsurprising because Complex IV uses oxygen as a substrate, and the relatively hypoxic environment of the mTAL means that a larger amount of Complex IV is necessary in order to produce the same hydrogen flux. On the other hand though, if we consider the two tissues' sensitivities to hypoxia in absolute terms we see that at an oxygen tension of 5 mmHg, the cytosolic ATP concentration in the mTAL is comparable to the baseline cytosolic ATP concentration in the PT. When the PT experiences an oxygen tension of 5 mmHg, it experiences ATP depletion sufficient to cause cell death. This is possible because Complex IV has a higher oxygen affinity in the mTAL in our model and experimentally [158]. That said, if we consider hypoxia relative to baseline oxygen tensions in each tissue, we see that the mTAL is at risk of cell death for 70% declines in the baseline oxygen tension whereas the PT is not at risk of cell death until 80-90% declines in oxygen tension from baseline. If we consider instead ATP homeostasis for higher rates of ATP consumption, we see that for a $Q_{ATP,max}$ that is 25% higher than typical in the mTAL (see the highest $Q_{ATP,max}$ in Table 3.7), we have a lower cytosolic ATP concentration than the PT does after a 25% increase in the maximal ATP consumption (see Table 3.6). This is despite the fact that the mTAL has a higher baseline cytosolic ATP concentration. This is due to the fact that the maximal ATP consumption in the PT is much lower than in the mTAL (1.5 M/s vs 2.1 M/s). In fact, after a 25% increase in the maximal ATP consumption in the PT, the PT's maximal ATP consumption is still lower than the baseline maximal ATP consumption in the mTAL. Ultimately then the PT is more sensitive to hypoxia below 10 mmHg oxygen tension. The mTAL is more sensitive to equivalent proportional decreases in oxygen tension than the PT is, to increased metabolic demand, and to Complex IV dysfunction. The mTAL is more sensitive to hypoxia and Complex IV dysfunction because of its baseline low oxygen tension, which can be demonstrated by considering its cytosolic ATP concentrations at comparable oxygen tensions to our PT hypoxia cases. The PT is more sensitive to oxygen tensions below

10 mmHg because Complex IV oxygen affinity in the mTAL is greater.

The proximal tubule is susceptible to OXPHOS dysfunction, for instance due to the accumulation of drugs reabsorbed from the nephron lumen [69]. Our results suggest that in the proximal tubule of the rat kidney, ATP concentrations are most sensitive to Complex III activity reductions, as can be seen in Figure 3.9. Based off of our results, we can predict that recovering Complex III function is the most promising target for mitochondria-mediated Fanconi syndrome if Complex III is affected. The predicted importance of Complex III, is compatible with experimental studies that suggest its importance to mitochondria-mediated renal pathology [127]. The additive relationship noted above between distinct OXPHOS deficiencies is indicative that this advice will remain true regardless of the combination of OXPHOS deficiencies.

Our model doesn't directly predict the production of reactive oxygen species, as we've noted before. However what it does predict presents an interesting case for how out-of-control reactive oxygen species production may depend on the supply of adenine nucleotides available during reperfusion. When ADP is not available within the mitochondrion, ATP Synthase is not able to shuttle hydrogen ions across the inner membrane of the mitochondrion. Without this, the electron transport chain is left in a reduced state and the proton motive force is increased. The adenine nucleotide levels (that is, the pooled concentration of ATP, ADP, and AMP) are experimentally observed to fall to roughly 30% of typical after clamping the renal pedicle (which includes the renal artery) for 60 minutes [34]. With a lower adenine nucleotide level, we see that the reperfused kidney's mitochondria are left in a reduced state in the PT and mTAL in our model as we expected, as discussed in Sections 3.3.12 and 3.3.13. This highly reduced state persists in our model unless the adenine nucleotide levels recover. The size of the adenine nucleotide pool is well-understood to be important to the respiration rate because adenine nucleotide translocase activity is frequently rate-limiting for mitochondrial respiration [4] and the size of the adenine nucleotide pool controls the flux through adenine nucleotide translocase [51]. Since it is important to the respiration rate, it is natural that with a smaller adenine nucleotide pool, that earlier steps in oxidative phosphorylation would be left in a reduced state for lack of a target to donate their electrons to.

Previous work [47] and our model predictions show that under 10 mmHg PT mitochondrial matrix oxygen tension, and our work predicts under 4 mmHg mTAL mitochondrial matrix oxygen tension, that some cells will experience ATP depletion. These estimates are much lower than tissue oxygen tensions linked to hypoxia [55], indicating that the hypoxia is more local than tissue-based measures can find, a result highly suggestive of microvascular ischemia, in accordance with the conventional microvascular view of renal hypoxia [50, 106, 119]. This suggests a role for microvascular ischemia in the development of renal hypoxia, rather than for macrovascular effects on renal hypoxia alone. Our findings for the threshold of hypoxic injury in the proximal tubule are compatible with experimental results [47].

We note above that for a physiologically reasonable metabolic demand, the mTAL can be sensitive to hypoxia. Understood relative to the PT's oxygen tension though, the mTAL is fairly resilient. We wish to identify the source of the mTAL's resilience to lower oxygen

tensions. We identified two factors in Section 3.3.11 which contribute to the resilience of the mTAL to ATP depletion during hypoxia: the mitochondrial volume fraction and Complex IV's oxygen affinity, which are recognized by physiologists as important to the resilience of the mTAL [158]. Our results noted in Section 3.3.11 suggest that mitochondrial volume fraction is very important to the mTAL's resilience, but that the higher oxygen affinity of Complex IV is part of what explains the mTAL's resilience. Our model predictions corroborate Schiffer et al's [158] hypothesis about the basis for the mTAL's resilience against hypoxia: that the mitochondrial volume density and Complex IV oxygen affinity both contribute to the robustness of the mTAL. This goes towards answering our comparative questions about the PT and mTAL.

Our predictions in our drug simulations indicate that the circumstances under which an uncoupler such as salicylate could cause proximal tubulopathy in rats are limited. We found that uncoupling was not a significant cause of ATP depletion in the cell in our model, although it could cause a significant increase in oxygen consumption (see Sections 3.3.6 and 3.3.7 for the results of the uncoupling case). Likely it requires underlying pre-existing conditions in the rat, for instance affecting delivery of oxygen to the kidney, such that the uncoupler is a more potent cause of hypoxia. Similarly, ifosfamide appears to be a less potent cause of kidney injury in rats according to our model (see Section 3.3.8). Ifosfamide primarily affects Complex I, and at experimentally noted ifosfamide-caused reductions in Complex I activity we did not observe significant ATP depletion in our model. This accords with observations that ifosfamide's nephrotoxicity is more concerning in children and patients taking cisplatin concurrently [89]. Ifosfamide could also produce an indirect impact through oxidative stress, a known consequence of Complex I dysfunction and ifosfamide use that is not within the scope of our model [163]. On the other hand, gentamicin is known to have common nephrotoxic effects via several mitochondrial mechanisms, including OXPHOS dysfunction and uncoupling [143], and our model indicates that these are sufficient to cause massive ATP depletion (see Section 3.3.8 and 3.3.9).

Aside from the above potential adverse outcomes, we studied oxygen consumption and how it was affected by many factors but principally uncoupling. Particularly in diabetes, uncoupling reduces the efficiency of aerobic respiration and increases the kidney's oxygen consumption [55]. Our work predicts increased oxygen consumption, but cannot predict the subsequent hypoxia because it treats mitochondrial partial pressure of oxygen as a clamped quantity, and thus not responsive to oxygen consumption. Future experimental and modelling work could go further by tying oxygen consumption to the partial pressure of oxygen via an estimated response curve of oxygen tension to oxygen consumption or a control ratio of the two quantities. However with this assumption of a clamped oxygen tension, we noted that a 10x increase in hydrogen leak produced a 37% increase in oxygen consumption in the PT, and that a 10x increase in hydrogen leak in produced a 27% increase in oxygen consumption in the mTAL. In light of the mTAL's inelastic supply of oxygen [47] and low baseline oxygen tension, it may nevertheless be more susceptible to uncoupling-mediated hypoxia.

In conclusion, our model accurately captures mitochondrial ATP generation and oxygen

consumption in the PT and mTAL. This model allows us to measure the efficiency of aerobic respiration in these two tissues, and the capacity of mitochondria to meet metabolic demand in the PT and mTAL. These predictions, found in Table 3.6 and 3.7, match well with experimental observations. We've also simulated OXPHOS dysfunction, uncoupling, hypoxia, and ischemia-reperfusion. Where possible we've identified thresholds for ATP depletion based on the above kinds of dysfunction. In the case of ischemia-reperfusion, we identify how to indirectly examine the production of reactive oxygen species from our model. We also examine different model descriptions of the process of reperfusion, demonstrating that the risk of reactive oxygen species production is much greater under some descriptions of reperfusion than others. More accurately capturing the feedback between tissue oxygen tension and oxygen consumption would be a valuable next step in capturing the negative consequences of uncoupling and other mitochondrial dysfunctions.

Chapter 4

A Model of Mitochondria in the Hepatocytes of Rats

4.1 Introduction

Mitochondria are crucial to understanding the pathophysiology of the liver in a wide array of circumstances. Some of the ways in which liver pathophysiology specifically is impacted by or mediated through mitochondria are not unique to the liver. Hypoxia is a common consequence of liver disease [179] and ischemia-reperfusion injury is a common consequence of liver transplantation [124] but they are certainly not unique to the liver. Other mitochondria-related pathophysiologies are unique to the liver. For instance alcoholic fatty liver disease is of course unique to the liver, and mitochondria are causally-connected to its development [195]. These unique problems for the liver also are associated with special adaptive responses. For instance during alcohol consumption, in healthy rats there is a large increase in liver oxygen tension [154]. This could potentially prevent hypoxia but could also increase oxidative stress, which is associated with alcohol-related liver injury [195]. In light of all these conditions, understanding mitochondria is crucial to understanding liver pathophysiology, but it is also necessary that the liver is recognized as the unique organ that it is when investigating mitochondria-related liver pathophysiology.

Since our interest is in a cellular organelle, we take a subcellular modelling approach to study this system. We study a system of ordinary differential equations which describe pyruvate oxidation, the tricarboxylic acid (TCA) cycle, and oxidative phosphorylation (OXPHOS). We take a model originally developed for cardiac muscle tissue [193], and since adapted to study the proximal tubule in the kidney [44], and adapt it into a model for hepatocytes. We opt to preferentially study hepatocytes within the liver because by volume the liver is composed of 80% hepatocytes [11]. The second-most common cell type, stellate cells, make up only 5-8% of liver cells [61]. Hepatocytes are also are the basis for many critical liver functions, including those related to energy metabolism, such as glycogenesis and gluconeogenesis [130].

We aim to develop a mathematical model of the hepatocyte mitochondrial function in both healthy and pathological conditions. Under baseline (healthy) conditions, we need to consider a range of values both to account for uncertainty and to account for heterogeneity between hepatocytes [12]. For our stated purpose of studying mitochondrial function, gradients of oxygen and preferences of metabolic pathways within liver lobules are particularly important. Other quantities are highly uncertain and must be varied for that reason. In particular ATP consumption and the contribution of glycolysis to liver function (the latter is also subject to spatial heterogeneity). When we examine the sensitivity of our model under health conditions, we'll be interested especially to identify the sensitivity of the default conditions to all the features mentioned here.

We then apply the model to investigate several causes of liver dysfunction, namely: mitochondrial disease (and especially those based on OXPHOS-mediated disorders), fatty liver disease (which especially causes oxidative stress, leading to OXPHOS dysfunction and Cytochrome C release), hypoxia, and acute alcohol consumption (which causes oxidative stress). Crucially, many of these either lead to or follow from OXPHOS dysfunction, and so our aim will be two-fold: to replicate conditions of a highly reduced OXPHOS chain, the natural preceding event to oxidative stress, and to consider OXPHOS dysfunction once it occurs.

4.2 Method

4.2.1 The Model

The model is adapted from a model for cells in the kidney of the rat. The biochemical reactions and transport kinetics in the two tissues are relatively similar, and so the model structure isn't significantly altered for this work. The only structural change to the kidney model is the introduction of glutamate dehydrogenase activity, described below. The key changes relative to either the PT or mTAL model were to the parameters, including some clamped states of the model. This happened in two phases: first we changed parameters that had been measured experimentally, and second we fitted some less measurable parameters. Section 4.2.2 addresses this second fitting phase. In this section we address experimentally determined parameter values.

Several important quantities for the model can be measured directly, they are listed in Table 4.1. ATP consumption ranges were chosen based on the activity of Na-K-ATPase in mice [80] and an estimate in rats that 20% of ATP consumption (via a proxy of oxygen consumption) is due to Na-K-ATPase [6]. This gave us a reasonable-appearing estimate that the maximal ATP consumption was roughly half of that of a proximal tubule cell in the kidney. $Q_{\text{ATP, max}}$ was chosen to be 8.75×10^{-4} M/s based on these measurements. Proximal tubule cells have particularly large energy requirements, suggesting this is reasonable [44]. Glycolysis-based ATP production (V_{Glyc}) was taken to be a third of the maximal glycolysis-mediated pyruvate and lactate production found in rats in Fedatto et al. [48], or 2.3×10^{-4}

Parameter	Values for Liver	Reference
Fractional Mitochondrial Volume (L mito/L cell)	0.23	[11]
Fractional Cytoplasmic Volume (L cyto/L cell)	0.70	[11]
Cytoplasm Water Fraction (L water/L cyto)	0.77	[172]
Mitochondria Water Fraction (L water/L mito)	0.58	[178]
Matrix NAD+NADH concentration (mmol/L matrix)	9.4×10^{-3}	[25]
Matrix concentration of co-enzyme Q (mmol/L matrix)	6.49×10^{-3}	[13]
Intermembrane concentration of Cytochrome C (mmol/L IM)	4.39×10^{-3}	[13]
Protein Density of Mitochondria (mg prot/L mito)	6.45×10^{5}	[97]
Liver-to-heart Ratio Complex I	1.2	[13]
Liver-to-heart Ratio Complex III	0.525	[13]
Liver-to-heart Ratio Complex IV	0.40	[13]
Mitochondrial Oxygen Tension (mmHg)	35	[121]
Cytosolic Potassium Concentration (mmol/L cyto)	88	[186]
Cytosolic pH	7.09	[177]
Cytosolic Magnesium Concentration (mmol/L cyto)	0.4	[136]
Cytosolic Pyruvate (mmol/L cyto)	1.2	[168]

Table 4.1: A list of parameters used in our model that were based on experimental data. One parameter noted above comes from murine data [25].

M/s.

The model structure was altered to include one additional flux, corresponding to the activity of glutamate dehydrogenase, which in mammalian cells converts glutamate into alphaketogluterate, a Krebs cycle intermediate. This flux was represented in our model with simplified kinetics as follows:

$$J_{\text{gdh}} = V_{\text{GDH}} \frac{[\text{GLU}]_{\text{x}}[\text{NAD}]_{\text{x}}}{K_{\text{M, GLU}} + [\text{GLU}]_{\text{x}}} \tag{4.1}$$

The activity of glutamate dehydrogenase is a source of alphaketogluterate and NADH in the mitochondrial matrix, and consumes glutamate and NAD^+ (see Equation 2.119). V_{GDH} and $K_{\text{M, GLU}}$ were chosen based on experimental measurements (to be 6.25 s^{-1} and 1.9x10^{-3} M respectively) [84]. That paper uses a model of the kinetics that was even simpler, not including NAD^+, for that reason, we treat that paper as measuring $V_{\text{max}} = X_{\text{GDH}} \frac{[NAD^+]_x}{K_{\text{NAD, ref}}}$, where $K_{\text{NAD, ref}}$ is a baseline concentration of NAD^+ present in the mitochondrial matrix. We use physiologically reasonable concentrations to choose $K_{\text{NAD, ref}}$, assume for calculation that this was the NAD^+ concentration present in the mitochondrial matrix in the work of Jonker et al. [84], and then V_{GDH} may be calculated simply as $V_{\text{GDH}} = \frac{X_{GDH}}{K_{\text{NAD, ref}}}$ (which Jonker et al. measure to be 2×10^{-10} M/s). Our model requires us to model the reaction's

dependence on NAD^+ concentration because otherwise the model may consume excessive NAD^+. Glutamate dehydrogenase consumes NAD^+ and for that reason exhibits a kinetic dependence on it [17].

Target Quantity	Measured	Source	Predicted
State 2 Oxygen Consumption (mM/s)	0.30	[72]	0.30
State 3 Oligomycin-Sensitive Oxygen Consumption (mM/s)	2.0	[72]	2.2

Table 4.2: Values used to fit unknown parameters and the predicted values.

4.2.2 Model Parameter Fitting

Along with the above experiment-based parameter changes, we decrease (23%) the hydrogen leak permeability relative to the proximal tubule model above ($P_{\text{H, Leak}}$ to 714, our adenine nucleotide translocase activity is the same as in the above PT model, that is X_{ANT} is 6.75 x 10^{-3}), we are able to find a suitable fit for the State 2 and 3 oxygen consumption as measured in isolated liver mitochondria [72]. In that work they measure the State 2 measurements of oxygen consumption to be 0.30 mM/s, and the State 3 measurements of oligomycin-sensitive (or Complex IV-dependent) oxygen consumption to be 2.0 mM/s. With adjustments to the hydrogen leak we get a good fit for the State 2 and 3 oxygen consumption. For other parameters we use values from Edwards et al. [44]. The results of the fit are recorded in Table 4.2.

4.2.3 Simulations

All simulations discussed below use an *in vivo* model, the State 2 and 3 respiration discussed in the previous section were measured using a different model structure that nevertheless shares most model equations (see the discussion in Chapter 2).

While there is a variety of mitochondria-mediated liver pathologies, they tend to progress through OXPHOS dysfunction or oxidative stress. The latter is attenuated by uncoupling effects, or hydrogen leak permeability. Uncoupling reduces the effect of oxidative stress because when the proton motive force is less strong, OXPHOS complexes are better able to transfer their electrons through the electron transport chain instead of staying in a reduced state that increases the risk of free radical formation. Oxidative stress can also initiate mitochondrial permeability transition (mPT), which may reduce the concentration of cytochrome C in the intermembrane space. Oxidative stress can also produce OXPHOS dysfunction.

OXPHOS dysfunction is represented by some combination of reductions in the activities of Complex I, III, IV, and ATP Synthase (X_{CI}, X_{CIII}, X_{CIV}, and X_{F1}, see Section 2.2). We consider combinations in reductions of these activities because many OXPHOS dysfunctions are not specific to one OXPHOS enzyme [104]. We consider successive reductions in the

activity of each OXPHOS enzyme by 25% to as low as a quarter of the baseline enzyme activity.

Oxidative stress is frequently a consequence of the cell being in an energized state where the redox state of the cell's electron transport chain is too reduced. We consider two mechanisms that are able to produce oxidative stress: high glycolysis (four times the default value for V_{Glyc}) or via reperfusion following a period of ischemia (ischemia involving zero oxygen tension, smaller adenine nucleotide (a 0.25 fold change in the concentrations of ATP, ADP, and AMP) and nicotinamide pools (a 0.5 fold change in NAD_{tot})). In the latter case, we consider the consequences of total hypoxia (no oxygen) over a period of 50,000 seconds (or roughly 14 hours) with a nicotinamide pool (the combined concentrations of NADH and NAD^+, or NAD_{tot}) that is half the normal size [86], and a pool of cytosolic adenine nucleotides (the combined concentrations of ATP, ADP, and AMP) that is a quarter of normal levels [86, 187]. Following this period of ischemia, liver oxygen tension returns to normal but other features of the cell do not. We then recorded the reperfusion behaviour until it appeared to settle at a new baseline.

Aside from the above cases, we consider uncoupling on its own and hypoxia. The latter is a known consequence of liver disease, and especially alcoholic liver disease in rats [154, 179]. We considered oxygen tensions reduced by tenths from the default oxygen tension of 36 mmHg, to a low of 3.6 mmHg. We also consider an oxygen tension of 0.5 mmHg to gauge the effects of more extreme hypoxia. For uncoupling, we consider 2x, 5x, and 10x typical hydrogen leak permeability ($P_{\text{H,leak}}$, see Equation 2.138).

4.3 Results

4.3.1 Baselines

Key model predictions are shown in Table 4.3. Under baseline conditions, the liver model predicts a cytosolic ATP concentration of 6.91 mM, and an ATP/ADP ratio of 18.11. These compare favourably with at least some experimental estimates. For instance Schwenke et al. measure the cytosolic ATP concentration to be 6.18 mM. The cytosolic ATP/ADP ratio was found to be 6.94 in the same study [162], although the ATP/ADP ratio varies widely between preparations [162, 198]. Other predicted measures of the energetic state of the liver also appear to accord well with at least some experimental results. For instance the electrical potential gradient across the inner membrane of liver mitochondria was predicted to be 167 mV (physiological conditions treated as a positive quantity). This is within experimentally observed ranges. Porter and Brand observe an electrical potential gradient of 149 mV [139]. Other studies on isolated hepatocytes have found the electrical potential gradient to be 154 mV in young rats [68]. Some studies report even lower values for the electrical potential gradient such as 108 mV [171] or 118 mV [123], both in perfused liver. Other studies working with isolated rat liver mitochondria have reported electric potential gradients as high as 188

	O_2 Consumption (nmol O_2 mg^{-1} s^{-1})	ATP Generation (nmol ATP mg^{-1} s^{-1})	P/O	Electrical Potential Gradient (mV)	Proton Motive Force (PMF, mV)	$[ATP]_c$ (mM)	$[ATP]_c$ /$[ADP]_c$
Base Case							
P_{O2} = 36mmHg pH_c = 7.09	0.62	2.04	1.64	166.85	167.71	6.91	18.11
P_{O2} Variation							
P_{O2} = 50mmHg	0.61	2.04	1.68	166.96	168.71	6.91	18.49
P_{O2} = 12mmHg	0.62	2.04	1.65	165.58	167.18	6.9	17.84
P_{O2} = 8mmHg	0.62	2.04	1.65	164.74	166.26	6.89	17.40
$Q_{ATP,max}$ Variation							
$Q_{ATP,max}$ x 0.75	0.45	1.27	1.4	167.21	169.03	6.94	20.01
$Q_{ATP,max}$ x 1.25	0.79	2.8	1.77	165.93	167.75	6.87	16.44
$Q_{ATP,max}$ x 1.5	0.96	3.56	1.86	164.99	167.26	6.80	14.30
pH_c Variations							
pH_c = 7.40	0.55	2.03	1.83	161.72	188.81	6.58	9.71
pH_c = 7.00	0.65	2.03	1.57	167.1	162.17	6.97	21.74
pH_c = 6.80	0.73	2.01	1.39	167.31	148.47	7.07	30.92
$[K^+]_c$ Variations							
$[K^+]_c$ = 60mM	0.63	2.03	1.61	176.53	168.15	6.93	19.57
$[K^+]_c$ = 140mM	0.61	2.04	1.66	153.77	167.63	6.86	15.97
$[Mg^{2+}]_c$ Variations							
$[Mg^{2+}]_c$ = 0.2mM	0.62	2.03	1.64	166.62	168.32	6.81	14.40
$[Mg^{2+}]_c$ = 0.8mM	0.62	2.05	1.64	166.59	168.30	7.01	24.89
Variations in H^+ and K^+ leak permeability							
No leaks	0.47	2.1	2.25	174.84	169.71	6.93	19.21
No H^+ leak	0.52	2.08	1.99	167.52	169.19	6.92	18.68
No H^+ leak, 10x $P_{K,leak}$	0.71	1.97	1.39	126.59	162.52	6.61	10.17
No K^+ leak, 10x $P_{H,leak}$	1.48	1.69	0.57	166.22	163.77	6.86	16.23
10x $P_{H,leak}$	1.42	1.71	0.6	160.56	163.82	6.85	15.97
10x $P_{K,leak}$	0.76	1.95	1.29	126.49	162.2	6.60	10.0
10x Leaks	1.18	1.77	0.75	125.82	159.96	6.50	8.77

Table 4.3: The model under typical conditions and various relevant deviations from normal conditions.

mV [137]. In the above cases, the proton motive force was also frequently measured. There is a wide range of experimental measurements, which encompasses our predictions, we predicted the proton motive force to be 168 mV. Experiments have found the proton motive force to range from 125 mV [171] to 191 mV [68].

We calculate the P/O ratio only taking into account oxygen consumption by the mitochondria. Unlike multiple experimental studies, the P/O ratio is calculated using only mitochondrial oxygen consumption (as well with non-mitochondrial oxygen consumption) by Brand, Harper, and Taylor [19]. Including only mitochondrial oxygen consumption, they find a P/O ratio of 1.69 [19]. This is comparable to our predicted P/O ratio of 1.64. The P/O ratio was calculated from the ATP generation, which under default conditions was found to be 2.04 nmol ATP mg^{-1} prot s^{-1} by ATP Synthase, and O_2 consumption which was found to be 0.62 nmol O_2 mg^{-1} prot s^{-1} (the P/O ratio is the ATP generation (or ATP Synthase activity) divided by 2x the oxygen consumption (or Complex IV activity)).

4.3.2 Parameter Sensitivity Analysis

Here we vary several important parameters, namely the leak permeabilities, cytosolic ion concentrations, maximal ATP consumption, and oxygen tension. For this analysis we consider large changes to these parameters and report the effects (the exact changes are noted in the first column of Table 4.3), rather than reporting local measures of sensitivity (see Table 4.3). Our sensitivity analysis indicates that only some of these perturbations have a strong impact on liver mitochondrial function, notably maximal ATP consumption and leak permeabilities.

The key parameters that most significantly alter the system's behaviour in the ranges considered here are the maximal ATP consumption and the leak permeabilities ($P_{\mathrm{H,\,leak}}$ and $P_{\mathrm{K,\,leak}}$, see Equations 2.138 and 2.139). Under a 1.5-fold increase in maximal ATP consumption, there's a slightly more than 1.6-fold increase in oxygen consumption. This suggests a larger maximal ATP consumption could lead to hypoxia, due to the significantly increased oxygen consumption. However the efficiency as measured by the P/O ratio of respiration also improves with increased ATP consumption (for higher ATP consumption, the P/O ratio may be as high as 1.87). Leak permeabilities also had a major impact on the oxygen consumption. When there is no potassium leak and a ten-fold increase in hydrogen leak, the oxygen consumption more than doubles. When there is a ten-fold increase in potassium and hydrogen leak, the ATP concentration reaches its minimum, 6.5 mM, the ATP/ADP ratio hits its minimum as well of 8.77, as did the proton motive force, which gets to a minimum of 160 mV.

These results suggest that uncoupling and greater ATP demand could trigger greater oxygen consumption, possibly producing hypoxic conditions.

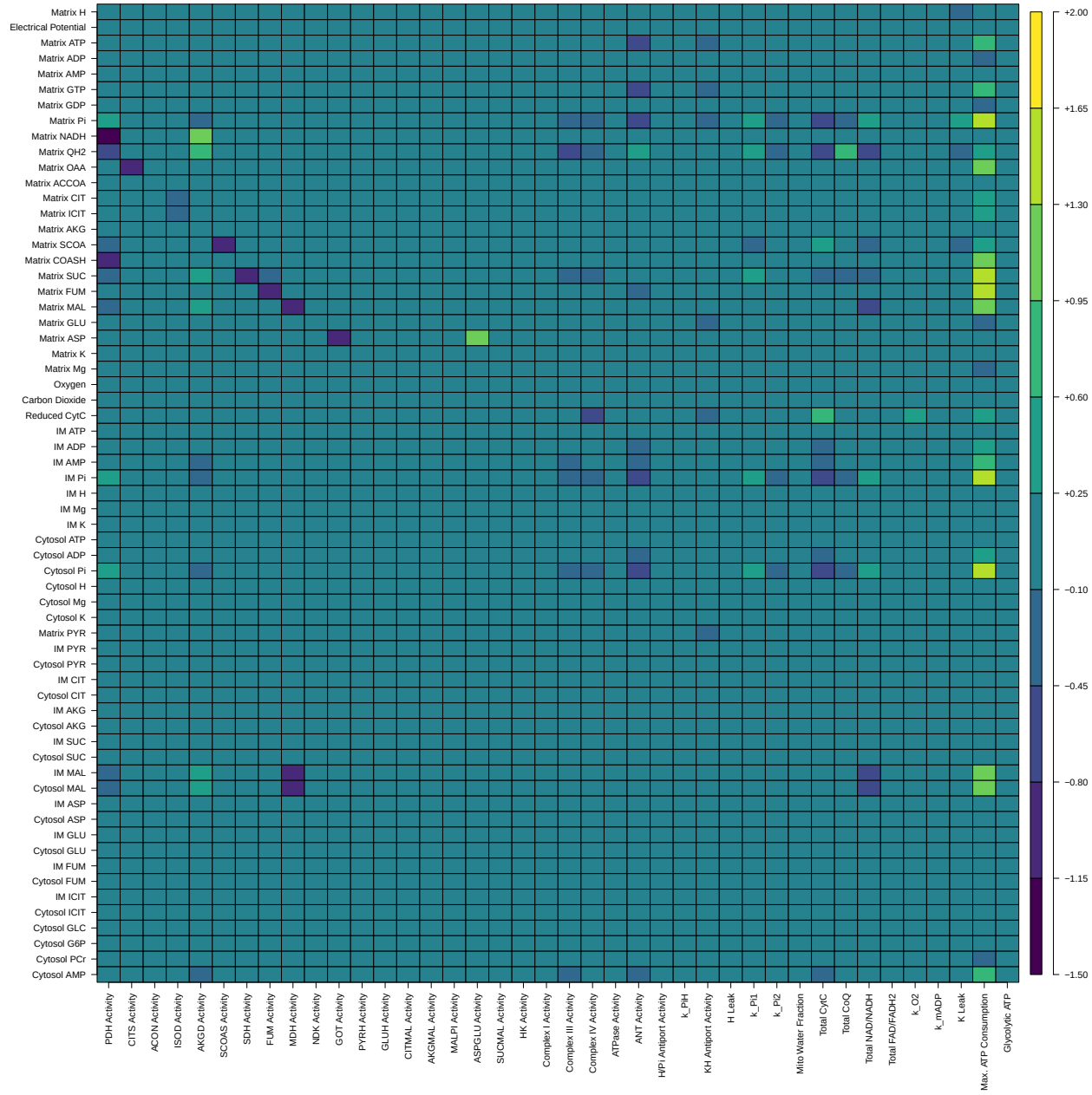

Figure 4.1: The full set of local sensitivities in the liver, for more information see section 4.3.3. CytC stands for cytochrome C, reduced cytochrome C refers to cytochrome C that has been donated an electron by Complex III.

4.3.3 Local Sensitivity Analysis

We consider the change in state variables in hepatocytes under a change in each parameter of our model. Below we show the derivative of each state variable against each parameter,

calculated using a central difference scheme with $\Delta p = 0.01p$ where p is the size of the parameter. The derivative is normalized relative to the baseline size of each state variable and the size of each parameter. The full local sensitivity analysis is reported in Figure 4.1. In Figure 4.2 we focus on several key variables and the parameters that are most impactful on those state variables. Hepatocytes in the liver appear to be fairly sensitive to many parameters. Several sensitivities are much higher than the comparable sensitivities in the PT and mTAL respectively. The NADH and reduced coenzyme Q concentrations were particularly sensitive to multiple key parameters. Cytosolic ATP concentrations are most sensitive to the maximal ATP consumption. The mechanism explaining the response of NADH concentrations to the activities of pyruvate dehydrogenase and alphaketogluterate dehydrogenase is the same as in the proximal tubule discussed above. Reduced coenzyme Q concentrations are strongly reactive to total NADH/NAD^+ concentrations, and thus to pyruvate dehydrogenase and alphaketogluterate dehydrogenase activity. Aside from those effects, the reduced coenzyme Q concentration is strongly sensitive to the total available coenzyme Q, and the pool available of cytochrome C, which is negatively associated with the quantity of reduced coenzyme Q. This indicates that the concentration of reduced coenzyme Q is restricted by the total amount of coenzyme Q to a moderate extent, and that the reduction state of the coenzyme Q is also controlled by the available cytochrome C to accept electrons from coenzyme Q. Overall this indicates that the coenzyme Q and cytochrome C pools are not present in great excess of what the mitochondrion needs.

4.3.4 OXPHOS Dysfunction

We describe our method for simulating dysfunction of oxidative phosphorylation (OXPHOS), that is activity of electron transport chain components and ATP synthase, above in Section 4.2.3. With a lowest OXPHOS complex activity of one quarter, there is little discernable consequence for cytosolic ATP consumption, and very little noticeable difference in the electrical potential gradient. With reduction to one quarter of all considered OXPHOS complex activities, the cytosolic ATP concentration differed by less than 2%. The electrical potential gradient never differed by more than 4%. Thus, impaired OXPHOS function was found to have little impact on ATP concentrations, or the electrical potential gradient of the liver. This result is consistent with the relatively few mitochondrial diseases known to affect the liver [104]. Those that do tend to be particularly severe, causing death in childhood, or progressive diseases leading ultimately to the depletion of mitochondrial DNA. The results were not significantly different under moderate hypoxia or reduced glycolysis.

Liver hepatocytes are predicted to be more robust than the proximal tubule (PT) of the kidney to OXPHOS dysfunction (results compiled in Table 4.4). The thick ascending limb (mTAL) is also more sensitive to OXPHOS dysfunction than the liver, but it has more confounding differences in tissue oxygen tension and mitochondrial volume fraction. We explore the reason for the difference between the PT and liver in robustness by considering the effect of reducing Complex III activity by 75% for hepatocyte mitochondria with PT-like parameter

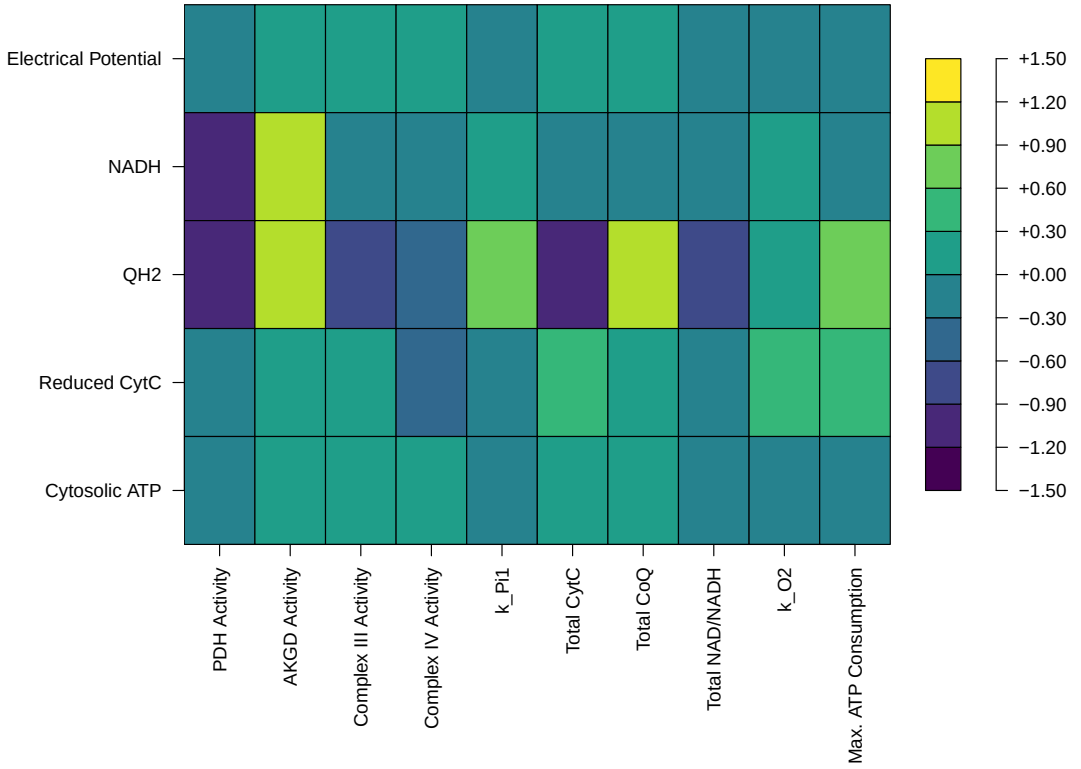

Figure 4.2: Local sensitivities of several important state variables in hepatocytes relative to certain significant parameters. CytC stands for cytochrome C, reduced cytochrome C refers to cytochrome C that has been donated an electron by Complex III. AKGD refers to alphaketogluterate dehydrogenase, PDH refers to pyruvate dehydrogenase, ANT refers to adenine nucleotide translocase, and QH_2 is the reduced form of coenzyme Q.

values for metabolic demand, glycolysis activity, or baseline OXPHOS enzyme activities (and combinations thereof). We consider another kind of robustness that the liver hepatocytes exhibit below (namely, to hypoxia). The PT has 74% of baseline cytosolic ATP concentrations under reduced Complex III activity. With no glycolysis (matching the PT) or PT-like baseline OXPHOS activities, the difference in cytosolic ATP concentration is negligible for a liver hepatocyte with Complex III dysfunction. With PT-like metabolic demand, we see 90% of baseline cytosolic ATP concentrations in hepatocytes. With both no glycolysis and PT-like metabolic demand, we see 78% of baseline cytosolic ATP concentrations. With PT-like OXPHOS activities and metabolic demand, we see 88% of baseline cytosolic ATP concentrations during Complex III dysfunction. With no glycolysis and PT-like baseline OXPHOS activities, we see negligible differences from baseline cytosolic ATP concentrations. With no glycolysis, PT-like metabolic demand, and PT-like baseline OXPHOS activities, we see 74% of baseline cytosolic ATP concentrations. This indicates that adjusting the glycolytic activity, OXPHOS activities, and metabolic demand to PT-like parameters is necessary and

Conditions	Relative Cytosolic ATP compared to typical Liver Hepatocytes
Liver hepatocyte with 75% dysfunction in Complex III	99%
Dysfunctional hepatocyte with PT-like metabolic demand	90%
Dysfunctional hepatocyte without glycolytic activity	97%
Dysfunctional hepatocyte with PT-like baseline OXPHOS activities	99%
Dysfunctional hepatocyte with PT-like metabolic demand and no glycolysis	78%
Dysfunctional hepatocyte with PT-like metabolic demand and baseline OXPHOS activities	88%
Dysfunctional hepatocyte with PT-like baseline OXPHOS activities and no glycolysis	96%
Dysfunctional hepatocyte with all three adjustments to be more like the PT	74%
PT Epithelial Cell with 75% dysfunction in Complex III	74%

Table 4.4: Variations in hepatocyte conditions and the consequences for cytosolic ATP concentrations under Complex III dysfunction.

together sufficient for us to observe PT-like sensitivity to OXPHOS dysfunction.

4.3.5 Conditions producing Oxidative Stress

Oxidative stress can occur under a range of circumstances. In our simulation work, high rates of glycolysis appear to be a particularly significant potential means of producing oxidative stress. We see in Figure 4.3 that under these glycolytic conditions, the proton motive force is extremely high (223 mV), supporting this conclusion. We consider high rates of maximal glcolysis, four times our default, similar to those observed in the presence of 20 mM of glucose [48]. This indicates that elevated glycolysis could generate reactive oxygen species in liver hepatocytes.

4.3.6 Uncoupling

Uncoupling is used by the cell as a means of relieving oxidative stress. However uncoupling also directly reduces the P/O ratio governing the efficiency of ATP generation, and increases oxygen consumption [161, 191], which may cause hypoxia. Titrating with FCCP, a potent uncoupler, until the respiratory rate was maximal, Schönfeld et al. was able to experimentally produce a 60% increase in oxygen consumption [161]. Our model reproduces this (see Table 4.5) proportional respiration rate increase with a five-fold increase in hydrogen leak (in this case, the P/O ratio was 0.93). Under a two fold increase in the hydrogen leak activity,

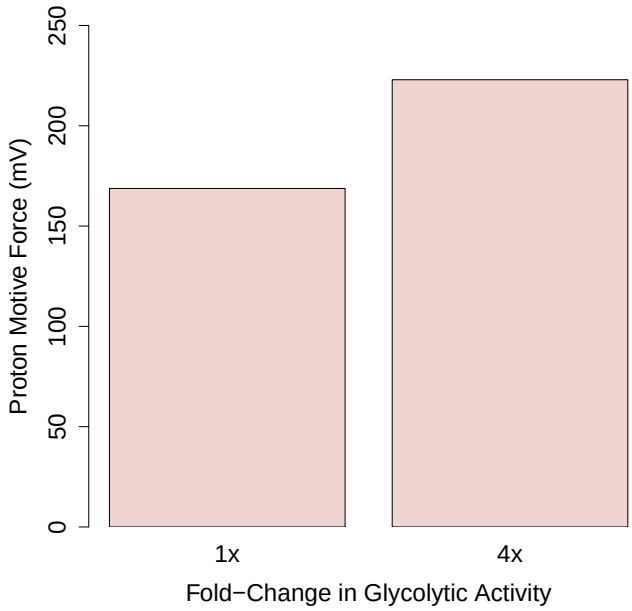

Figure 4.3: The left is the steady state proton motive force for the baseline model, and the right is the value under high rates of glycolysis (a quadrupled glycolytic activity).

	O_2 Consumption (nmol O_2 mg^{-1} s^{-1})	ATP Generation (nmol ATP mg^{-1} s^{-1})	P/O	Electrical Potential Gradient (mV)	Proton Motive Force (PMF, mV)	$[ATP]_c$ (mM)	$[ATP]_c$ /$[ADP]_c$
Base Case							
36 mmHg	0.62	2.04	1.64	166.85	167.71	6.91	18.11
Hypoxia							
0.5 mmHg	0.31	1.85	2.98	144.55	145.69	4.92	2.61
3.6 mmHg	0.60	2.03	1.7	158.44	159.61	6.76	13.21
18 mmHg	0.62	2.04	1.65	164.7	166.23	6.89	17.39
Uncoupling Cases							
2x H^+ Leak	0.72	2.0	1.38	166.24	166.96	6.9	17.78
5x H^+ Leak	1.01	1.88	0.93	164.84	165.2	6.88	16.91

Table 4.5: Additional predictions for simulations referred to in relation to hypoxia and uncoupling (see Sections 4.3.7 and 4.3.6).

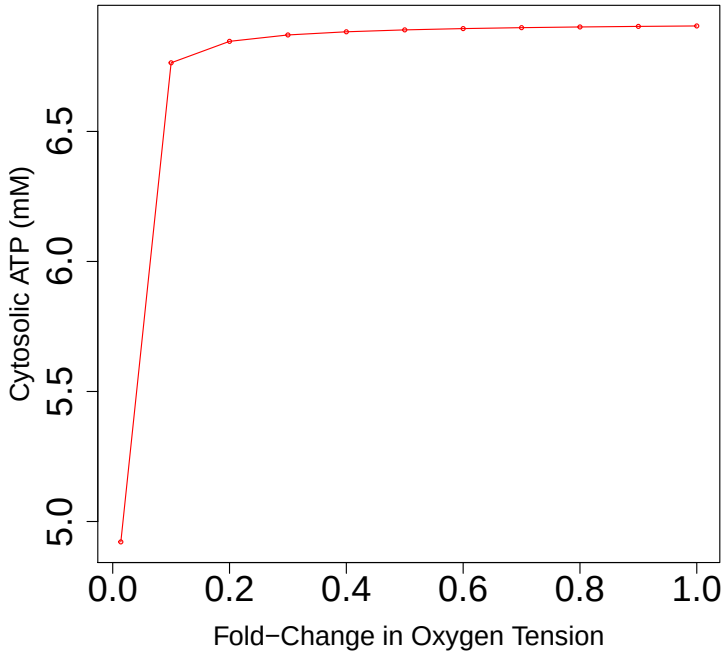

Figure 4.4: The response of cytosolic ATP levels in hepatocytes to changes in the liver's oxygen tension, the curve joins the points considered in a piecewise linear fashion.

we predict a 16% increase in oxygen consumption, which in an organ with already quite significant oxygen gradients within each liver lobule might be quite important. Already under a two-fold increase in the hydrogen leak, the P/O ratio predicted by the model to be as low as 1.38, compared to a baseline of 1.64, a 24% decrease. Thus we see a significant dependence of oxygen consumption on the extent of uncoupling.

4.3.7 Hypoxia

Our hypoxic simulations are outlined above in Section 4.2.3. The liver is only at-risk of ATP depletion under significant reductions in the oxygen tension in mitochondria (see Table 4.5). At an oxygen tension of 0.5 mmHg the cytosolic ATP concentration is reduced by 29% (to 4.9 mM). However at a tenth of normoxic oxygen tension (3.6 mmHg), cytosolic ATP concentrations are reduced by less than 4%. These results may seem inconsistent with the understood possibility of hypoxic liver injury but they are not. Another way that hypoxia can lead to mitochondria-mediated injury is discussed below in Section 4.3.8. Now we turn to the mechanism that explains this robustness.

Comparing ATP depletion between liver hepatocytes and the kidney, we see that hepatocytes are more robust to hypoxia. We simulate hepatocytes with PT-like metabolic demand

Conditions	Relative Cytosolic ATP compared to typical Liver Hepatocytes
Liver Hepatocyte with 10% of typical oxygen tension	98%
Hypoxic Hepatocyte with PT-like metabolic demand	57%
Hypoxic Hepatocyte without glycolytic activity	95%
Hypoxic Hepatocyte with PT-like baseline OXPHOS activities	97%
Hypoxic Hepatocyte with PT-like metabolic demand and no glycolysis	40%
Hypoxic Hepatocyte with PT-like metabolic demand and baseline OXPHOS activities	46%
Hypoxic Hepatocyte with all three adjustments to be more like the PT	31%
PT Epithelial Cell with 10% of typical oxygen tension	57%

Table 4.6: Variations in hepatocyte conditions and the consequences for cytosolic ATP concentrations under 10% of baseline oxygen tensions.

($Q_{ATP,\,max}$), glycolysis (V_{Glyc}), and baseline OXPHOS activity (X_{CI}, X_{CIII}, and X_{CIV}) in order to determine the differences that explain why they differ. We choose to compare to the PT because of the more comparable baseline oxygen tension. With 10% of baseline oxygen tension, the PT has 57% of its typical cytosolic ATP concentration. For PT-like metabolic demand, we have 57% of typical cytosolic ATP concentrations in the hypoxic hepatocyte. Without glycolysis, we have 95% of typical cytosolic ATP concentrations in the hypoxic hepatocyte. With both higher metabolic demand and no glycolysis, we have 40% of typical cytosolic ATP concentrations in the hypoxic hepatocytes. With PT-like metabolic demand, no glycolysis, and PT-like OXPHOS activity, we see 31% of typical cytosolic ATP concentrations. Ultimately this indicates that the hepatocyte's robustness against hypoxia is multifactorial, but that the lower metabolic demand plays a dominant role in explaining the hepatocyte's robustness to hypoxia.

4.3.8 Ischemia-Reperfusion Injury

Ischemia-reperfusion causes oxidative stress by leaving the electron transport chain in a highly reduced state temporarily. This is dangerous to the cell and the body, and can even lead to multiple organ dysfunction [131]. We wish to capture ischemia-reperfusion injury in our model and consider some candidate methods for preventing ischemia-reperfusion injury. To achieve this, we will simulate ischemia, and then we will simulate reperfusion in multiple ways. Then, we will study reperfusion in combination with interventions using pyruvate and dichloroacetate. During ischemia, the cell experiences a decline in both pyruvate and oxygen concentrations. As a consequence of ischemia, the adenine nucleotide (AMP/ADP/ATP) and nicotinamide adenine dinucleotide ($NADH/NAD^+$) pools become significantly smaller.

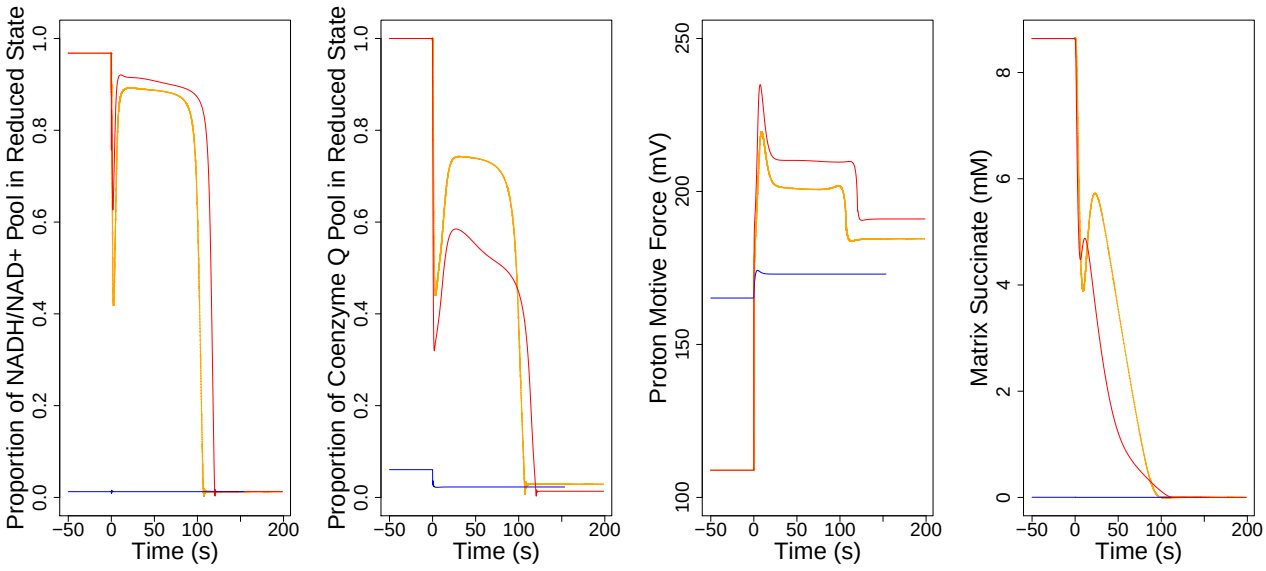

Figure 4.5: The effects of reperfusion (starting at time zero, with the ischemic steady state before that point) with a smaller pool of adenine nucleotides on NADH/NAD$^+$ & coenzyme Q redox state, the proton motive force, and the succinate concentration (red). The effects of reperfusion with a smaller pool of adenine nucleotides and OXPHOS dysfunction are in orange. The effects of reperfusion with a smaller pool of adenine nucleotides after more minor hypoxia (a 90% reduction in oxygen tension) are in blue.

The former shrinks by three quarters [86, 187], and the latter by one half [86]. Ischemia also causes OXPHOS dysfunction that reduces the activity of Complex I, III, and IV.

For our model, we consider a shrunken pool of AMP, ADP, ATP, NADH, and NAD$^+$ during reperfusion on top of restoration of typical oxygen levels after a bout of severe hypoxia (0 mmHg). We shrink the pool of adenine nucleotides by three quarters and the pool of nicotinamide adenine nucleotides by half following experimental results from Kamiike et al [86]. In this case, shown in Figure 4.5, we see that the NADH/NAD$^+$ and coenzyme Q pools are in a significantly reduced state for several minutes after reperfusion, and that the proton motive force is extremely elevated during the same period of time. This matches the timescale expected from experimental work, where it has been observed that reactive oxygen species are produced rapidly in a short period following reperfusion or reoxygenation [81]. In another trial, we consider the consequences of also including OXPHOS dysfunction. We include OXPHOS dysfunction by reducing the activity of Complex I, III, and IV by 15%, 70%, and 50% respectively following experimental results from Baniene et al. [199]. Under these circumstances, shown in Figure 4.5, we predictably see a somewhat more reduced coenzyme Q pool with a somewhat lower but still very high proton motive force. This is to be expected because a reduced rate of oxidative phosphorylation means that it will take longer to oxidize coenzyme Q. In other trials, we consider more moderate hypoxia (one tenth of typical) and

we do not observe the same long transients. We show the response to reperfusion in this less extreme case in Figure 4.5. This is demonstrably due to a lack of succinate build up because when we increase the succinate levels in these trials to levels comparable to our more extreme hypoxic case, we again see long transients.

4.4 Discussion

Our model simulations tell a simple story: the liver is highly effective at maintaining ATP homeostasis, but possibly quite sensitive to phenomena known to cause oxidative stress. These two features of liver mitochondria happen for overlapping reasons. The liver has a high capacity for glycolytic activity [48]. This capacity means the mitochondria do not have to satisfy the hepatocyte's metabolic burden on their own, but also can leave the mitochondria in a highly reduced state for lack of ADP to phosphorylate. This underlies our findings shown in Figure 4.3 that at the rates of glycolysis observed by Fedatto et al. [48] in healthy rats experiencing hyperglycemia, the electrical potential gradient is larger across the inner membrane of the mitochondria. This trade off of, on the one hand, being able to satisfy the cell's energetic requirements but on the other, risking oxidative stress, appears to be valuable for interpreting our results. We note reasons for this robustness in Sections 4.3.4 and 4.3.7. Our results demonstrate that it is a combination of several factors that explains the differences in robustness observed in liver hepatocytes compared to the proximal tubule in the kidney, a tissue that is far less robust to ATP depletion. Our results indicate that the liver's glycolytic activity, lower metabolic demand, and higher basline OXPHOS activites all contribute to the liver's robustness to dysfunction of Complex III, the rate-limiting step of the electron transport chain, and all must be changed to PT-like values in order to produce PT-like sensitivity to OXPHOS dysfunction. Similarly we need to change all three of these features of the hepatocyte in order to see PT-like sensitivity to ATP depletion during hypoxia. The hepatocyte simply has more electron transport activity servicing a smaller metabolic demand with a larger contribution from glycolysis, and this makes it more robust to significant kinds of ATP depletion.

This ability to satisfy the cell's energetic requirements may be examined in several ways. First of all, the cell is predicted to maintain a steady concentration of ATP even under a 50% increase in the maximal ATP consumption, as shown in Table 4.3. Second, as noted above in Section 4.3.4, if the rates of glycolysis are reduced we also see that the mitochondria can make up the difference by increasing their ATP generation. Each of these model simulations support our contention that the mitochondria may robustly provide for the hepatocyte's ATP needs. These observations should not surprise us, since ATP depletion is not frequently observed in mitochondria-mediated liver pathologies, unlike oxidative stress [195, 124].

Ischemia-reperfusion injury is frequently caused by a temporary excessively reduced redox state of the electron transport chain causing oxidative stress during reperfusion [15]. We represent ischemia in our model by decreased oxygen tension and pyruvate concentra-

tion. During reperfusion we include a decreased supply of adenine nucleotides, based on a study that indicates a 75% smaller adenine nucleotide following ischemia [86]. We observe a transient redox state change as recorded in Figure 4.5. We also consider added effects from OXPHOS dysfunction. When we include these effects, we see a more reduced coenzyme Q pool and a marginally lower transient proton motive force relative to the ischemia-reperfusion case without OXPHOS dysfunction, as shown in Figure **??**. Both resemble experimentally observed timescales for the enhanced production of ROS following ischemia [30, 66, 81]. However the results in the latter case should be interpreted carefully. Reperfusion injury harms the electron transport chain, and it is often difficult to study the effects of ischemia on oxidative phosphorylation independently from the effects of reperfusion. For this reason, the levels of OXPHOS dysfunction used in Figure **??** should be treated as potential overestimates. These limitations are not a major problem because we are able to reproduce the appropriate timescale of reperfusion transients with or without OXPHOS dysfunction as noted above.

The saturation of the electron transport chain with electrons during reperfusion appears to be closely tied to the build up of succinate in ischemia, and the associated consumption of succinate following reperfusion. This coincides with suggested mechanisms for reperfusion injury in cardiac tissue [30]. As Chouchani et al. [30] notes, succinate build up has a preponderance of evidence indicating its importance to mitochondria-mediated ischemia-reperfusion injury. Under more moderate hypoxia in other cases considered, where succinate build up is not observed in the same way, we do not see the same indicators of risk of ROS production that we note above.

In rats, it has been observed that chronic alcohol consumers have worse hepatic oxygen homeostasis relative to control non-alcoholic rats [154]. That is, in the event of acute alcohol consumption, chronic alcohol consumers may experience extremely low hepatic oxygen tensions. Sato et al. found that chronic alcohol consumers had a median oxygen tension upon acute alcohol consumption of 8 mmHg and oxygen tensions could be indistinguishable from zero [154], that is less than 3 mmHg. This is comparable to the hypoxic simulation case discussed in the previous paragraph. This suggests a mechanism by which alcohol consumption in individuals with alcoholic liver disease may trigger oxidative stress in a tissue, accelerating the progression of the disease.

While glycolysis may be elevated to levels like those noted previously in severe hyperglycemia, there are other ways to produce comparably elevated glycolysis as well. Fedatto et al. [48] studied hepatic tissue of rats with adjuvant arthritis (triggered by heat-killed *Mycobacterium tuberculosis*). The maximal rate of glycolysis was found to be roughly 30% higher in the arthritic rats. This presents another means of producing elevated glycolysis, which is potentially a trigger for oxidative stress. Fedatto et al. hypothesize other illnesses causing circulating inflammatory mediators may produce the same glycolytic effects [48], suggesting a range of diseases that could be causing oxidative stress in hepatocytes.

Our work can predict various indicators of oxidative stress, but cannot predict ROS production or the subsequent oxidative stress. Future work could our model with realistic models of ROS production. The former problem may be resolved by adapting existing models

of ROS production [60] to the liver and incorporating them into our model. Predicting oxidative stress requires progress in the study of mitohormesis for the liver, so that thresholds for pathological ROS production may be found. As it stands we know that a moderate amount of ROS production may be a good thing [135]. Another contribution that could improve our model would be to integrate it with models of other pathways of hepatic metabolism, models of this kind exist for at least parts of hepatic metabolism [35]. Finally, our parameter estimates draw from a heterogeneous set of sources, including some experimental estimates from mice, namely, the Na-K-ATPase activity (discussed in Section 4.2.1), the cytosolic potassium concentration [186], and the pooled NADH/NAD^+ concentration [25]. With more data from rats, it is possible we would have better predictions.

We include glutamate dehydrogenase activity in our model. Jonker et al. [84] found sexual dimorphism in the parameter $K_{\text{NAD, ref}}$ in rat hepatocytes. Periportal hepatocyte $K_{\text{NAD, ref}}$ were estimated to be 2.7 mmHg in male and female rats, and in the pericentral hepatocytes of female rats the average was estimated to be as high as 3.7. For the purpose of this work an intermediate value was chosen between the sexes (3 mmHg), but future work could expand on ours by creating a sex-specific version of the model that included this sexual dimorphism in glutamate dehydrogenase dynamics. Valle et al. [182] notes sexual dimorphism in OXPHOS capacity and mitochondrial protein content as well. These differences are likely to be the most impactful on mitochondrial behaviour since as we mentioned before, OXPHOS capacity is a key factor that explains the liver's robustness to OXPHOS dysfunction.

In conclusion, we have developed a model of hepatocytes in mitochondria that predicts ATP generation, oxygen consumption, and risk factors of ROS production & oxidative stress. Our findings agree with empirical findings that ATP depletion is not a major risk in the liver, and seems to support the view that oxidative stress might be important to liver pathophysiology in many cases.

Chapter 5

Effects of Diabetes on Mitochondrial Function in Renal Epithelial Cells and Hepatocytes

5.1 Introduction

Roughly half a billion people globally suffer from diabetes [116]. Diabetes is a major burden due to the mortality risk and the systemic impacts of diabetes on multiple organ systems and ultimately, quality of life [114, 116]. Treatment of diabetes requires the management of both the immediate effects of diabetes on blood sugar, and its downstream complications. In this work we contribute to the latter aim, by exploring the effects of blood sugar dysregulation on cellular respiration in the kidney and liver, which may contribute to diabetic end organ damage. We do this with an ordinary differential equations model of mitochondrial ATP generation and oxygen consumption (see Chapter 2). The effects of diabetes on key determinants of mitochondrial function are not systematically understood, and differ significantly between studies and model systems (see Table 5.1). While this work is constrained to rat physiology, this still leaves considerable variation based on the kind of model of diabetes used. Parameter estimates for models of type I diabetes, especially streptozotocin-caused diabetes, were most common [21, 37, 41, 85, 87, 95, 117, 118, 125, 129, 148, 190, 194]. Thus we have more confidence that our results resemble the streptozotocin case than others. However we consider parameter ranges from other experimental models where available as a starting point for considering other models. We identify ranges for diabetic impacts on cellular respiration and perform parameter sensitivity analyses across these ranges. In doing so, we hope to capture some effects of mitochondrial dysfunction that could play a part in diabetic end organ damage.

There are many animal models of diabetes [88]. In finding parameter estimates for our work we primarily consider rat models of diabetes where experimental measurements useful

to our model were recorded. We also sparingly use results from murine models of diabetes. We ultimately identified several relevant parameters that differ during diabetes: Complex I, III, and IV activity, cytochrome C and coenzyme Q concentrations, mitochondrial volume fraction, and total protein content. Our measurements came from multiple experimental rat models of diabetes, including diet-induced diabetes using a 20% high fructose corn syrup diet [31], streptozotocin- and alloxan-induced diabetes (many, but for example Wu, Luo, and Yan [194]), genetically impaired glucose response using Goto-Kakizaki rats [153], and genetic obesity using the Zucker fatty rat [147]. Due to the heterogeneity both in diabetes and in experimental models of diabetes, we do not identify a single mathematical model of diabetes. Instead we identify parameter ranges that are observed under at least some experimental model of diabetes in order to give a range of predictions for the effects of diabetes on mitochondrial function.

The parameter measurements included in Table 5.1 capture the effects of diabetes on oxidative phosphorylation (OXPHOS) as a result of dysregulated reactive oxygen species (ROS) production. However there are other sources of physiological damage: in response to increased ROS production, mitochondria respond by increasing hydrogen leak [55], or uncoupling, in order to avoid leaving the OXPHOS system in such a reduced state as to produce significant amounts of ROS. While this response is meant to be adaptive and is part of mitohormesis, it can cause hypoxia, because uncoupling reduces the efficiency of cellular respiration, leading to greater oxygen consumption. This renders the cell susceptible to oxidative stress, hypoxia, or both, a dangerous condition to be in. Thus aside from the above measurements of OXPHOS systems, we consider a wide range of values for uncoupling and oxygen tension.

The uncoupling activity, oxygen tension, and activities or concentrations of OXPHOS components together capture a large portion of the significant differences of mitochondrial function in diabetes. Within this framework we predict several quantities of interest to the study of the diabetic liver and kidney: cytosolic ATP concentrations, ATP generation, oxygen consumption, the P/O ratio, and the redox state of the NADH/NAD^+ pool, cytochrome C, and coenzyme Q. ATP depletion leads to cell death, changes to oxygen consumption lead to hypoxia, and the redox states of the above electron carriers determine the risk of out-of-control ROS production. While this doesn't capture all the risks to the cell from mitochondrial dysfunction, it captures some of the most important ones.

5.2 Methods

5.2.1 Parameter Collection

As noted above, several physical quantities were identified that appear to differ between healthy rodents and rodents experiencing early diabetes. We use these to develop our model of diabetic mitochondria. Oxidative phosphorylation is altered in numerous ways by diabetes.

Parameter Measured	Species	Organ	Diabetes	Parameter Change	Paper
Complex I Activity	Rat	Kidney	STZ	None	[129]
Complex I Activity	Rat	Kidney	STZ	$<$ 25% Reduction	[194]
Complex I Activity	Mouse	Kidney	STZ	$\sim$ 33% Reduction	[41]
Complex I Activity	Rat	Liver	STZ	None	[21]
Complex I Activity	Rat	Liver	Al	$\sim$ 25% Reduction	[118]
Complex I Activity	Rat	Liver	GO	$\sim$ 50% Reduction	[147]
Complex III Activity	Rat	Kidney	STZ	$<$ 25% Reduction	[129]
Complex III Activity	Mouse	Kidney	GO	$\sim$ 25% Reduction	[200]
Complex III Activity	Rat	Liver	STZ	$<$ 25% Reduction	[148]
Complex IV Activity	Rat	Kidney	STZ	$\sim$ 50% Reduction	[37]
Complex IV Activity	Rat	Kidney	STZ	None	[129]
Complex IV Activity	Mouse	Kidney	STZ	$\sim$ 75% Reduction	[41]
Complex IV Activity	Rat	Liver	STZ	$\sim$ 75% Increase	[21]
Complex IV Activity	Rat	Liver	GO	$<$ 75% Reduction	[147]
[Coenzyme Q]	Rat	Kidney	STZ	$\sim$17% Reduction	[125]
[Coenzyme Q]	Mouse	Kidney	GO	$\sim$ 50% Reduction	[173]
[Coenzyme Q]	Mouse	Kidney	GO	None	[192]
[Coenzyme Q]	Rat	Liver	STZ	$\sim$ 80% Reduction	[95]
[Coenzyme Q]	Rat	Liver	GD	$\sim$ 100% Increase	[153]
[Cytochrome C]	Rat	Kidney	STZ	$<$ 25% Reduction	[87]
[Cytochrome C]	Mouse	Kidney	STZ	$\sim$ 60% Reduction	[117]
[Cytochrome C]	Rat	Liver	STZ	None	[21]
[Cytochrome C]	Mouse	Liver	DO	$<$ 75% Reduction	[31]
Mito. Protein Content	Rat	Liver	STZ	$\sim$ 20% Increase	[85]
Mito. Volume Fraction	Mouse	Kidney	GO	$\sim$ 15% Increase	[117]
Mito. Volume Fraction	Rat	Liver	STZ	$\sim$ 50% Increase	[190]

Table 5.1: Parameter estimates for diabetes-specific fold changes in parameter values. The diabetes column lists the diabetes model by kind. STZ stands for streptozotocin-induced (a model of Type I diabetes), Al for alloxan-induced (Type I), GO for genetic obesity (Type II), GD for genetic non-obese Type II diabetes, and DO for dietary obesity (Type II). When identifying changes in Coenzyme Q concentrations, concentration changes that were mitochondria-specific were preferred to non-organelle-specific estimates where both existed. However no such estimates were available for the kidney. Several liver-specific quantities were reported per mass of mitochondrial protein, in these cases the mitochondrial protein content fold change reported in this table was used to facilitate comparison.

We collect these parameter estimates in Table 5.1. We see that the most used model of diabetes in the respirometry experiments that we identified was streptozotocin (STZ), a drug-based model of type I diabetes. However, we also identified parameter measurements

from alloxan-treated rats (Al), another model of type I diabetes, diet-induced obesity leading to a model of type II diabetes (DO), and genetic obesity models producing type II diabetes (GO). For all parameters considered, estimates could be found in rats for both the liver and the kidney. We report several results in mice for completeness, and to help identify where measurements in rats may give a conservative range for the potential changes in the parameters considered.

In several cases, care is necessary in interpreting the fold changes reported in the literature. Coenzyme Q for instance is not unique to mitochondria, it is found throughout the cell. But in the rat kidney, the only reports of fold-changes in concentration for the rat kidney we could identify were concentrations for the whole tissue, rather than organelle-specific [173]. In some cases, quantities were reported per mass of protein [148, 192]. However experimental work has found that the diabetic liver has significantly elevated protein content [85]. Thus the fold change in activity must be calculated taking the relative protein content into consideration as well.

OXPHOS deficiency, uncoupling, and hypoxia in the liver and kidney has been the subject of previous modelling work (see Sections 3.3.8, 3.3.9, 3.3.10, 3.3.11, 4.3.4, and 4.3.7 but also 44). However there are multiple reasons why the case of diabetes is different: namely, coenzyme Q concentrations and mitochondrial volume in each tissue differ between diabetic and non-diabetic individuals, and the fact that the differences in OXPHOS activity are well-understood in the diabetic case as discussed above. For the below simulations in the kidney, both the proximal tubule (PT) and medullary thick ascending limb of the loop of Henle (mTAL), we use a 17% reduction in mitochondrial coenzyme Q concentrations, no reduction in cytochrome C concentrations, and a 15% increase in mitochondrial volume fraction. In the liver we use a 80% reduction in coenzyme Q concentration (the more extreme case), no decrease in cytochrome C concentration, and a 50% increase in mitochondrial volume fraction. For OXPHOS dysfunction, the follow the experimental measurements in Table 5.1. In the kidney that means we consider fold-changes in Complex I activity of 0.67, 0.75, or no change, Complex III activity changes of 0.75 or no change, and Complex IV activity changes of 0.25, 0.5, 0.75, or no change. In the liver hepatocytes we consider fold-changes in Complex I activity of 0.5, 0.75, or no change, Complex III activity changes of 0.75 or no change, and Complex IV activity changes of 0.25, 0.5, 0.75, 1.75, or no change. We consider a spread of uncoupling levels and hypoxia in both tissues, with fold-changes in the hydrogen leak activity of 1.15, 1.5, 5, 10, or no change and fold-changes in the oxygen tension of 0.1, 0.5, or no change.

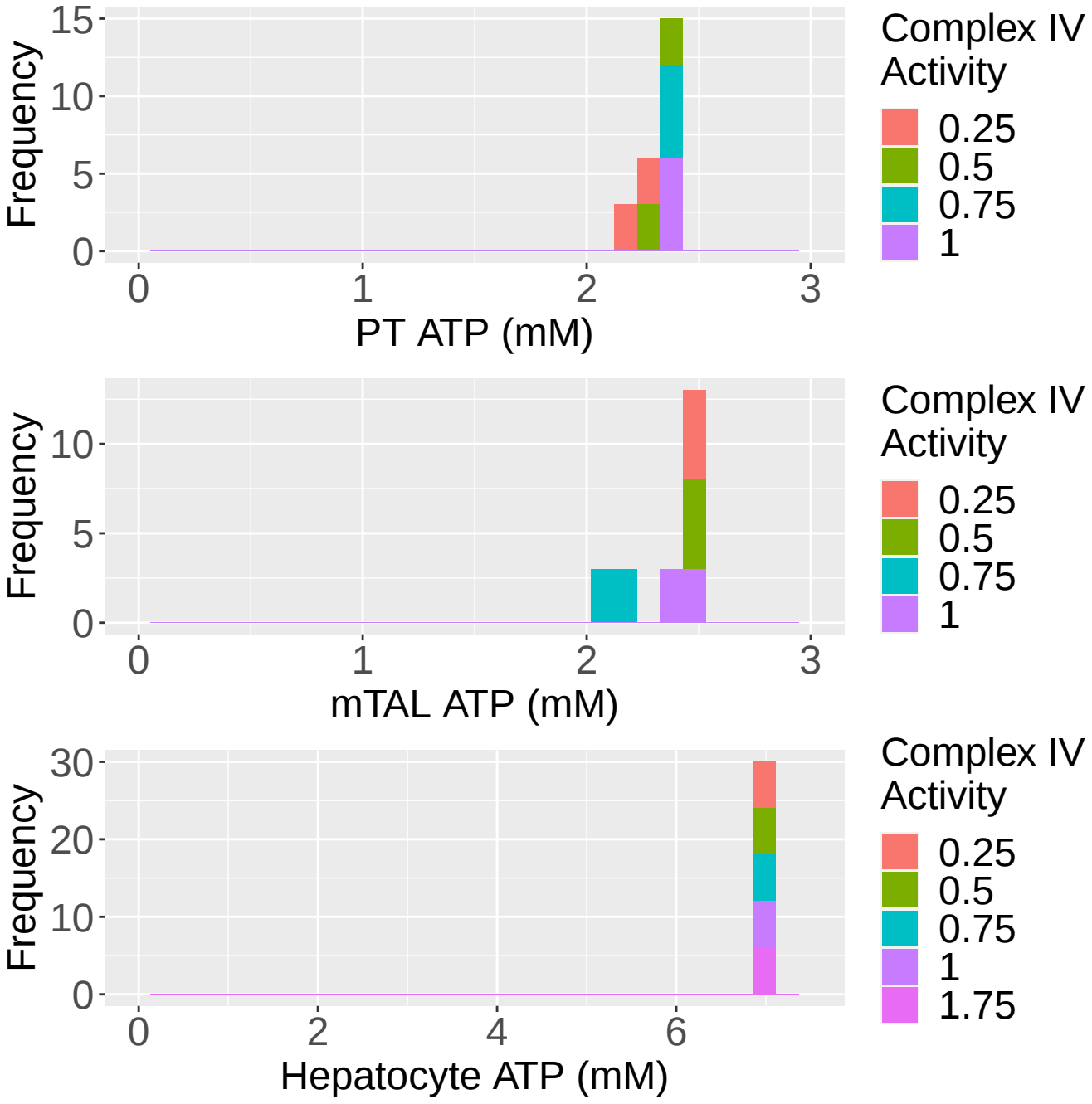

Figure 5.1: The ATP levels under all perturbations of OXPHOS function considered, coloured by the fold-change in the activity of Complex IV as reported in each legend.

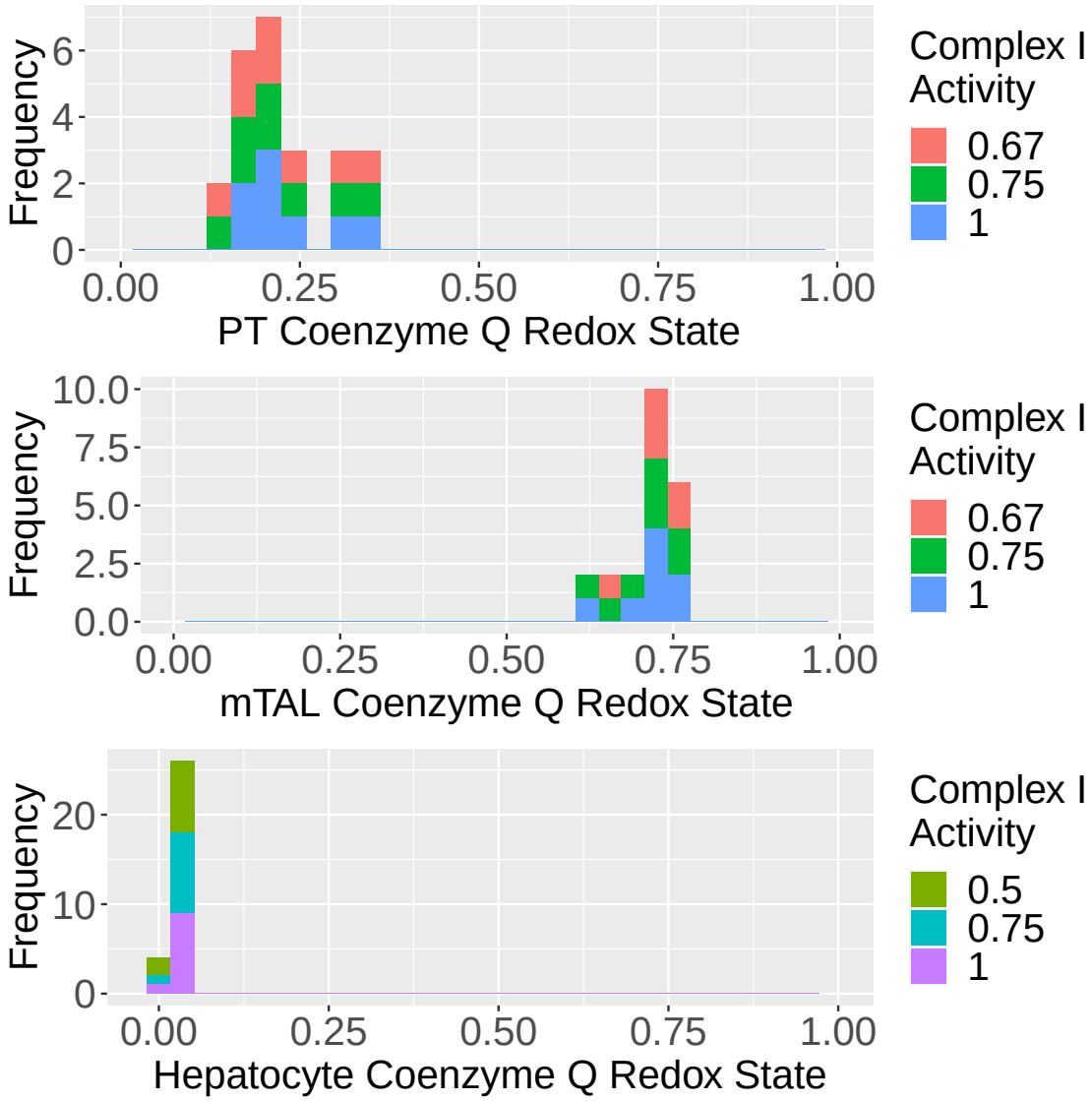

Figure 5.2: The proportion of the pool of coenzyme Q that is in a reduced state in the PT, mTAL, and liver hepatocytes, coloured by the activity of Complex IV, under various perturbations to OXPHOS function. The legend is reported as the fold-change to the activity observed in healthy tissues.

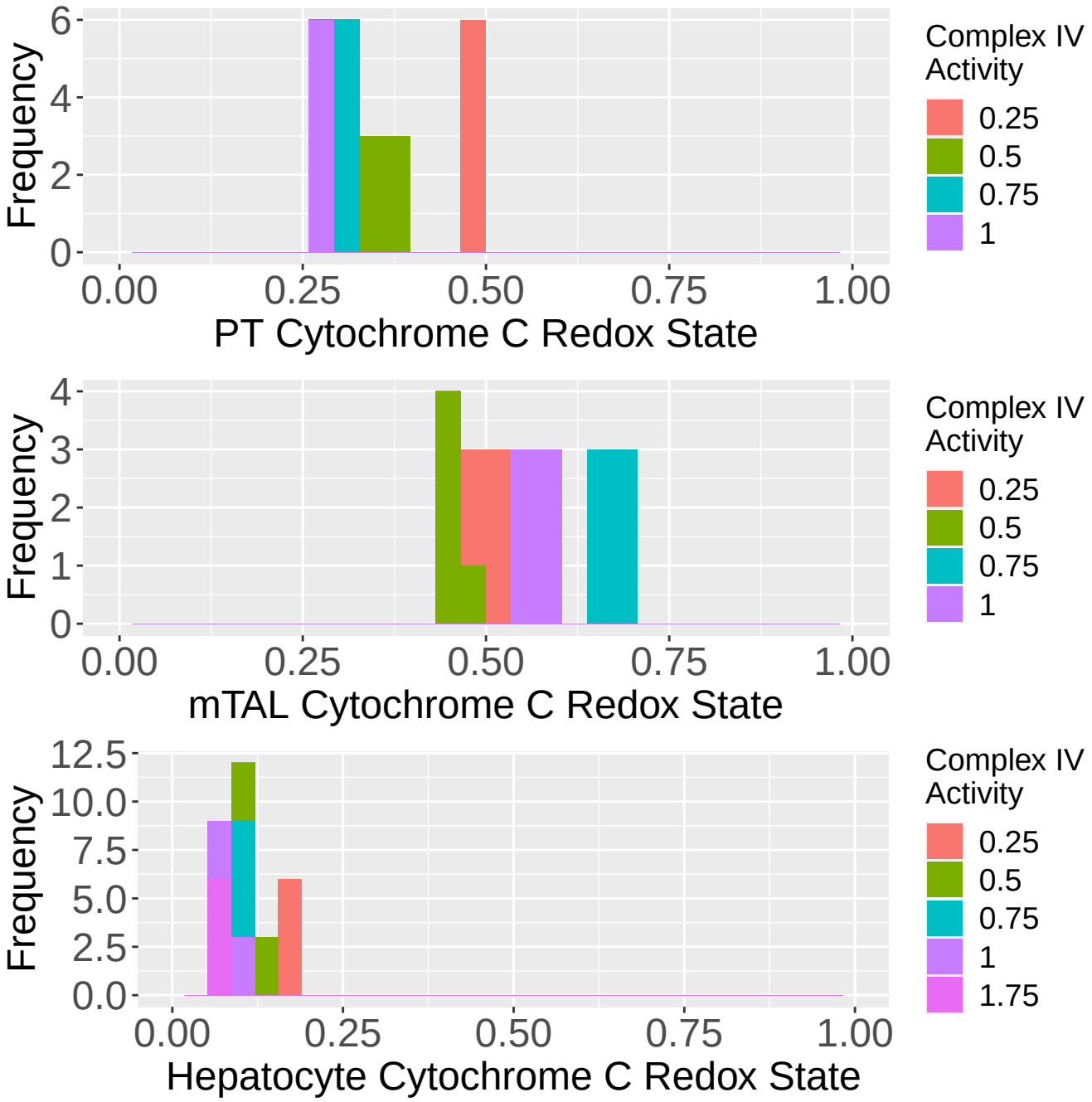

Figure 5.3: The proportion of the pool of cytochrome C that is in a reduced state in the PT, mTAL, and liver hepatocytes, coloured by the activity of Complex IV, under various perturbations to OXPHOS function. The legend is reported as the fold-change to the activity observed in healthy tissues.

5.3 Results

5.3.1 OXPHOS Dysfunction

We consider combinations of change in OXPHOS activity across the range found experimentally in diabetes. For the kidney, we consider reductions in Complex I function by one third and one quarter, in Complex III by one quarter, and in Complex IV by one, two, or three quarters. For the liver, we consider reductions in Complex I activity by one half or one quarter, reductions in Complex III activity by one quarter, increases in Complex IV activity by 70%, and reductions in Complex IV activity by one, two, three quarters, and an increase by three quarters. These values are chosen based on the experimentally observed effects noted in Table 5.1. Under the degrees of OXPHOS dysfunction observed experimentally without any changes to uncoupling or oxygen tension, we see few major impacts on any important features of cellular function, such as cytosolic ATP concentration, cellular polarity, and the redox state of coenzyme Q and cytochrome C. This is the case in both the kidney and liver, with the exception of the coenzyme Q redox state in the mTAL. While the PT has significantly higher coenzyme Q redox state, it is well-below a fully reduced state (a value of 1). Thus, there is coenzyme Q available to accept electrons from Complex I in the PT tissue, which should prevent out-of-control reactive oxygen species production. The coenzyme Q pool can be significantly closer to a fully reduced state under physiologically reasonable (for diabetes) reductions in Complex I and IV activity, a condition that could drive reactive oxygen species production at Complex III and IV. We can see the results for coenzyme Q reduction state in Figure 5.2. These results are comparable to previous findings on OXPHOS dysfunction in healthy kidney and liver tissues above (see Sections 3.3.8, 3.3.9, and 4.3.4).

5.3.2 Uncoupling and Hypoxia

Uncoupling can lead to hypoxia through reduced efficiency of oxygen consumption. We consider 15%, 50%, five-fold, and ten-fold increases in hydrogen leak permeability, and 90% and 50% decreases in oxygen tension. In Figure 5.4 we see ATP depletion and redox states of key electron carriers under combinations of uncoupling and hydrogen leak for the PT, mTAL, and liver hepatocytes. We see that ATP depletion can be a consequence of significant hypoxia combined with hydrogen leak in the PT and mTAL. At one tenth of normal oxygen tension, the PT and mTAL are both below thresholds where you may expect to see dangerous ATP depletion [115]. Uncoupling in combination with this, even relatively minor uncoupling, can reduced the cytosolic ATP concentration by a further physiologically significant amount. There was no strong or universal effect of uncoupling on electron carrier redox state. The liver hepatocytes do not demonstrate the same sensitivity to hypoxia and uncoupling. Under significant hypoxia, the pools of coenzyme Q and cytochrome C are both left in a fairly reduced state in the PT and mTAL. However this may not lead to the significant production

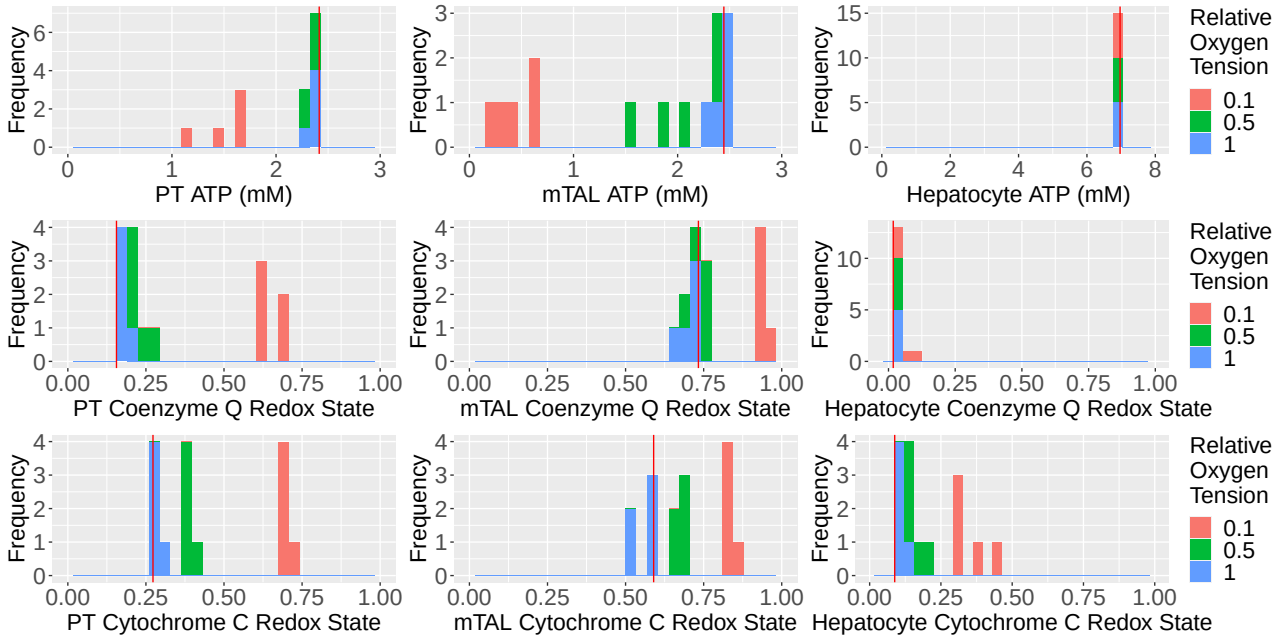

Figure 5.4: PT, mTAL, and hepatocyte predictions for cytosolic ATP concentration and the reduced proportion of the coenzyme Q and cytochrome C pools under various perturbations to the hydrogen leak permeability and mitochondrial oxygen tension. The ATP depletion in the tenth of normal oxygen tension case (0.1x) is below the threshold for the cell to undergo programmed cell death [115] in the PT and mTAL. The legend is reported as the fold-change from normoxic conditions for that tissue.

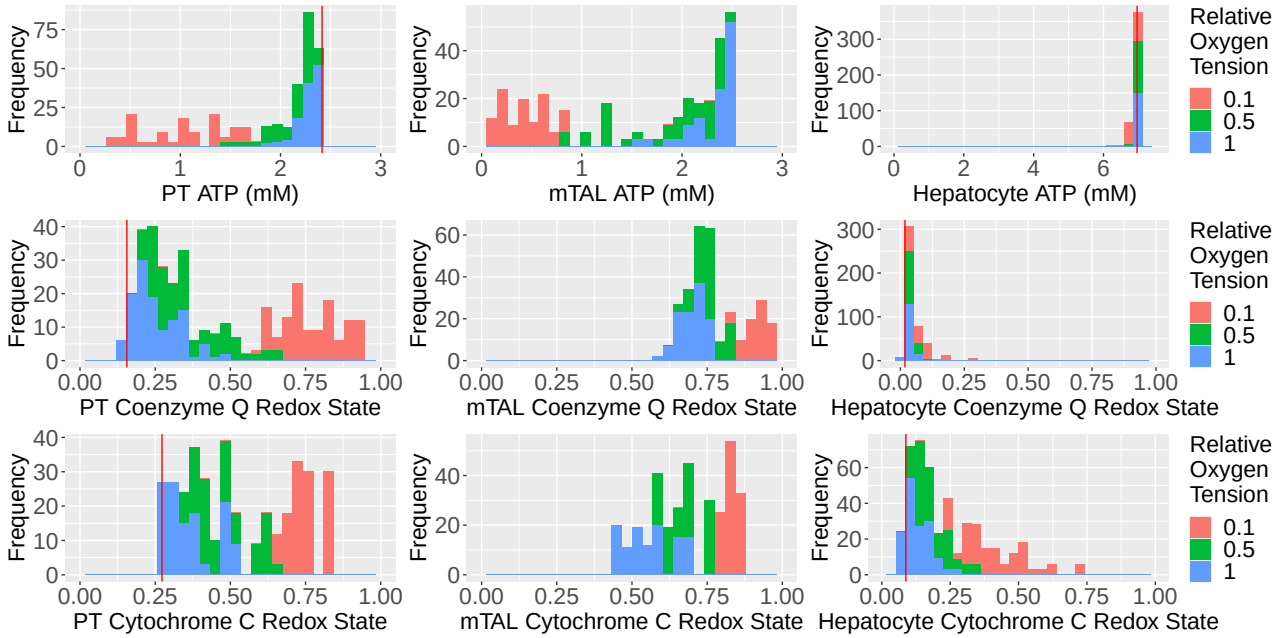

Figure 5.5: The cytosolic ATP concentrations, proportions of the coenzyme Q pool in a reduced state, and proportions of the cytochrome C pool in a reduced state for the proximal tubule (first column), medullary thick ascending limb (second column), and liver hepatocytes (third column) under various degrees of hypoxia, uncoupling, and OXPHOS dysfunction. The vertical line in each graph represents the health cell's value. The bars in the histogram are coloured according to the proportion of typical oxygen tension, with red representing 10% of typical oxygen tension, green 50% of typical, and blue normoxia.

of ROS due to the lower oxygen tension (recall, oxygen is a substrate for ROS production). The production of ROS during hypoxia has been found to increase by some experimental work, indicating that these changes to redox state could be significant despite hypoxia being the absence of a key substrate for ROS production [78].

5.3.3 OXPHOS Dysfunction, Hypoxia, and Uncoupling

The processes above frequently happen simultaneously. This requires a broader range of simulated cases. Below we consider of the above considered OXPHOS dysfunctions, uncoupling, and hypoxia. When we consider this range of cases, we naturally see a wider range of outcomes. The predictions from these cases are shown in Figure 5.5. In the PT and mTAL, we can see major ATP depletion. Physiologically significant ATP depletion can occur in the PT under uncoupling, OXPHOS dysfunction, and minor hypoxia (in our simulations, a 50% reduction in oxygen tension). In the mTAL, more significant hypoxia (a 90% reduction in oxygen tension) is necessary to produce ATP depletion. In liver hepatocytes on the other hand, we do not see significant ATP depletion. Earlier model simulations regarding

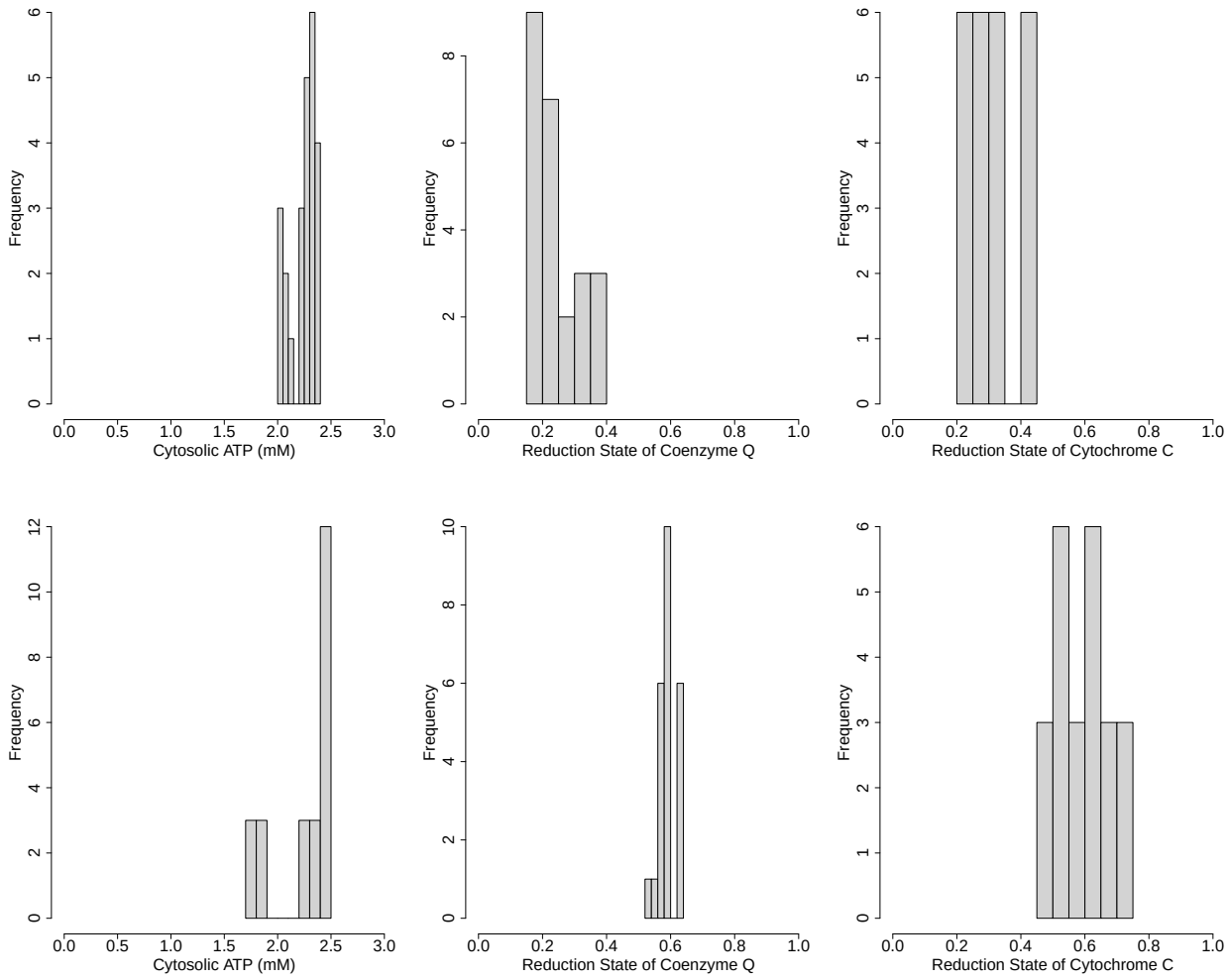

Figure 5.6: The responses of cytosolic ATP, coenzyme Q, and cytochrome C to uncoupling and hypoxia levels like those observed in mice in the PT (top) and mTAL (bottom) [55].

the resilience of the liver to hypoxia and OXPHOS dysfunction found in Section 4.3.4 and 4.3.7 (see also Section 4.4) found that this was due the greater OXPHOS activities, lower metabolic demand, and higher rates of glycolysis in the liver. This is compatible with the known greater risk of kidney disease than liver disease in diabetes [46, 167].

For levels of uncoupling and hypoxia observed in diabetic mouse kidneys [55, 44], that is, 30% lower oxygen tension in the PT, 20% lower oxygen tension in the medulla, and 2.5x greater hydrogen leak activity, the worst ATP depletion observed (see Figure 5.6) is no more than 18% in the proximal tubule, and the mTAL only sees dangerous ATP depletion under severe Complex IV dysfunction (dangerous meaning more than 75% loss of activity). The electron transport chain is left in a somewhat more reduced state under these circumstances.

Risk factors for ROS production as we noted exist in the mTAL in the presence of OX-

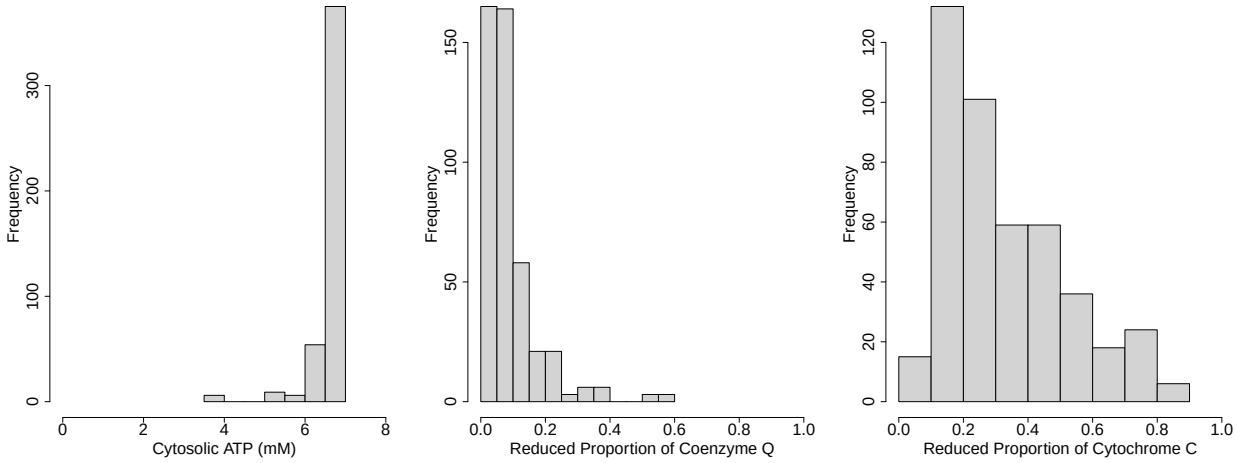

Figure 5.7: The range of cytosolic ATP concentrations, coenzyme Q reduction state, and cytochrome C reduction state in hepatocytes across comparable simulated cases in the liver for kidney-like baseline coenzyme Q, cytochrome C, and cytosolic hydrogen ion concentrations.

PHOS dysfunction alone but hypoxia can make matters worse in multiple tissues. We see the coenzyme Q and cytochrome C pools are in a significantly more reduced state in the PT and mTAL, as is the cytochrome C pool in liver hepatocytes. As is clear from these figures, the redox states of coenzyme Q and cytochrome C are most influenced by the oxygen tension. ROS production is crucial to the development of complications from diabetes in the rat liver and kidney, as indicated by the positive response to antioxidants in diabetic rat liver and kidney [63, 185].

Simulations indicated above (see Section 4.3.7) that the basis for the liver's more effective ATP homeostasis are related to its higher OXPHOS activities, lower metabolic demand, and greater rate of glycolysis. Further simulations (see Figure 5.7) indicate that the greater susceptibility to full coenzyme Q and cytochrome C reduction in the kidney is related to the comparatively smaller pools of these electron carriers in the kidney and the higher pH in the kidney cytosol. When we adjust the liver's mitochondria to have kidney-like parameters in these respects, we observe that they are much more reduced, and in particular the cytochrome C pool may be more than 80% reduced in some simulated cases.

5.4 Discussion

Our key cases involve changes to the mitochondrial volume fraction, cytochrome C content, coenzyme Q content, and OXPHOS activities. Under these conditions, each tissue the cell is still able to continue its typical ATP generation (see Figure 5.1) but we observe that due to the lower coenzyme Q concentration in the kidney of streptozotocin-treated rats [125], the

coenzyme Q pool is in fairly reduced state by default in the mTAL (see Figure 5.2). When combined with Complex IV activity reductions (75%) observed in streptozotocin-treated mice [41], more than 75% of the coenzyme Q pool is in a reduced state by default. Under Complex IV activity reductions (50%) observed in streptozotocin-treated rats, we still see the coenzyme Q is in a more reduced state (∼70%). When the coenzyme Q pool is left in a more reduced state, this leaves Complexes I and III in a more reduced state, and this leads to the generation of reactive oxygen species [128]. However it is difficult to predict the extent that this will negatively impact the mTAL. Reduced and oxidized coenzyme Q bind to the same site on Complex I, and so reduced coenzyme Q competes with oxidized coenzyme Q for the binding site [111]. This suppresses the oxidation of Complex I over and above the decreased supply of available oxidized coenzyme Q when the coenzyme Q pool is in a reduced state. For an experimental analogue of the effects of reduced coenzyme Q, we can look to rotenone. Rotenone can bind to the same site on Complex I with greater affinity than coenzyme Q, mimicking the effects of a highly reduced coenzyme Q pool. Rotenone can be shown to cause large amounts of Complex I-mediated reactive oxygen species production [111]. Comparably, if the coenzyme Q pool is in a reduced state then there can be increased reactive oxygen species production.

The cell is able to survive the stresses of diabetes, which is unsurprising. If all cells died from catastrophic failures of mitochondrial respiration, then there would be no rodents to study diabetes in. The more realistic concern, and the concern addressed by our other diabetes simulations, is that the cell will be more sensitive to stresses frequently associated with diabetes. There are strong interactions between the effects of hypoxia or uncoupling, and diabetic OXPHOS dysfunction. Without diabetic OXPHOS dysfunction, hypoxia and uncoupling may lead to ATP depletion in the PT when oxygen tension gets as low as 5 mmHg, the same threshold for ATP depletion as in the healthy kidney cortex, as observed in Figure 5.4 (cf. discussion of hypoxia in Chapter 3). Hypoxia and uncoupling independent of diabetic OXPHOS dysfunction do not appear to be a significant danger to the hepatocytes in the liver under otherwise typical diabetic conditions. On the other hand, with diabetic OXPHOS dysfunction, both the PT and mTAL are at risk of ATP depletion (see Figures 5.5). In both cases, while the OXPHOS dysfunction is very important to the development of the simulated ATP depletion, hypoxia is necessary for pushing these effects over the top.

We know that the diabetic kidney in alloxan-treated mice will express more of Uncoupling Protein 2 (UCP-2), which increases the hydrogen leak activity of the mitochondrion [55]. This mechanism most likely is meant to help ensure the flow of electrons through the electron transport chain, instead of to reactive oxygen species production. However instead it has been shown using UCP-2 knockout mice that the consequent hypoxia from this UCP-2 overexpression in the kidney is more dangerous than the observed reactive oxygen species production in mice [55]. Hypoxia is a consequence of uncoupling because hydrogen leakage increases the oxygen consumption of Complex IV while not producing new ATP for the cell, driving down the oxygen efficiency of mitochondrial respiration. In the aforementioned work in mice they find a roughly 30% decrease in oxygen tension in the PT and 20% decrease in

oxygen tension in the mTAL. For those degrees of hypoxia and with the 2.5x greater hydrogen leak activity used by Edwards, Palm, and Layton [44], we do not see more than 20% cytosolic ATP depletion. Experimentally, 30% ATP depletion is necessary to increase the risk of apoptosis in mice proximal tubule cells [115] and so our predicted ATP depletion is insufficient. While the diabetic kidney is much more sensitive to hypoxia and uncoupling, cells are not at immediate risk of apoptosis from ATP depletion at typical observed diabetic kidney oxygen tensions and mitochondrial uncoupling levels. That said, when the oxygen tension is lower, the cell is at greater risk of ATP depletion and oxidative stress due to diabetic OXPHOS dysfunction (see Figure 5.5). Hypoxia and uncoupling are greater threats to the bioenergetics of the diabetic kidney than they are to a healthy kidney due to OXPHOS dysfunction in the diabetic kidney (cf. our results for hypoxia in Chapter 3).

Reactive oxygen species production is a particularly important mechanism by which diabetes triggers end-organ damage [183]. Our findings indicate that key electron intermediates will be in a highly reduced state across tissues in the diabetic rat kidney when they experience hypoxia. Under these circumstances, the coenzyme Q and the cytochrome C pool will be in a reduced state in the diabetic kidney, compared to non-hypoxic diabetic kidney tissue (see Figure 5.5). These indicate that both Complex I (in the PT and mTAL) and III (in the PT, mTAL, and liver) may be involved in reactive oxygen species production in diabetes [60]. Complex I can over-produce reactive oxygen species when the coenzyme Q pool is in a highly reduced state. If the coenzyme Q pool is in a reduced state, then Complex I does not have enough substrate to donate electrons to, leading to Complex I producing reactive oxygen species. Complex III can over-produce reactive oxygen species when the cytochrome C pool is in a reduced state because similarly, it must donate its electrons to cytochrome C. Complex III reactive oxygen species production will be worse if the coenzyme Q pool is also in a reduced state. Since coenzyme Q donates electrons to Complex III, if the coenzyme Q pool is in a highly reduced state as well, then Complex III will be further saturated with electrons. These changes, especially for cytochrome C reduction states, are explained in large part by the combination of hypoxia and lower Complex IV activities. We can see in Figure 5.5 that hypoxia strongly impacts the reduction state of cytochrome C and coenzyme Q in the diabetic kidney. The higher reduction state of cytochrome C than noted in any of our previous work is explained by the combined effects of a lower Complex IV activity and hypoxia. Both lower the flux through Complex IV, which is the only means of oxidizing cytochrome C. These results indicate that it may not be true under all circumstances that the cytochrome C pool will be in a reduced state because experimental measurements of diabetic Complex IV activity vary widely (see Table 5.1 for several measurements of Complex IV activity in rodents using various experimental models of diabetes). In fact, Complex IV activity is measured to be higher in the livers of rats treated with streptozotocin [21]. Since streptozotocin treatment is a model for type I diabetes, this suggests that hepatocytes in the liver of type I diabetic rats may in fact be less susceptible to Complex III-mediated oxidative stress. This might be an adaptive response to hyperglycemia by the liver.

Mitochondrial respirometry is a mature field with an unusually rich collection of ex-

perimental measurements of electron transport activity. This allows for the tissue-specific modelling of the effects of diabetes on mitochondria, based on measurements like those collected below in Table 5.1. In this work we attempt to model known effects on mitochondria of diabetes. We use a variety of experimental measurements to produce an ensemble of predictions, accounting for the significant differences between diabetes caused by different mechanisms, and the variation in diabetic phenotypes even among cases of diabetes in the same kind of experimental model. Our findings indicate the importance of Complex IV activity to determining the risk of oxidative stress in diabetes, and that diabetes makes the cell more sensitive to common stresses, in particular hypoxia. As personalized measurement becomes more important to medicine, particularly in light of real-world variation like that captured in Table 5.1, so will the identification of important parameters, a task that this work contributes to.

Chapter 6

Conclusions

So what should we make of the above? We've studied three tissues and described where they differ in response to many different perturbations of state and model structure. The proximal tubule (PT) and medullary thick ascending limb of the loop of Henle (mTAL) consume significant amounts of ATP by volume, and this makes them more sensitive to dysfunctions of oxidative phosphorylation (OXPHOS) & hypoxia (see Sections 3.3.8, 3.3.9, 3.3.10, and 3.3.11) compared to other tissue like the liver. Our mechanistic comparisons with the liver indicate that PT and mTAL's higher metabolic demand, low glycolytic activity, and comparatively low OXPHOS activity are all relevant to explaining this sensitivity (see Section 4.3.4). If we compare the PT and mTAL, we see that the mTAL is more sensitive to Complex IV dysfunction than the PT (see Section 3.3.9). Our follow-up simulations with mTAL-like conditions but PT-like oxygen tension (see Section 3.3.9) indicate that this is due to the low oxygen tension in the mTAL. The liver by contrast is more sensitive to causes of oxidative stress, such as high rates of glycolysis and reperfusion following ischemic hypoxia. We see a long transient in the electron carriers of the electron transport chain and the proton motive force during reperfusion in the liver, which seems to be due to the build-up of succinate during ischemia (see Section 4.3.8). Chouchani et al. [30] argues that this is a unifying pathway for mitochondria-mediated ischemia-reperfusion injury, which gives us greater confidence in these predictions. This transient appears to act on a comparable timescale to what we observe in liver reperfusion injury [81] and in reperfusion injury in myocardial tissue [30, 66]. Myocardial and liver tissue both are known to experience mitochondria-mediated ROS production during reperfusion [82]. If we consider the diabetic mitochondrion, our model predicts that the PT and mTAL are particularly at-risk for both ATP depletion and oxidative stress (see Section 5.3.3). On the other hand, the liver appears to be less sensitive to mitochondria-mediated diabetic end-organ damage according to our model (again see Section 5.3.3). Altogether these results indicate a greater sensitivity of the kidney to ATP depletion and diabetic oxidative stress, and the liver to oxidative stress from glycolytic activity and reperfusion.

Ultimately then, our results indicate that each of the tissues we considered have characteristic ways that they are sensitive to mitochondrial dysfunction, or mitochondria-mediated

injury. These ways can be connected to a range of mitochondrial and tissue-scale factors. For instance, the activity of OXPHOS enzymes is crucial to the robustness of the liver and is a mitochondrial-scale factor (once again see Section 4.3.4). On the other hand, tissue-scale factors such as high metabolic demand (necessary in the kidney for instance for urine concentration [5]) and oxygen tension appear in our model to be crucial for understanding the risks from mitochondrial diseases (once again see Section 3.3.9). This opens up space for extending our model: we know that the tissue may affect the mitochondria, but in aggregate, mitochondria may also affect the tissue. A limitation of our model is that tissue-scale factors are not modelled as dynamically responsive to mitochondrial functioning. For example, oxygen tension is clamped in our model, meaning that regardless of local oxygen consumption the tissue's oxygen tension remains the same. Consequently, if we want to understand the effect of a certain degree of uncoupling (which increases oxygen consumption), we have no better method of pursuing this than simply seeing how it affects the mitochondria to combine that level of uncoupling with various degrees of hypoxia, without any way of predicting the appropriate degree of hypoxia. This limitation points towards a corresponding ambition however: multi-scale modelling of metabolism. We believe the best way to expand on this work is to integrate it into larger models of oxygen transport, and of the factors determining local metabolic demand. Appropriate multi-scale models of metabolism will involve more than just placing our mitochondrial models inside of a larger scale (and ultimately, hopefully whole-body) model with appropriate interfaces. A first step along the way to this would be incorporating our mitochondrial model into larger models of the energy-intensive processes in the kidney and liver. In the kidney, that means models of epithelial transport in the nephron [43, 98, 100, 112, 99, 101, 102]. On the other hand in the liver, the primary ATP-consuming processes are urea synthesis [22], gluconeogenesis [22], and active ion transport [144]. With a model that includes ATP generation (by the mitochondria) and consumption (by the processes above), a natural follow-up step would be to integrate these models with a model of the tissue's oxygenation. In the kidney there are many models that could be used for this work [28, 166, 165, 56, 27, 57, 29]. While in the liver has been subject to less sustained modelling attention, its spatial heterogeneity is well-understood [12]. Due to the liver's highly regular structure of lobules it should be highly tractable to model liver oxygenation. While the liver and kidney are particularly important to whole-body homeostasis, every tissue has mitochondria and most tissues are susceptible to mitochondrial dysfunction or mitochondria-mediated injury. For a whole-body multiscale model of metabolism then, we need models of mitochondrial respiration in other tissues.

That is the spirit in which we introduce the quote in the dedication (pg. vi): what I've done here is provide an account of the key differences in mitochondrial respiration between several important tissues; that is, I've provided a map for the local understanding of respiration. While this provides useful information about mitochondrial disease, hypoxia, and reperfusion injury, it is ultimately half of the picture. The gap from local to global information is not just important for the sake of better understanding our problems or on aesthetic grounds. As pointed out by Hester [77], the majority of measurements taken of patients are macroscale measurements (e.g. pulse, eGFR, or blood pressure) and the majority of outcomes they're

interested in are also macroscale. If mathematical physiologists are to be clinically relevant, we ought to connect ourselves to events on a scale that medical practitioners document.

References

[1] Charlotte L Alston, Mariana C Rocha, Nichola Z Lax, Doug M Turnbull, and Robert W Taylor. The genetics and pathology of mitochondrial disease. *The Journal of pathology*, 241(2):236–250, 2017.

[2] Corrado Angelini, L Bello, M Spinazzi, and C Ferrati. Mitochondrial disorders of the nuclear genome. *Acta Myologica*, 28(1):16, 2009.

[3] Nadine Assmann, Katja Dettmer, Johann MB Simbuerger, Carsten Broeker, Nadine Nuernberger, Kathrin Renner, Holly Courtneidge, Enriko D Klootwijk, Axel Duerkop, Andrew M Hall, et al. Renal fanconi syndrome is caused by a mistargeting-based mitochondriopathy. *Cell Reports*, 15(7):1423–1429, 2016.

[4] Anna Atlante, Teresa Maria Seccia, Ersilia Marra, and Salvatore Passarella. The rate of atp export in the extramitochondrial phase via the adenine nucleotide translocator changes in aging in mitochondria isolated from heart left ventricle of either normotensive or spontaneously hypertensive rats. *Mechanisms of ageing and development*, 132(10):488–495, 2011.

[5] Mun Aw, Tamara M Armstrong, C Michele Nawata, Sarah N Bodine, Jeeeun J Oh, Guojun Wei, Kristen K Evans, Mohammad Shahidullah, Timo Rieg, and Thomas L Pannabecker. Body mass-specific na+-k+-atpase activity in the medullary thick ascending limb: implications for species-dependent urine concentrating mechanisms. *American Journal of Physiology-Regulatory, Integrative and Comparative Physiology*, 314(4):R563–R573, 2018.

[6] TY Aw and Dean P Jones. Atp concentration gradients in cytosol of liver cells during hypoxia. *American Journal of Physiology-Cell Physiology*, 249(5):C385–C392, 1985.

[7] Robert S Balaban. Modeling mitochondrial function. *American Journal of Physiology-Cell Physiology*, 291(6):C1107–C1113, 2006.

[8] Antoni Barrientos and Carlos T Moraes. Titrating the effects of mitochondrial complex i impairment in the cell physiology. *Journal of Biological Chemistry*, 274(23):16188–16197, 1999.

[9] Jason N Bazil, Daniel A Beard, and Kalyan C Vinnakota. Catalytic coupling of oxidative phosphorylation, atp demand, and reactive oxygen species generation. *Biophysical journal*, 110(4):962–971, 2016.

[10] Daniel A Beard and Hong Qian. *Chemical biophysics: quantitative analysis of cellular systems*, volume 126. Cambridge University Press Cambridge, 2008.

[11] B Beauvoit, T Kitai, and B Chance. Contribution of the mitochondrial compartment to the optical properties of the rat liver: a theoretical and practical approach. *Biophysical Journal*, 67(6):2501–2510, 1994.

[12] Shani Ben-Moshe and Shalev Itzkovitz. Spatial heterogeneity in the mammalian liver. *Nature Reviews Gastroenterology & Hepatology*, 16(7):395–410, 2019.

[13] Giovanni Benard, Benjamin Faustin, Emilie Passerieux, Anne Galinier, Christophe Rocher, Nadege Bellance, J-P Delage, Louis Casteilla, Thierry Letellier, and Rodrigue Rossignol. Physiological diversity of mitochondrial oxidative phosphorylation. *American Journal of Physiology-Cell Physiology*, 291(6):C1172–C1182, 2006.

[14] Richard Bertram, Morten Gram Pedersen, Dan S Luciani, and Arthur Sherman. A simplified model for mitochondrial atp production. *Journal of theoretical biology*, 243(4):575–586, 2006.

[15] Jianbin Bi, Jia Zhang, Yifan Ren, Zhaoqing Du, Qingshan Li, Yue Wang, Shasha Wei, Lifei Yang, Jingyao Zhang, Chang Liu, et al. Irisin alleviates liver ischemia-reperfusion injury by inhibiting excessive mitochondrial fission, promoting mitochondrial biogenesis and decreasing oxidative stress. *Redox biology*, 20:296–306, 2019.

[16] Ralf Bohnensack. Control of energy transformation in mitochondria. analysis by a quantitative model. *Biochimica et Biophysica Acta (BBA)-Bioenergetics*, 634:203–218, 1981.

[17] Dennis Botman, Wikky Tigchelaar, and Cornelis JF Van Noorden. Determination of glutamate dehydrogenase activity and its kinetics in mouse tissues using metabolic mapping (quantitative enzyme histochemistry). *Journal of Histochemistry & Cytochemistry*, 62(11):802–812, 2014.

[18] Nadine Bouby, Lise Bankir, Marie-Marcelle Trinh-Trang-Tan, Will W Minuth, and Wilhelm Kriz. Selective adh-induced hypertrophy of the medullary thick ascending limb in brattleboro rats. *Kidney international*, 28(3):456–466, 1985.

[19] Martin D Brand, Mary-Ellen Harper, and Heather C Taylor. Control of the effective p/o ratio of oxidative phosphorylation in liver mitochondria and hepatocytes. *Biochemical Journal*, 291(3):739–748, 1993.

[20] Martin D Brand and David G Nicholls. Assessing mitochondrial dysfunction in cells. *Biochemical Journal*, 435(2):297–312, 2011.

[21] JA Brignone, Clara M Campos de Brignone, RR Rodriguez, Blanca N Badano, and AOM Stoppani. Modified oscillation behavior and decreased d-3-hydroxybutyrate dehydrogenase activity in diabetic rat liver mitochondria. *Archives of biochemistry and biophysics*, 214(2):581–588, 1982.

[22] Guy C Brown. Control of respiration and atp synthesis in mammalian mitochondria and cells. *Biochemical Journal*, 284(1):1–13, 1992.

[23] Irene V Budunova and Leonid A Mittelman. The effect of k+/h+ antiporter nigericin on gap junction permeability. *Cell biology and toxicology*, 8(1):63–73, 1992.

[24] Paolo Calzavacca, Roger G Evans, Michael Bailey, Rinaldo Bellomo, and Clive N May. Cortical and medullary tissue perfusion and oxygenation in experimental septic acute kidney injury. *Critical care medicine*, 43(10):e431–e439, 2015.

[25] Juliana Camacho-Pereira, Mariana G Tarragó, Claudia CS Chini, Veronica Nin, Carlos Escande, Gina M Warner, Amrutesh S Puranik, Renee A Schoon, Joel M Reid, Antonio Galina, et al. Cd38 dictates age-related nad decline and mitochondrial dysfunction through an sirt3-dependent mechanism. *Cell metabolism*, 23(6):1127–1139, 2016.

[26] T Cavalier-Smith. The simultaneous symbiotic origin of mitochondria, chloroplasts, and microbodies. *Annals of the New York Academy of Sciences*, 503(1):55–71, 1987.

[27] Jing Chen, Aurélie Edwards, and Anita T Layton. A mathematical model of o2 transport in the rat outer medulla. ii. impact of outer medullary architecture. *American Journal of Physiology-Renal Physiology*, 297(2):F537–F548, 2009.

[28] Jing Chen, Aurélie Edwards, and Anita T Layton. Effects of ph and medullary blood flow on oxygen transport and sodium reabsorption in the rat outer medulla. *American Journal of Physiology-Renal Physiology*, 298(6):F1369–F1383, 2010.

[29] Jing Chen, Anita T Layton, and Aurélie Edwards. A mathematical model of o2 transport in the rat outer medulla. i. model formulation and baseline results. *American Journal of Physiology-Renal Physiology*, 297(2):F517–F536, 2009.

[30] Edward T Chouchani, Victoria R Pell, Edoardo Gaude, Dunja Aksentijević, Stephanie Y Sundier, Ellen L Robb, Angela Logan, Sergiy M Nadtochiy, Emily NJ Ord, Anthony C Smith, et al. Ischaemic accumulation of succinate controls reperfusion injury through mitochondrial ros. *Nature*, 515(7527):431–435, 2014.

[31] Kate S Collison, Soad M Saleh, Razan H Bakheet, Rana K Al-Rabiah, Angela L Inglis, Nadine J Makhoul, Zakia M Maqbool, Marya Zia Zaidi, Mohammed A Al-Johi, and Futwan A Al-Mohanna. Diabetes of the liver: the link between nonalcoholic fatty liver disease and hfcs-55. *Obesity*, 17(11):2003–2013, 2009.

[32] Sonia Cortassa, Miguel A Aon, Eduardo Marbán, Raimond L Winslow, and Brian O'Rourke. An integrated model of cardiac mitochondrial energy metabolism and calcium dynamics. *Biophysical journal*, 84(4):2734–2755, 2003.

[33] Michael M Cox and David L Nelson. *Lehninger principles of biochemistry*, volume 5. Wh Freeman New York, 2008.

[34] SK Cunningham, TV Keaveny, and P Fitzgerald. Effect of allopurinol on tissue atp, adp and amp concentrations in renal ischaemia. *Journal of British Surgery*, 61(7):562–565, 1974.

[35] Tanja Cvitanović Tomaš, Žiga Urlep, Miha Moškon, Miha Mraz, and Damjana Rozman. Liversex computational model: Sexual aspects in hepatic metabolism and abnormalities. *Frontiers in physiology*, 9:360, 2018.

[36] OV Demin, II Gorianin, BN Kholodenko, and HV Westerhoff. Kinetic modeling of energy metabolism and generation of active forms of oxygen in hepatocyte mitochondria. *Molekuliarnaia biologiia*, 35(6):1095–1104, 2001.

[37] Maria Antonietta Di Noia, Sarah Van Driesche, Ferdinando Palmieri, Li-Ming Yang, Shuo Quan, Alvin I Goodman, and Nader G Abraham. Heme oxygenase-1 enhances renal mitochondrial transport carriers and cytochrome c oxidase activity in experimental diabetes. *Journal of Biological Chemistry*, 281(23):15687–15693, 2006.

[38] Francisca Diaz and Carlos T Moraes. Mitochondrial biogenesis and turnover. *Cell calcium*, 44(1):24–35, 2008.

[39] Karolina Dominiak, Agnieszka Koziel, and Wieslawa Jarmuszkiewicz. The interplay between mitochondrial reactive oxygen species formation and the coenzyme q reduction level. *Redox biology*, 18:256–265, 2018.

[40] T Dowd, M Barac-Nieto, RK Gupta, and A Spitzer. 31p nuclear magnetic resonance and saturation transfer studies of the isolated perfused rat kidney. *Kidney and Blood Pressure Research*, 12(3):161–170, 1989.

[41] Laura L Dugan, Young-Hyun You, Sameh S Ali, Maggie Diamond-Stanic, Satoshi Miyamoto, Anne-Emilie DeCleves, Aleksander Andreyev, Tammy Quach, San Ly, Grigory Shekhtman, et al. Ampk dysregulation promotes diabetes-related reduction of superoxide and mitochondrial function. *The Journal of clinical investigation*, 123(11), 2013.

[42] Jaroslaw Dzbek and Bernard Korzeniewski. Control over the contribution of the mitochondrial membrane potential ($\delta\psi$) and proton gradient (δph) to the protonmotive force (δp): in silico studies. *Journal of Biological Chemistry*, 283(48):33232–33239, 2008.

[43] Aurélie Edwards, Hayo Castrop, Kamel Laghmani, Volker Vallon, and Anita T Layton. Effects of nkcc2 isoform regulation on nacl transport in thick ascending limb and macula densa: a modeling study. *American Journal of Physiology-Renal Physiology*, 307(2):F137–F146, 2014.

[44] Aurélie Edwards, Fredrik Palm, and Anita T Layton. A model of mitochondrial o2 consumption and atp generation in rat proximal tubule cells. *American Journal of Physiology-Renal Physiology*, 318(1):F248–F259, 2020.

[45] Messoud Efendiev. *Mathematical Modeling of Mitochondrial Swelling*. Springer, 2018.

[46] Hashem B El-Serag, Thomas Tran, and James E Everhart. Diabetes increases the risk of chronic liver disease and hepatocellular carcinoma. *Gastroenterology*, 126(2):460–468, 2004.

[47] Roger G Evans, Duncan Goddard, Gabriela A Eppel, and Paul M O'Connor. Factors that render the kidney susceptible to tissue hypoxia in hypoxemia. *American Journal of Physiology-Regulatory, Integrative and Comparative Physiology*, 300(4):R931–R940, 2011.

[48] Z Jr Fedatto, EL Ishii-Iwamoto, C Bersani-Amado, ER Martins Maciel, A Bracht, and AM Kelmer-Bracht. Glucose phosphorylation capacity and glycolysis in the liver of arthritic rats. *Inflammation Research*, 49(3):128–132, 2000.

[49] Thorsten Feldkamp, Joel M Weinberg, Markus Hörbelt, Christina Von Kropff, Oliver Witzke, Jens Nürnberger, and Andreas Kribben. Evidence for involvement of nonesterified fatty acid-induced protonophoric uncoupling during mitochondrial dysfunction caused by hypoxia and reoxygenation. *Nephrology Dialysis Transplantation*, 24(1):43–51, 2009.

[50] Josephine M Forbes and David R Thorburn. Mitochondrial dysfunction in diabetic kidney disease. *Nature Reviews Nephrology*, 14(5):291, 2018.

[51] NG Forman and DF Wilson. Dependence of mitochondrial oxidative phosphorylation on activity of the adenine nucleotide translocase. *Journal of Biological Chemistry*, 258(14):8649–8655, 1983.

[52] Laura Formentini, Marta P Pereira, Laura Sánchez-Cenizo, Fulvio Santacatterina, José J Lucas, Carmen Navarro, Alberto Martínez-Serrano, and José M Cuezva. In vivo inhibition of the mitochondrial h+-atp synthase in neurons promotes metabolic preconditioning. *The EMBO journal*, 33(7):762–778, 2014.

[53] Dominique M Freeman, Sylvia Bartlett, George Radda, and Brian Ross. Energetics of sodium transport in the kidney: saturation transfer 31p-nmr. *Biochimica et Biophysica Acta (BBA)-Molecular Cell Research*, 762(2):325–336, 1983.

[54] Dominique M Freeman, Laurence Chan, Haliru Yahaya, Paul Holloway, and Brian D Ross. Magnetic resonance spectroscopy for the determination of renal metabolic rate in vivo. *Kidney international*, 30(1):35–42, 1986.

[55] M Friederich-Persson, Patrik Persson, Peter Hansell, and Fredrik Palm. Deletion of uncoupling protein-2 reduces renal mitochondrial leak respiration, intrarenal hypoxia and proteinuria in a mouse model of type 1 diabetes. *Acta Physiologica*, 223(4):e13058, 2018.

[56] Brendan C Fry, Aurélie Edwards, and Anita T Layton. Impact of nitric-oxide-mediated vasodilation and oxidative stress on renal medullary oxygenation: a modeling study. *American Journal of Physiology-Renal Physiology*, 310(3):F237–F247, 2016.

[57] Brendan C Fry, Aurélie Edwards, Ioannis Sgouralis, and Anita T Layton. Impact of renal medullary three-dimensional architecture on oxygen transport. *American Journal of Physiology-Renal Physiology*, 307(3):F263–F272, 2014.

[58] Ramindhu Galgamuwa, Kristine Hardy, Jane E Dahlstrom, Anneke C Blackburn, Elize Wium, Melissa Rooke, Jean Y Cappello, Padmaja Tummala, Hardip R Patel, Aaron Chuah, et al. Dichloroacetate prevents cisplatin-induced nephrotoxicity without compromising cisplatin anticancer properties. *Journal of the American Society of Nephrology*, 27(11):3331–3344, 2016.

[59] Ramindhu Galgamuwa, Kristine Hardy, Jane E Dahlstrom, Anneke C Blackburn, Elize Wium, Melissa Rooke, Jean Y Cappello, Padmaja Tummala, Hardip R Patel, Aaron Chuah, et al. Dichloroacetate prevents cisplatin-induced nephrotoxicity without compromising cisplatin anticancer properties. *Journal of the American Society of Nephrology*, 27(11):3331–3344, 2016.

[60] Laura D Gauthier, Joseph L Greenstein, Sonia Cortassa, Brian O'Rourke, and Raimond L Winslow. A computational model of reactive oxygen species and redox balance in cardiac mitochondria. *Biophysical journal*, 105(4):1045–1056, 2013.

[61] Albert Geerts. History, heterogeneity, developmental biology, and functions of quiescent hepatic stellate cells. In *Seminars in liver disease*, volume 21, pages 311–336. Copyright© 2001 by Thieme Medical Publishers, Inc., 333 Seventh Avenue, New ..., 2001.

[62] Nahum D Gershon, Keith R Porter, and Benes L Trus. The cytoplasmic matrix: its volume and surface area and the diffusion of molecules through it. *Proceedings of the National Academy of Sciences*, 82(15):5030–5034, 1985.

[63] Selda Gezginci-Oktayoglu, Hasan Basaraner, Refiye Yanardag, and Sehnaz Bolkent. The effects of combined treatment of antioxidants on the liver injury in stz diabetic rats. *Digestive diseases and sciences*, 54(3):538–546, 2009.

[64] Carlotta Giorgi, Chiara Agnoletto, Angela Bononi, Massimo Bonora, Elena De Marchi, Saverio Marchi, Sonia Missiroli, Simone Patergnani, Federica Poletti, Alessandro Rimessi, et al. Mitochondrial calcium homeostasis as potential target for mitochondrial medicine. *Mitochondrion*, 12(1):77–85, 2012.

[65] Marcela González-Granillo, Christina Savva, Xidan Li, Mark Fitch, Matteo Pedrelli, Marc Hellerstein, Paolo Parini, Marion Korach-André, and Jan-Åke Gustafsson. Erβ activation in obesity improves whole body metabolism via adipose tissue function and enhanced mitochondria biogenesis. *Molecular and cellular endocrinology*, 479:147–158, 2019.

[66] D Neil Granger and Peter R Kvietys. Reperfusion injury and reactive oxygen species: the evolution of a concept. *Redox biology*, 6:524–551, 2015.

[67] Michael W Gray. Lynn margulis and the endosymbiont hypothesis: 50 years later. *Molecular biology of the cell*, 28(10):1285–1287, 2017.

[68] Tory M Hagen, David L Yowe, James C Bartholomew, Carol M Wehr, Katherine L Do, Jin-Y Park, and Bruce N Ames. Mitochondrial decay in hepatocytes from old rats: membrane potential declines, heterogeneity and oxidants increase. *Proceedings of the National Academy of Sciences*, 94(7):3064–3069, 1997.

[69] Andrew M Hall, Paul Bass, and Robert J Unwin. Drug-induced renal fanconi syndrome. *QJM: An International Journal of Medicine*, 107(4):261–269, 2014.

[70] Andrew M Hall, George J Rhodes, Ruben M Sandoval, Peter R Corridon, and Bruce A Molitoris. In vivo multiphoton imaging of mitochondrial structure and function during acute kidney injury. *Kidney international*, 83(1):72–83, 2013.

[71] Andrew M Hall and Robert J Unwin. The not so 'mighty chondrion': emergence of renal diseases due to mitochondrial dysfunction. *Nephron Physiology*, 105(1):p1–p10, 2007.

[72] Arnaldur Hall, Anna K Larsen, Ladan Parhamifar, Kathrine D Meyle, Lin-Ping Wu, and S Moein Moghimi. High resolution respirometry analysis of polyethylenimine-mediated mitochondrial energy crisis and cellular stress: Mitochondrial proton leak and inhibition of the electron transport system. *Biochimica et Biophysica Acta (BBA)-Bioenergetics*, 1827(10):1213–1225, 2013.

[73] Barry Halliwell and John MC Gutteridge. *Free radicals in biology and medicine*. Oxford University Press, USA, 2015.

[74] Jung Min Han and Vipul Periwal. A mathematical model of calcium dynamics: Obesity and mitochondria-associated er membranes. *PLoS computational biology*, 15(8):e1006661, 2019.

[75] Margit Heiske, Thierry Letellier, and Edda Klipp. Comprehensive mathematical model of oxidative phosphorylation valid for physiological and pathological conditions. *The FEBS Journal*, 284(17):2802–2828, 2017.

[76] DA Hems and G Gaja. Carbohydrate metabolism in the isolated perfused rat kidney. *Biochemical Journal*, 128(2):421–426, 1972.

[77] Robert L Hester, Radu Iliescu, Richard Summers, and Thomas G Coleman. Systems biology and integrative physiological modelling. *The Journal of physiology*, 589(5):1053–1060, 2011.

[78] David L Hoffman, Jason D Salter, and Paul S Brookes. Response of mitochondrial reactive oxygen species generation to steady-state oxygen tension: implications for hypoxic cell signaling. *American Journal of Physiology-Heart and Circulatory Physiology*, 292(1):H101–H108, 2007.

[79] Hanne Hoitzing, Payam A Gammage, Lindsey Van Haute, Michal Minczuk, Iain G Johnston, and Nick S Jones. Energetic costs of cellular and therapeutic control of stochastic mitochondrial dna populations. *PLoS computational biology*, 15(6):e1007023, 2019.

[80] Silvia Iannello, Paolina Milazzo, and Francesco Belfiore. Animal and human tissue na, k-atpase in obesity and diabetes: a new proposed enzyme regulation. *The American journal of the medical sciences*, 333(1):1–9, 2007.

[81] Hartmut Jaeschke and Jerry R Mitchell. Mitochondria and xanthine oxidase both generate reactive oxygen species in isolated perfused rat liver after hypoxic injury. *Biochemical and biophysical research communications*, 160(1):140–147, 1989.

[82] Wayel Jassem and Justin Roake. The molecular and cellular basis of reperfusion injury following organ transplantation. *Transplantation Reviews*, 12(1):14–33, 1998.

[83] Qusheng Jin and Craig M Bethke. Kinetics of electron transfer through the respiratory chain. *Biophysical Journal*, 83(4):1797–1808, 2002.

[84] Ard Jonker, Willie JC Geerts, Rob Charles, Wouter H Lamers, and Cornelis JF Van Noorden. The dynamics of local kinetic parameters of glutamate dehydrogenase in rat liver. *Histochemistry and cell biology*, 106(4):437–443, 1996.

[85] Antonio Jordá, Ernesto Pérez-Pastor, and Manuel Portolés. Effect of streptozotocin-diabetes on rat liver mitochondrial adenosine triphosphatase turnover. *Biochemical Journal*, 251(2):621–624, 1988.

[86] Wataru Kamiike, Fusao Watanabe, Tadao Hashimoto, Kunio Tagawa, Yoshikazu Ikeda, Kazuyasu Nakao, and Yasunaru Kawashima. Changes in cellular levels of atp and its catabolites in ischemic rat liver. *The Journal of Biochemistry*, 91(4):1349–1356, 1982.

[87] SS Katyare and JG Satav. Effect of streptozotocin-induced diabetes on oxidative energy metabolism in rat kidney mitochondria. a comparative study of early and late effects. *Diabetes, Obesity and Metabolism*, 7(5):555–562, 2005.

[88] Aileen JF King. The use of animal models in diabetes research. *British journal of pharmacology*, 166(3):877–894, 2012.

[89] Jean Klastersky. Side effects of ifosfamide. *Oncology*, 65(Suppl. 2):7–10, 2003.

[90] MICHAEL C Kohn, MURRAY J Achs, and DAVID Garfinkel. Computer simulation of metabolism in pyruvate-perfused rat heart. ii. krebs cycle. *American Journal of Physiology-Regulatory, Integrative and Comparative Physiology*, 237(3):R159–R166, 1979.

[91] Michael C Kohn and David Garfinkel. Computer simulation of metabolism in palmitate-perfused rat heart. ii. behavior of complete model. *Annals of biomedical engineering*, 11(6):511–531, 1983.

[92] Michael C Kohn and David Garfinkel. Computer simulation of metabolism in palmitate-perfused rat heart. ii. behavior of complete model. *Annals of biomedical engineering*, 11(6):511–531, 1983.

[93] Tímea Komlódi, Fanni F Geibl, Matilde Sassani, Attila Ambrus, and László Tretter. Membrane potential and delta ph dependency of reverse electron transport-associated hydrogen peroxide production in brain and heart mitochondria. *Journal of bioenergetics and biomembranes*, 50(5):355–365, 2018.

[94] A Kowald and TBL Kirkwood. Mitochondrial mutations, cellular instability and ageing: modelling the population dynamics of mitochondria. *Mutation Research/DNAging*, 295(3):93–103, 1993.

[95] J Kucharska, Z Braunova, O Ulicna, L Zlatos, and A Gvozdjakova. Deficit of coenzyme q in heart and liver mitochondria of rats with streptozotocin-induced diabetes. *Physiological research*, 49(4):411–418, 2000.

[96] Adrian J Lambert and Martin D Brand. Superoxide production by nadh: ubiquinone oxidoreductase (complex i) depends on the ph gradient across the mitochondrial inner membrane. *Biochemical Journal*, 382(2):511–517, 2004.

[97] AJ Lambert, B Wang, J Yardley, J Edwards, and BJ Merry. The effect of aging and caloric restriction on mitochondrial protein density and oxygen consumption. *Experimental gerontology*, 39(3):289–295, 2004.

[98] Anita T Layton, Aurélie Edwards, and Volker Vallon. Adaptive changes in gfr, tubular morphology, and transport in subtotal nephrectomized kidneys: modeling and analysis. *American Journal of Physiology-Renal Physiology*, 313(2):F199–F209, 2017.

[99] Anita T Layton, Kamel Laghmani, Volker Vallon, and Aurélie Edwards. Solute transport and oxygen consumption along the nephrons: effects of na+ transport inhibitors. *American Journal of Physiology-Renal Physiology*, 311(6):F1217–F1229, 2016.

[100] Anita T Layton and Harold E Layton. A computational model of epithelial solute and water transport along a human nephron. *PLoS computational biology*, 15(2):e1006108, 2019.

[101] Anita T Layton and Volker Vallon. Sglt2 inhibition in a kidney with reduced nephron number: modeling and analysis of solute transport and metabolism. *American Journal of Physiology-Renal Physiology*, 314(5):F969–F984, 2018.

[102] Anita T Layton, Volker Vallon, and Aurélie Edwards. A computational model for simulating solute transport and oxygen consumption along the nephrons. *American Journal of Physiology-Renal Physiology*, 311(6):F1378–F1390, 2016.

[103] AT Layton and A Edwards. *Mathematical Modeling in Renal Physiology*, volume 862. Springer, 2014.

[104] Way S Lee and Ronald J Sokol. Liver disease in mitochondrial disorders. In *Seminars in liver disease*, volume 27, page 259. NIH Public Access, 2007.

[105] Ann LeFurgey, Anthony J Spencer, William R Jacobs, Peter Ingram, and Lazaro J Mandel. Elemental microanalysis of organelles in proximal tubules. i. alterations in transport and metabolism. *Journal of the American Society of Nephrology*, 1(12):1305–1320, 1991.

[106] Matthieu Legrand, Egbert G Mik, Tanja Johannes, Didier Payen, and Can Ince. Renal hypoxia and dysoxia after reperfusion of the ischemic kidney. *Molecular medicine*, 14(7):502–516, 2008.

[107] Guy Lemieux, James Berkofsky, and Christiane Lemieux. Renal tissue metabolism in the rat during chronic metabolic alkalosis: importance of glycolysis. *Canadian journal of physiology and pharmacology*, 64(11):1419–1426, 1986.

[108] T Letellier, F Bédes, M Malgat, B Korzeniewski, LS Jouaville, and Ramuné Morkuniene. Metabolic control analysis and threshold effect in oxidative phosphorylation: implications for mitochondrial pathologies. *Molecular and cellular biochemistry*, 174(1):143–148, 1997.

[109] A Leung, D Ohadi, G Pekkurnaz, and P Rangamani. Systems modeling predicts that mitochondria er contact sites regulate the postsynaptic energy landscape. *NPJ systems biology and applications*, 7(1):1–14, 2021.

[110] William Lewis, Brian J Day, and William C Copeland. Mitochondrial toxicity of nrti antiviral drugs: an integrated cellular perspective. *Nature Reviews Drug Discovery*, 2(10):812–822, 2003.

[111] Nianyu Li, Kathy Ragheb, Gretchen Lawler, Jennie Sturgis, Bartek Rajwa, J Andres Melendez, and J Paul Robinson. Mitochondrial complex i inhibitor rotenone induces apoptosis through enhancing mitochondrial reactive oxygen species production. *Journal of Biological Chemistry*, 278(10):8516–8525, 2003.

[112] Qianyi Li, Alicia A McDonough, Harold E Layton, and Anita T Layton. Functional implications of sexual dimorphism of transporter patterns along the rat proximal tubule: modeling and analysis. *American Journal of Physiology-Renal Physiology*, 315(3):F692–F700, 2018.

[113] X Li, RK Dash, RK Pradhan, F Qi, M Thompson, KC Vinnakota, F Wu, F Yang, and DA Beard. A database of thermodynamic quantities for the reactions of glycolysis and the tricarboxylic acid cycle. *The Journal of Physical Chemistry B*, 114(49):16068–16082, 2010.

[114] UD Lichtenauer, J Seissler, and WA Scherbaum. Diabetic complications. micro and macroangiopathic end-organ damage. *Der Internist*, 44(7):840–6, 2003.

[115] Wilfred Lieberthal, Sarah A Menza, and Jerrold S Levine. Graded atp depletion can cause necrosis or apoptosis of cultured mouse proximal tubular cells. *American Journal of Physiology-Renal Physiology*, 274(2):F315–F327, 1998.

[116] Xiling Lin, Yufeng Xu, Xiaowen Pan, Jingya Xu, Yue Ding, Xue Sun, Xiaoxiao Song, Yuezhong Ren, and Peng-Fei Shan. Global, regional, and national burden and trend of diabetes in 195 countries and territories: an analysis from 1990 to 2025. *Scientific reports*, 10(1):1–11, 2020.

[117] Runa SJ Lindblom, Gavin C Higgins, Tuong-Vi Nguyen, Maryann Arnstein, Darren C Henstridge, Cesare Granata, Matthew Snelson, Vicki Thallas-Bonke, Mark E Cooper, Josephine M Forbes, et al. Delineating a role for the mitochondrial permeability transition pore in diabetic kidney disease by targeting cyclophilin d. *Clinical Science*, 134(2):239–259, 2020.

[118] Oxana Lukivskaya, Eleonora Patsenker, and Vyacheslav U Buko. Protective effect of ursodeoxycholic acid on liver mitochondrial function in rats with alloxan-induced diabetes: link with oxidative stress. *Life sciences*, 80(26):2397–2402, 2007.

[119] Shuai Ma, Roger G Evans, Naoya Iguchi, Marianne Tare, Helena C Parkington, Rinaldo Bellomo, Clive N May, and Yugeesh R Lankadeva. Sepsis-induced acute kidney injury: A disease of the microcirculation. *Microcirculation*, 26(2):e12483, 2019.

[120] Gerhard Magnus and Joel Keizer. Model of β-cell mitochondrial calcium handling and electrical activity. ii. mitochondrial variables. *American Journal of Physiology-Cell Physiology*, 274(4):C1174–C1184, 1998.

[121] Egbert G Mik, Tanja Johannes, Coert J Zuurbier, Andre Heinen, Judith HPM Houben-Weerts, Gianmarco M Balestra, Jan Stap, Johan F Beek, and Can Ince. In vivo mitochondrial oxygen tension measured by a delayed fluorescence lifetime technique. *Biophysical Journal*, 95(8):3977–3990, 2008.

[122] JT Miyahara and R Karler. Effect of salicylate on oxidative phosphorylation and respiration of mitochondrial fragments. *Biochemical Journal*, 97(1):194–198, 1965.

[123] Maria P Mollica, Susanna Iossa, Giovanna Liverini, and Sibylle Soboll. Steady state changes in mitochondrial electrical potential and proton gradient in perfused liver from rats fed a high fat diet. *Molecular and cellular biochemistry*, 178(1):213–217, 1998.

[124] Eduardo E Montalvo-Jave, Tomas Escalante-Tattersfield, Jose A Ortega-Salgado, Enrique Piña, and David A Geller. Factors in the pathophysiology of the liver ischemia-reperfusion injury. *Journal of Surgical Research*, 147(1):153–159, 2008.

[125] PI Moreira, AP Rolo, C Sena, R Seica, CR Oliveira, and MS Santos. Insulin attenuates diabetes-related mitochondrial alterations: a comparative study. *Medicinal Chemistry*, 2(3):299–308, 2006.

[126] Bhanu Chandra Mulukutla, Andrew Yongky, Simon Grimm, Prodromos Daoutidis, and Wei-Shou Hu. Multiplicity of steady states in glycolysis and shift of metabolic state in cultured mammalian cells. *PloS one*, 10(3):e0121561, 2015.

[127] Shankar Munusamy and Lee Ann MacMillan-Crow. Mitochondrial superoxide plays a crucial role in the development of mitochondrial dysfunction during high glucose exposure in rat renal proximal tubular cells. *Free Radical Biology and Medicine*, 46(8):1149–1157, 2009.

[128] Michael P Murphy. How mitochondria produce reactive oxygen species. *Biochemical journal*, 417(1):1–13, 2009.

[129] Georgian T Mustata, Mariana Rosca, Klaus M Biemel, Oliver Reihl, Mark A Smith, Ashwini Viswanathan, Christopher Strauch, Yunpeng Du, Jie Tang, Timothy S Kern, et al. Paradoxical effects of green tea (camellia sinensis) and antioxidant vitamins in diabetic rats: improved retinopathy and renal mitochondrial defects but deterioration of collagen matrix glycoxidation and cross-linking. *Diabetes*, 54(2):517–526, 2005.

[130] Shilpa R Nagarajan, Moumita Paul-Heng, James R Krycer, Daniel J Fazakerley, Alexandra F Sharland, and Andrew J Hoy. Lipid and glucose metabolism in hepatocyte cell lines and primary mouse hepatocytes: a comprehensive resource for in vitro studies of hepatic metabolism. *American Journal of Physiology-Endocrinology and Metabolism*, 316(4):E578–E589, 2019.

[131] Constantinos Nastos, Konstantinos Kalimeris, Nikolaos Papoutsidakis, Marios-Konstantinos Tasoulis, Panagis M Lykoudis, Kassiani Theodoraki, Despoina Nastou, Vassilios Smyrniotis, and Nikolaos Arkadopoulos. Global consequences of liver ischemia/reperfusion injury. *Oxidative medicine and cellular longevity*, 2014, 2014.

[132] Itzhak Nissim, Oksana Horyn, Yevgeny Daikhin, Ilana Nissim, Bohdan Luhovyy, Peter C Phillips, and Marc Yudkoff. Ifosfamide-induced nephrotoxicity: mechanism and prevention. *Cancer research*, 66(15):7824–7831, 2006.

[133] Molly O'Reilly, Luke Young, Nerissa K Kirkwood, Guy P Richardson, Corné J Kros, and Anthony L Moore. Gentamicin affects the bioenergetics of isolated mitochondria and collapses the mitochondrial membrane potential in cochlear sensory hair cells. *Frontiers in cellular neuroscience*, 13:416, 2019.

[134] Valeria Padovano, Christine Podrini, Alessandra Boletta, and Michael J Caplan. Metabolism and mitochondria in polycystic kidney disease research and therapy. *Nature Reviews Nephrology*, 14(11):678–687, 2018.

[135] Carlos Marques Palmeira, João Soeiro Teodoro, João Alves Amorim, Clemens Steegborn, David A Sinclair, and Anabela Pinto Rolo. Mitohormesis and metabolic health: The interplay between ros, camp and sirtuins. *Free Radical Biology and Medicine*, 141:483–491, 2019.

[136] Tushar Patel, Steven F Bronk, Gregory J Gores, et al. Increases of intracellular magnesium promote glycodeoxycholate-induced apoptosis in rat hepatocytes. *The Journal of clinical investigation*, 94(6):2183–2192, 1994.

[137] Patrice X Petit, José E O'Connor, Didier Grunwald, and Spencer C Brown. Analysis of the membrane potential of rat-and mouse-liver mitochondria by flow cytometry and possible applications. *European journal of biochemistry*, 194(2):389–397, 1990.

[138] Walter Pfaller and Michael Rittinger. Quantitative morphology of the rat kidney. In *Biochemical Aspects of Renal Function*, pages 17–22. Elsevier, 1980.

[139] Richard K Porter and Martin D Brand. Causes of differences in respiration rate of hepatocytes from mammals of different body mass. *American Journal of Physiology-Regulatory, Integrative and Comparative Physiology*, 269(5):R1213–R1224, 1995.

[140] JL Purvis and EC Slater. The effect of magnesium on oxidative phosphorylation and mitochondrial adenosine triphosphatase. *Experimental Cell Research*, 16(1):109–117, 1959.

[141] GARY A Quamme and LJ Dai. Presence of a novel influx pathway for mg2+ in mdck cells. *American Journal of Physiology-Cell Physiology*, 259(3):C521–C525, 1990.

[142] Gary A Quamme and Christian de Rouffignac. Epithelial magnesium transport and regulation by the kidney. *Front Biosci*, 5(D694-711):15, 2000.

[143] Yaremi Quiros, Laura Vicente-Vicente, Ana I Morales, José M López-Novoa, and Francisco J López-Hernández. An integrative overview on the mechanisms underlying the renal tubular cytotoxicity of gentamicin. *Toxicological sciences*, 119(2):245–256, 2011.

[144] Michael Rabkin and JJ Blum. Quantitative analysis of intermediary metabolism in hepatocytes incubated in the presence and absence of glucagon with a substrate mixture containing glucose, ribose, fructose, alanine and acetate. *Biochemical Journal*, 225(3):761–786, 1985.

[145] Rabary M Rajerison, May Faure, and François Morel. Effects of temperature, ouabain and diuretics on the cell sodium and potassium contents of isolated rat kidney tubules. *Pflügers Archiv*, 406(3):285–290, 1986.

[146] Hena R Ramay and Marko Vendelin. Diffusion restrictions surrounding mitochondria: a mathematical model of heart muscle fibers. *Biophysical journal*, 97(2):443–452, 2009.

[147] Haider Raza, Annie John, and Frank Christopher Howarth. Increased oxidative stress and mitochondrial dysfunction in zucker diabetic rat liver and brain. *Cellular Physiology and Biochemistry*, 35(3):1241–1251, 2015.

[148] Haider Raza, Subbuswamy K Prabu, Annie John, and Narayan G Avadhani. Impaired mitochondrial respiratory functions and oxidative stress in streptozotocin-induced diabetic rats. *International journal of molecular sciences*, 12(5):3133–3147, 2011.

[149] David FS Rolfe, AJ Hulbert, and Martin D Brand. Characteristics of mitochondrial proton leak and control of oxidative phosphorylation in the major oxygen-consuming tissues of the rat. *Biochimica et Biophysica Acta (BBA)-Bioenergetics*, 1188(3):405–416, 1994.

[150] Mahua Roy and Stacey D Finley. Computational model predicts the effects of targeting cellular metabolism in pancreatic cancer. *Frontiers in physiology*, 8:217, 2017.

[151] Alberto Saa and Kellen M Siqueira. Modeling the atp production in mitochondria. *Bulletin of mathematical biology*, 75(9):1636–1651, 2013.

[152] Lynn Sagan. On the origin of mitosing cells. *Journal of theoretical biology*, 14(3):225–IN6, 1967.

[153] Maria S Santos, Dario L Santos, Carlos M Palmeira, Raquel Seiça, António J Moreno, and Catarina R Oliveira. Brain and liver mitochondria isolated from diabetic goto-kakizaki rats show different susceptibility to induced oxidative stress. *Diabetes/metabolism research and reviews*, 17(3):223–230, 2001.

[154] Nobuhiro Sato, Takenobu Kamada, Sunao Kawano, Norio Hayashi, Yutaka Kishida, Haruya Meren, Harumasa Yoshihara, and Hiroshi Abe. Effect of acute and chronic ethanol consumption on hepatic tissue oxygen tension in rats. *Pharmacology Biochemistry and Behavior*, 18:443–447, 1983.

[155] Andrew M Schaefer, Robert W Taylor, Douglass M Turnbull, and Patrick F Chinnery. The epidemiology of mitochondrial disorders—past, present and future. *Biochimica et Biophysica Acta (BBA)-Bioenergetics*, 1659(2-3):115–120, 2004.

[156] Tomas A Schiffer, Michael Christensen, Håkan Gustafsson, and Fredrik Palm. The effect of inactin on kidney mitochondrial function and production of reactive oxygen species. *PloS one*, 13(11):e0207728, 2018.

[157] Tomas A Schiffer, Michael Christensen, Håkan Gustafsson, and Fredrik Palm. The effect of inactin on kidney mitochondrial function and production of reactive oxygen species. *PloS one*, 13(11):e0207728, 2018.

[158] Tomas A Schiffer, Håkan Gustafsson, and Fredrik Palm. Kidney outer medulla mitochondria are more efficient compared with cortex mitochondria as a strategy to sustain atp production in a suboptimal environment. *American Journal of Physiology-Renal Physiology*, 315(3):F677–F681, 2018.

[159] Tom JJ Schirris, G Herma Renkema, Tina Ritschel, Nicol C Voermans, Albert Bilos, Baziel GM van Engelen, Ulrich Brandt, Werner JH Koopman, Julien D Beyrath, Richard J Rodenburg, et al. Statin-induced myopathy is associated with mitochondrial complex iii inhibition. *Cell metabolism*, 22(3):399–407, 2015.

[160] Sabine Schmitt, Sabine Schulz, Eva-Maria Schropp, Carola Eberhagen, Alisha Simmons, Wolfgang Beisker, Michaela Aichler, and Hans Zischka. Why to compare absolute numbers of mitochondria. *Mitochondrion*, 19:113–123, 2014.

[161] Peter Schönfeld, Mariusz R Wiêckowski, and Lech Wojtczak. Thyroid hormone-induced expression of the adp/atp carrier and its effect on fatty acid-induced uncoupling of oxidative phosphorylation. *FEBS letters*, 416(1):19–22, 1997.

[162] WD Schwenke, S Soboll, HJ Seitz, and H Sies. Mitochondrial and cytosolic atp/adp ratios in rat liver in vivo. *Biochemical Journal*, 200(2):405–408, 1981.

[163] Gerald Schwerdt, Nader Gordjani, Andreas Benesic, Ruth Freudinger, Brigitte Wollny, Antje Kirchhoff, and Michael Gekle. Chloroacetaldehyde-and acrolein-induced death of human proximal tubule cells. *Pediatric nephrology*, 21(1):60–67, 2006.

[164] Philipp F Secker, Sascha Beneke, Nadja Schlichenmaier, Johannes Delp, Simon Gutbier, Marcel Leist, and Daniel R Dietrich. Canagliflozin mediated dual inhibition of mitochondrial glutamate dehydrogenase and complex i: an off-target adverse effect. *Cell death & disease*, 9(2):1–13, 2018.

[165] Ioannis Sgouralis, Roger G Evans, Bruce S Gardiner, Julian A Smith, Brendan C Fry, and Anita T Layton. Renal hemodynamics, function, and oxygenation during cardiac surgery performed on cardiopulmonary bypass: a modeling study. *Physiological reports*, 3(1):e12260, 2015.

[166] Ioannis Sgouralis, Roger G Evans, and Anita T Layton. Renal medullary and urinary oxygen tension during cardiopulmonary bypass in the rat. *Mathematical medicine and biology: a journal of the IMA*, 34(3):313–333, 2017.

[167] Yanjue Shen, Rongrong Cai, Jie Sun, Xue Dong, Rong Huang, Sai Tian, and Shaohua Wang. Diabetes mellitus as a risk factor for incident chronic kidney disease and end-stage renal disease in women compared with men: a systematic review and meta-analysis. *Endocrine*, 55(1):66–76, 2017.

[168] Elmar A Siess, Dietrich G Brocks, Herbert K Lattke, and Otto H Wieland. Effect of glucagon on metabolite compartmentation in isolated rat liver cells during gluconeogenesis from lactate. *Biochemical Journal*, 166(2):225–235, 1977.

[169] Jan A Smeitink, Massimo Zeviani, Douglass M Turnbull, and Howard T Jacobs. Mitochondrial medicine: a metabolic perspective on the pathology of oxidative phosphorylation disorders. *Cell metabolism*, 3(1):9–13, 2006.

[170] Anthony C Smith, Filmon Eyassu, Jean-Pierre Mazat, and Alan J Robinson. Mitocore: a curated constraint-based model for simulating human central metabolism. *BMC systems biology*, 11(1):1–13, 2017.

[171] Sibylle Soboll, Rembert Elbers, Roland Scholz, and Hans-Walter Heldt. Subcellular distribution of di-and tricarboxylates and ph gradients in perfused rat liver. *Hoppe-Seyler's Zeitschrift fur physiologische Chemie*, 361(1):69–76, 1980.

[172] Andrew P Somlyo, Avril V Somlyo, and Henry Shuman. Electron probe analysis of vascular smooth muscle. composition of mitochondria, nuclei, and cytoplasm. *The Journal of cell biology*, 81(2):316–335, 1979.

[173] Karly C Sourris, Brooke E Harcourt, Peter H Tang, Amy L Morley, Karina Huynh, Sally A Penfold, Melinda T Coughlan, Mark E Cooper, Tuong-Vi Nguyen, Rebecca H Ritchie, et al. Ubiquinone (coenzyme q10) prevents renal mitochondrial dysfunction in an experimental model of type 2 diabetes. *Free Radical Biology and Medicine*, 52(3):716–723, 2012.

[174] Peter W Stacpoole. Therapeutic targeting of the pyruvate dehydrogenase complex/pyruvate dehydrogenase kinase (pdc/pdk) axis in cancer. *JNCI: Journal of the National Cancer Institute*, 109(11), 2017.

[175] Anatoly A Starkov and Gary Fiskum. Regulation of brain mitochondrial h2o2 production by membrane potential and nad (p) h redox state. *Journal of neurochemistry*, 86(5):1101–1107, 2003.

[176] Isaac E Stillman, Mayer Brezis, Samuel N Heyman, Franklin H Epstein, Kate Spokes, and Seymour Rosen. Effects of salt depletion on the kidney: changes in medullary oxygenation and thick ascending limb size. *Journal of the American Society of Nephrology*, 4(8):1538–1545, 1994.

[177] MARIO Strazzabosco, SHOTARO Sakisaka, TOMIHIRO Hayakawa, and JAMES L Boyer. Effect of udca on intracellular and biliary ph in isolated rat hepatocyte couplets and perfused livers. *American Journal of Physiology-Gastrointestinal and Liver Physiology*, 260(1):G58–G69, 1991.

[178] SQ Sun, S-L Shi, JA Hunt, and RD Leapman. Quantitative water mapping of cryosectioned cells by electron energy-loss spectroscopy. *Journal of microscopy*, 177(1):18–30, 1995.

[179] Tomohiro Suzuki, Satoko Shinjo, Takatomo Arai, Mai Kanai, and Nobuhito Goda. Hypoxia and fatty liver. *World Journal of Gastroenterology: WJG*, 20(41):15087, 2014.

[180] Shruti N Tapiawala, Kathryn J Tinckam, Carl J Cardella, Jeffrey Schiff, Daniel C Cattran, Edward H Cole, and S Joseph Kim. Delayed graft function and the risk for death with a functioning graft. *Journal of the American Society of Nephrology*, 21(1):153–161, 2010.

[181] M Tsimaratos, F Roger, D Chabardes, D Mordasini, U Hasler, A Doucet, P-Y Martin, and E Feraille. C-peptide stimulates na+, k+-atpase activity via pkc alpha in rat medullary thick ascending limb. *Diabetologia*, 46(1):124–131, 2003.

[182] Adamo Valle, Rocio Guevara, Francisco J Garcia-Palmer, Pilar Roca, and J Oliver. Sexual dimorphism in liver mitochondrial oxidative capacity is conserved under caloric restriction conditions. *American Journal of Physiology-Cell Physiology*, 293(4):C1302–C1308, 2007.

[183] Caroline Maria Oliveira Volpe, Pedro Henrique Villar-Delfino, Paula Martins Ferreira Dos Anjos, and José Augusto Nogueira-Machado. Cellular death, reactive oxygen species (ros) and diabetic complications. *Cell death & disease*, 9(2):1–9, 2018.

[184] N Vrbjar, V Javorkova, and O Pechanova. Changes of sodium and atp affinities of the renal na, k-atpase during and after nitric oxide-deficient hypertension. *Physiological research*, 51(5):475–482, 2002.

[185] Guo Guang Wang, Xiao Hua Lu, Wei Li, Xue Zhao, and Cui Zhang. Protective effects of luteolin on diabetic nephropathy in stz-induced diabetic rats. *Evidence-Based Complementary and Alternative Medicine*, 2011, 2011.

[186] Kening Wang and Robert Wondergem. Hepatocyte water volume and potassium activity during hypotonic stress. *The Journal of membrane biology*, 135(2):137–144, 1993.

[187] Fusao Watanabe, Wataru Kamiike, Tadashi Nishimura, Tadao Hashimoto, and Kunio Tagawa. Decrease in mitochondrial levels of adenine nucleotides and concomitant mitochondrial dysfunction in ischemic rat liver. *The Journal of Biochemistry*, 94(2):493–499, 1983.

[188] BA Watts 3rd and David W Good. Effects of ammonium on intracellular ph in rat medullary thick ascending limb: mechanisms of apical membrane nh4+ transport. *The Journal of general physiology*, 103(5):917–936, 1994.

[189] Joel M Weinberg and H David Humes. Mechanisms of gentamicin-induced dysfunction of renal cortical mitochondria: I. effects on mitochondrial respiration. *Archives of biochemistry and biophysics*, 205(1):222–231, 1980.

[190] K Welt, J Weiss, R Martin, D Dettmer, T Hermsdorf, K Asayama, S Meister, and G Fitzl. Ultrastructural, immunohistochemical and biochemical investigations of the rat liver exposed to experimental diabetes und acute hypoxia with and without application of ginkgo extract. *Experimental and Toxicologic Pathology*, 55(5):331–345, 2004.

[191] Lech Wojtczak and Peter Schönfeld. Effect of fatty acids on energy coupling processes in mitochondria. *Biochimica et Biophysica Acta (BBA)-Bioenergetics*, 1183(1):41–57, 1993.

[192] LE Wold, D Muralikrishnan, CB Albano, FL Norby, M Ebadi, and J Ren. Insulin-like growth factor i (igf-1) supplementation prevents diabetesinduced alterations in coenzymes q 9 and q 10. *Acta diabetologica*, 40(2):85–90, 2003.

[193] Fan Wu, Feng Yang, Kalyan C Vinnakota, and Daniel A Beard. Computer modeling of mitochondrial tricarboxylic acid cycle, oxidative phosphorylation, metabolite transport, and electrophysiology. *Journal of Biological Chemistry*, 282(34):24525–24537, 2007.

[194] Jinzi Wu, Xiaoting Luo, and Liang-Jun Yan. Two dimensional blue native/sds-page to identify mitochondrial complex i subunits modified by 4-hydroxynonenal (hne). *Frontiers in physiology*, 6:98, 2015.

[195] Shunhei Yamashina, Nobuhiro Sato, Kazuyoshi Kon, Kenichi Ikejima, and Sumio Watanabe. Role of mitochondria in liver pathophysiology. *Drug Discovery Today: Disease Mechanisms*, 6(1-4):e25–e30, 2009.

[196] John W Yarham, Joanna L Elson, Emma L Blakely, Robert McFarland, and Robert W Taylor. Mitochondrial trna mutations and disease. *Wiley Interdisciplinary Reviews: RNA*, 1(2):304–324, 2010.

[197] Hai-Tao Yu, Xiao-Yi Fu, Bing Liang, Shuang Wang, Jian-Kang Liu, Shu-Ran Wang, and Zhi-Hui Feng. Oxidative damage of mitochondrial respiratory chain in different organs of a rat model of diet-induced obesity. *European journal of nutrition*, 57(5):1957–1967, 2018.

[198] Richard A Zager. Mitochondrial free radical production induces lipid peroxidation during myohemoglobinuria. *Kidney international*, 49(3):741–751, 1996.

[199] Cecilia Zazueta, Mabel Buelna-Chontal, Arturo Macías-López, Nadia G Román-Anguiano, Héctor González-Pacheco, Natalia Pavón, Rashidi Springall, Alberto Aranda-Frausto, Rafael Bojalil, Alejandro Silva-Palacios, et al. Cytidine-5'-diphosphocholine protects the liver from ischemia/reperfusion injury preserving mitochondrial function and reducing oxidative stress. *Liver Transplantation*, 24(8):1070–1083, 2018.

[200] Hua Zhang, Hong-Mei Zhang, Li-Ping Wu, Dun-Xian Tan, Amrita Kamat, Yun-Qing Li, Michael S Katz, Hanna E Abboud, Russel J Reiter, and Bin-Xian Zhang. Impaired mitochondrial complex iii and melatonin responsive reactive oxygen species generation in kidney mitochondria of db/db mice. *Journal of pineal research*, 51(3):338–344, 2011.

[201] Wensheng Zhang and Aurélie Edwards. Oxygen transport across vasa recta in the renal medulla. *American Journal of Physiology-Heart and Circulatory Physiology*, 283(3):H1042–H1055, 2002.

[202] Xiao Zhang, Ranjan K Dash, Anne V Clough, Dexuan Xie, Elizabeth R Jacobs, and Said H Audi. Integrated computational model of lung tissue bioenergetics. *Frontiers in physiology*, 10:191, 2019.

[203] Xiao Zhang, Ranjan K Dash, Elizabeth R Jacobs, Amadou KS Camara, Anne V Clough, and Said H Audi. Integrated computational model of the bioenergetics of isolated lung mitochondria. *PloS one*, 13(6):e0197921, 2018.

[204] Kenneth Zierler. Whole body glucose metabolism. *American Journal of Physiology-Endocrinology and Metabolism*, 276(3):E409–E426, 1999.

[205] M Zoratti, M Favaron, D Pietrobon, and V Petronilli. Nigericin-induced transient changes in rat-liver mitochondria. *Biochimica et Biophysica Acta (BBA)-Bioenergetics*, 767(2):231–239, 1984.

[206] Francesco Zurlo, Karen Larson, Clifton Bogardus, Eric Ravussin, et al. Skeletal muscle metabolism is a major determinant of resting energy expenditure. *The Journal of clinical investigation*, 86(5):1423–1427, 1990.